

AD-A153 767

AFWAL TR-84-3085

IMPROVED STATISTICAL ANALYSIS METHOD FOR PREDICTION OF MAXIMUM INLET
DISTORTION

Dennis Sedlock

Aerodynamics and Airframe Branch
Aeromechanics Division

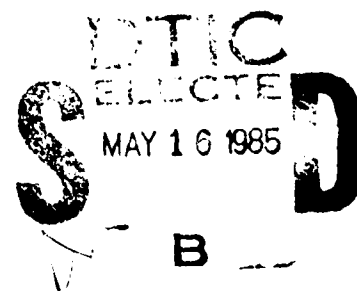


March 1985

Final Report for Period January 1983 - March 1984

Approved for Public Release; Distribution Unlimited

FLIGHT DYNAMICS LABORATORY
AIR FORCE WRIGHT AERONAUTICAL LABORATORIES
AIR FORCE SYSTEMS COMMAND
WRIGHT-PATTERSON AIR FORCE BASE, OHIO 45433



NOTICE

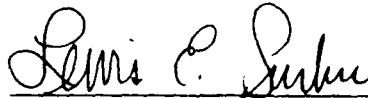
When Government drawings, specifications, or other data are used for any purpose other than in connection with a definitely related Government procurement operation, the United States Government thereby incurs no responsibility nor any obligation whatsoever; and the fact that the government may have formulated, furnished, or in any way supplied the said drawings, specifications, or other data, is not to be regarded by implication or otherwise as in any manner licensing the holder or any other person or corporation, or conveying any rights or permission to manufacture use, or sell any patented invention that may in any way be related thereto.

This report has been reviewed by the Office of Public Affairs (ASD/PA) and is releasable to the National Technical Information Service (NTIS). At NTIS, it will be available to the general public, including foreign nations.

This technical report has been reviewed and is approved for publication.



DENNIS SEDLOCK
Senior Aerospace Engineer



LEWIS E. SURBER
Technical Manager

FOR THE COMMANDER



ALFRED C. DRAPER
Asst for Research & Technology
Aeromechanics Division

"If your address has changed, if you wish to be removed from our mailing list, or if the addressee is no longer employed by your organization please notify AFWAL/FTT, W-PARS, DH 46433 to help us maintain a current mailing list".

Copies of this report should not be returned unless return is required by security considerations, contractual obligations, or notice on a specific document.

Unclassified

SECURITY CLASSIFICATION OF THIS PAGE

REPORT DOCUMENTATION PAGE

1a. REPORT SECURITY CLASSIFICATION UNCLASSIFIED			1b. RESTRICTIVE MARKINGS		
2a. SECURITY CLASSIFICATION AUTHORITY			3. DISTRIBUTION/AVAILABILITY OF REPORT Approved for public release; distribution unlimited.		
2b. DECLASSIFICATION/DOWNGRADING SCHEDULE					
4. PERFORMING ORGANIZATION REPORT NUMBER(S) AFWAL-TR-84-3085			5. MONITORING ORGANIZATION REPORT NUMBER(S)		
6a. NAME OF PERFORMING ORGANIZATION Aerodynamics & Airframe Branch		6b. OFFICE SYMBOL (If applicable) AFWAL/FIMM		7a. NAME OF MONITORING ORGANIZATION	
6c. ADDRESS (City, State and ZIP Code) Air Force Wright Aeronautical Laboratories Wright-Patterson AFB OH 45433				7b. ADDRESS (City, State and ZIP Code)	
8a. NAME OF FUNDING/SPONSORING ORGANIZATION		8b. OFFICE SYMBOL (If applicable)		9. PROCUREMENT INSTRUMENT IDENTIFICATION NUMBER	
8c. ADDRESS (City, State and ZIP Code)				10. SOURCE OF FUNDING NOS.	
				PROGRAM ELEMENT NO.	PROJECT NO.
11. TITLE (Include Security Classification) Improved Statistical Analysis Method for Prediction of Maximum Inlet Distortion (U)				2404	240410 24041062
12. PERSONAL AUTHOR(S) Sedlock, Dennis					
13a. TYPE OF REPORT Final		13b. TIME COVERED FROM 1 Feb 84 TO 31 Mar 84		14. DATE OF REPORT (Yr., Mo., Day) 1985 March	
15. PAGE COUNT 116					
16. SUPPLEMENTARY NOTATION JAN 83					
17. COSATI CODES			18. SUBJECT TERMS (Continue on reverse if necessary and identify by block number)		
FIELD	GROUP	SUB GR.	Time-Variant Distortion Inlet Analysis Inlet-Engine Compatibility Statistical Method		
21	05				
01	01				
19. ABSTRACT (Continue on reverse if necessary and identify by block number) This report presents the results of an investigation to develop an analytical method that uses inlet total pressure statistical properties and a random number process to predict the most probable maximum pressure distortion and pressure distortion map. The validity of the method is demonstrated by comparing predicted maximum distortion levels and pressure contour maps with measured peak distortion levels and pressure contour maps obtained from analog screening of inlet pressure data.					
20. DISTRIBUTION/AVAILABILITY OF ABSTRACT UNCLASSIFIED/UNLIMITED <input type="checkbox"/> SAME AS RPT. <input checked="" type="checkbox"/> OTIC USERS <input type="checkbox"/>			21. ABSTRACT SECURITY CLASSIFICATION Unclassified		
22a. NAME OF RESPONSIBLE INDIVIDUAL Dennis Sedlock			22b. TELEPHONE NUMBER (Include Area Code) 513-255-6207		22c. OFFICE SYMBOL AFWAL/FIMM

FOREWORD

This report was prepared by Dennis Sedlock of the Aerodynamics and Airframe Branch, Aeromechanics Division, Flight Dynamics Laboratory, Air Force Wright Aeronautical Laboratories, Wright-Patterson Air Force Base, Ohio under Project 2404, "Aeromechanics Technology," Task 240410, "Aeronautics and Airframe Propulsion Technology", Work Unit 24041062, "Inlet Integration Technology".

The work reported herein was performed during the period 1 ^{JAN.} ~~February~~ 1983 to 31 March 1984. The report was released by the author in July 1984.

The author expresses his appreciation to Mr Joseph Marous of the Hybrid Simulation Division, Aeronautical Systems Division Computer Center, for his contribution in the development of the computer programs and to Ms Tammy A. Wall of the Aerodynamics and Airframe Branch for her contribution in the preparation of this report.

DTIC
ELECTE
MAY 16 1985
S B D

Accession For	
NTIS GRA&I	<input checked="" type="checkbox"/>
DTIC TAB	<input type="checkbox"/>
Unannounced	<input type="checkbox"/>
Distribution	
PER CALL JC	
Availability Codes	
Avail and/or	
Unannounced	
A-1	

DOC
QUALITY
INSPECTED
1

TABLE OF CONTENTS

SECTION	PAGE
I. INTRODUCTION	1
II. BACKGROUND	5
III. BASIC MODEL ANALYSIS	12
Statistical Prediction Model Description	12
Inlet Data Base and Engine Distortion Parameters	12
Basic Model Results	14
Correlation Analysis	32
Digital Filter Development	43
IV. IMPROVED MODEL ANALYSIS	49
Improved Statistical Prediction Model Description	49
Prediction Model with Filtering	51
Prediction Model with Filtering and Map Averaging	74
Prediction Model Using Eight Turbulence Values	91
V. SUMMARY AND CONCLUSIONS	103
VI. REFERENCES	105

LIST OF ILLUSTRATIONS

FIGURE	PAGE
1. Deterministic Method for Peak Pressure Distortion	2
2. Time Variant Pressure Model	8
3. Basic Statistical Prediction Model	13
4. Basic Method (GE_1) - Comparison of Predicted to Measured Distortion	16
5. Basic Method (GE_1) - Percent RMS Difference	17
6. Basic Method (GE_1) - Pressure Contour Map and Histogram, Low Turbulence	18
7. Basic Method (GE_1) - Pressure Contour Map and Histogram, Moderate Turbulence	19
8. Basic Method (GE_1) - Pressure Contour Map and Histogram, High Turbulence	20
9. Basic Method (PWA) - Comparison of Predicted to Measured Distortion	22
10. Basic Method (PWA) - Percent RMS Difference	23
11. Basic Method (PWA) - Pressure Contour Map and Histogram, Low Turbulence	24
12. Basic Method (PWA) - Pressure Contour Map and Histogram, Moderate Turbulence	26
13. Basic Method (PWA) - Pressure Contour Map and Histogram, High Turbulence	27
14. Basic Method (GE_2) - Comparison of Predicted to Measured Distortion	28
15. Basic Method (GE_2) - Percent RMS Difference	29
16. Basic Method (GE_2) - Pressure Contour Map and Histogram, Low Turbulence	30
17. Basic Method (GE_2) - Pressure Contour Map and Histogram, Moderate Turbulence	31
18. Basic Method (GE_2) - Pressure Contour Map and Histogram, High Turbulence	33

19. Probe-to-Probe Cross Correlation	35
20. Probe-to-Probe Cross Correlation	35
21. RMS Pressure - Frequency Correlation	37
22. Probe-to-Probe Cross Correlation	38
23. Probe-to-Probe Cross Correlation	40
24. Probe-to-Probe Cross Correlation	41
25. Probe-to-Probe Cross Correlation	42
26. Generalized Random Number PSD with Non-Recursive Filter . .	46
27. Random Number PSD with Recursive Filter	46
28. Improved Statistical Prediction Model	50
29. Improved Method (GE_1) - Comparison of Predicted to Measured Distortion (Filtered)	52
30. Improved Method (GE_1) - Percent RMS Difference	54
31. Improved Method (GE_1) - Pressure Contour Map and Histogram, Low Turbulence (Filtered)	55
32. Improved Method (GE_1) - Pressure Contour Map and Histogram, Moderate Turbulence (Filtered)	56
33. Improved Method (GE_1) - Pressure Contour Map and Histogram, High Turbulence (Filtered)	57
34. Distribution of Probe Recovery Difference (GE_1)	58
35. Improved Method (PWA) - Comparison of Predicted to Measured Distortion (Filtered)	60
36. Improved Method (PWA) - Percent RMS Difference	61
37. Improved Method (PWA) - Pressure Contour Map and Histogram, Low Turbulence (Filtered)	62
38. Improved Method (PWA) - Pressure Contour Map and Histogram, Moderate Turbulence (Filtered)	64
39. Improved Method (PWA) - Pressure Contour Map, High Turbulence (Filtered)	65
40. Distribution of Probe Recovery Difference (PWA)	66

41. Improved Method (GE_2) - Comparison of Predicted to Measured Distortion, (Filtered)	67
42. Improved Method (GE_2) - Percent RMS Difference, (Filtered)	69
43. Improved Method (GE_2) - Pressure Contour Map and Histogram, Low Turbulence (Filtered)	70
44. Improved Method (GE_2) - Pressure Contour Map and Histogram, Moderate Turbulence (Filtered)	71
45. Improved Method (GE_2) - Pressure Contour Map and Histogram, High Turbulence (Filtered)	72
46. Distribution of Probe Recovery Difference (GE_2)	73
47. Improved Method (GE_1) - Pressure Contour Map and Histogram, Low Turbulence (Filtered and Map Averaged) . .	76
48. Improved Method (GE_1) - Pressure Contour Map and Histogram, Moderate Turbulence (Filtered and Map Averaged)	77
49. Improved Method (GE_1) - Pressure Contour Map and Histogram, High Turbulence (Filtered and Map Averaged). .	78
50. Improved Method (PWA) - Pressure Contour Map and Histogram, Moderate Turbulence (Filtered and Map Averaged)	79
51. Improved Method (PWA) - Pressure Contour Map and Histogram, High Turbulence (Filtered and Map Averaged). .	80
52. Improved Method (PWA) - Pressure Contour Map and Histogram, Moderate Turbulence (Filtered and Map Averaging).	82
53. Improved Method (GE_2) - Pressure Contour Map and Histogram, Moderate Turbulence (Filtered and Map Averaged).	83
54. Improved Method (GE_2) - Pressure Contour Map and Histogram, High Turbulence (Filtered and Map Averaged). .	84
55. Improved Method (GE_2) - Pressure Contour Map and Histogram, High Turbulence (Filter and Map Averaged). . .	85
56. Percent RMS Difference (GE_1).	87
57. Predicted Pressures within $\pm 2\%$ Measured P_{T_i} (GE_1)	88
58. Percent RMS Difference (PWA)	89
59. Predicted Pressures within $\pm 2\%$ Measured P_{T_i} (PWA)	90
60. Percent RMS Difference (GE_2)	92

61.	Predicted Pressures within $\pm 2\%$ Measured P_{T_i} (GE_2)	93
62.	Improved Method (GE_1) - Pressure Contour Map and Histogram - 8 RMS Turbulence Measurements, Low Turbulence	95
63.	Improved Method (GE_1) - Pressure Contour Map and Histogram - 8 RMS Turbulence Measurements, Moderate Turbulence	96
64.	Improved Method (GE_1) - Pressure Contour Map and Histogram - 8 RMS Turbulence Measurements, High Turbulence	97
65.	Improved Method (PWA) - Pressure Contour Map and Histogram - 8 RMS Turbulence Measurements, Moderate Turbulence	98
66.	Improved Method (GE_2) - Pressure Contour Map and Histogram - 8 RMS Turbulence Measurements, Moderate Turbulence	99
67.	Percent RMS Difference (8 vs 40 RMS Turbulence Values).	101
68.	Predicted Pressures within $\pm 2\%$ Measured P_{T_i}	102

LIST OF SYMBOLS

f_c	cut-off filter frequency
h_o, h_k	filter weighting coefficient
M	$(N-1)/2$
N	number of samples averaged
P_T	total pressure
P_T/P_{T0}	total pressure recovery
$\Delta P_{T_{RMS}}/P_T, T$	turbulence, T
r	probe radius
RMS	Root-Mean-Square
RN	Random Number
S	distance between probes
X	filter input
Y_n, Y_o	filter output

Subscripts

Dyn	dynamic
f	fluctuating
i	i th pressure
j	j th pressure
o	free stream
ss	steady-state

SECTION I

INTRODUCTION

This report presents the results of an investigation to develop an analytical method which predicts the maximum pressure distortion level and provides a synthesized pressure distortion map at the entrance to the turbine engine compression system. The method uses the steady-state total pressures and the statistical properties of the time-variant total pressures measured at the compressor face plane.

A high degree of compatibility between the inlet and engine is necessary for an aerodynamically stable propulsion system. An essential element in assessing that compatibility is the determination of the time-variant total pressure distortion generated by the inlet. A deterministic analysis procedure, shown in Figure 1, has evolved for processing time-variant pressure distortion data. Filtered high-response compressor face pressure data are combined with their respective steady-state total pressure component and input to a set of engine distortion parameter equations. Peak distortion levels and pressure distortion maps are determined. If the peak distortion level is less than some limit value related to an engine surge margin allocation, a compatible inlet-engine combination exists. The procedure has been a successful but conservative approach to the problem.

Analog editing systems have been used extensively to provide that assessment of inlet-engine compatibility. One such system called DYNADEC (Dynamic Data Eding and Computing), utilizes a modern state-of-the-art hybrid computer (Reference 1). DYNADEC provides for the continuous solution of the distortion parameter equations and the handling of the massive quantities of data in a timely and cost-effective manner. Entire data records can be screened in a real-time environment with final results available immediately. The high degree of system flexibility allows program parameters to be easily changed and thus provides for an efficient analysis process.

While the analysis process appears to be well in-hand, the acquisition of dynamic pressure data has become an increasingly expensive proposition due to higher wind tunnel operational costs, the use of large

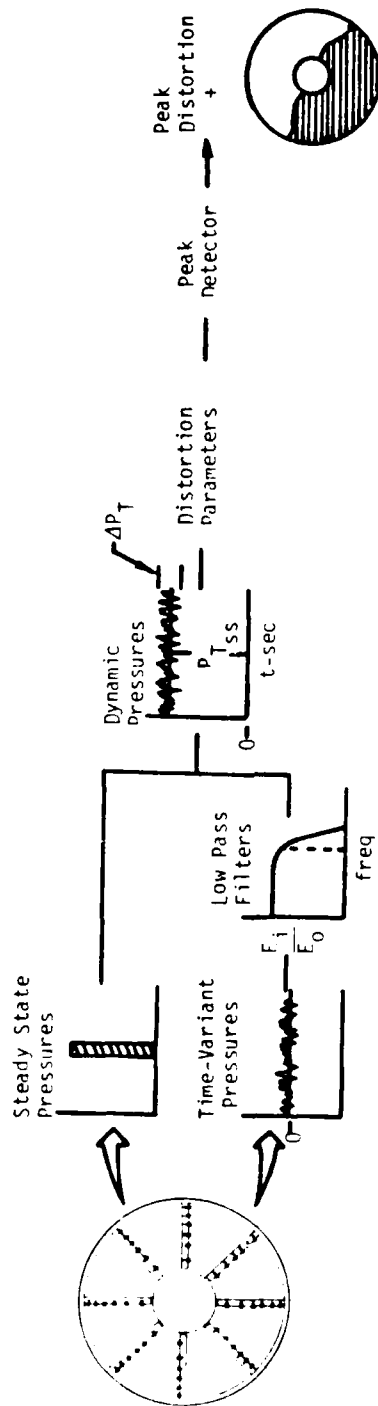


Figure 1 Deterministic Method for peak pressure distortion

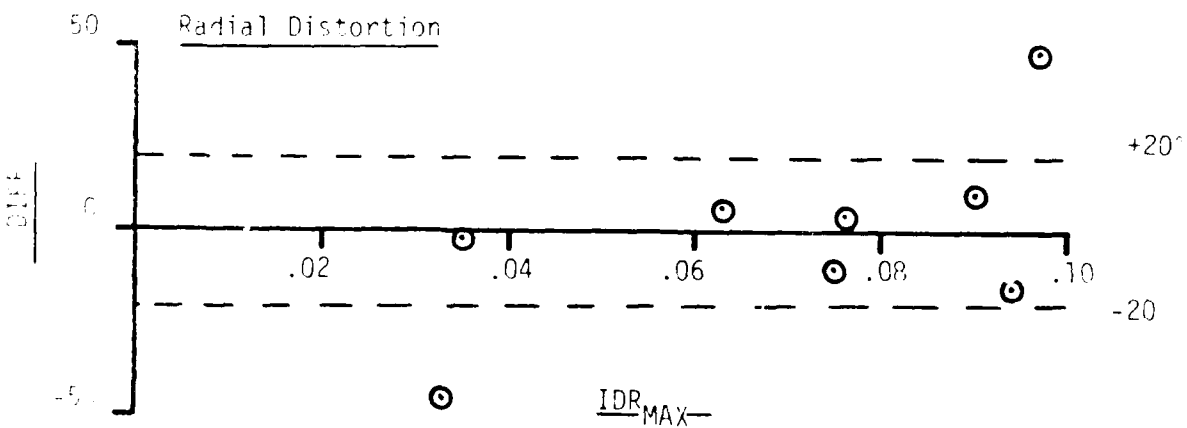
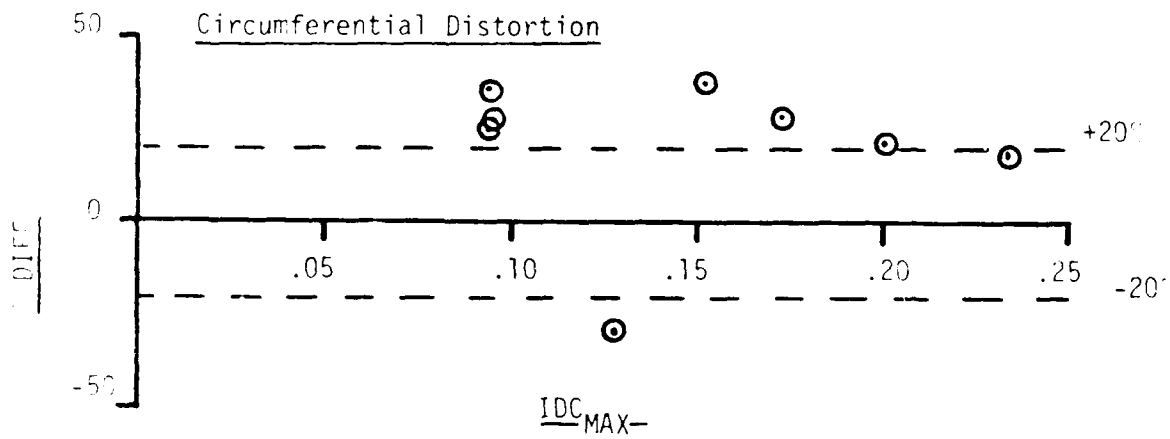
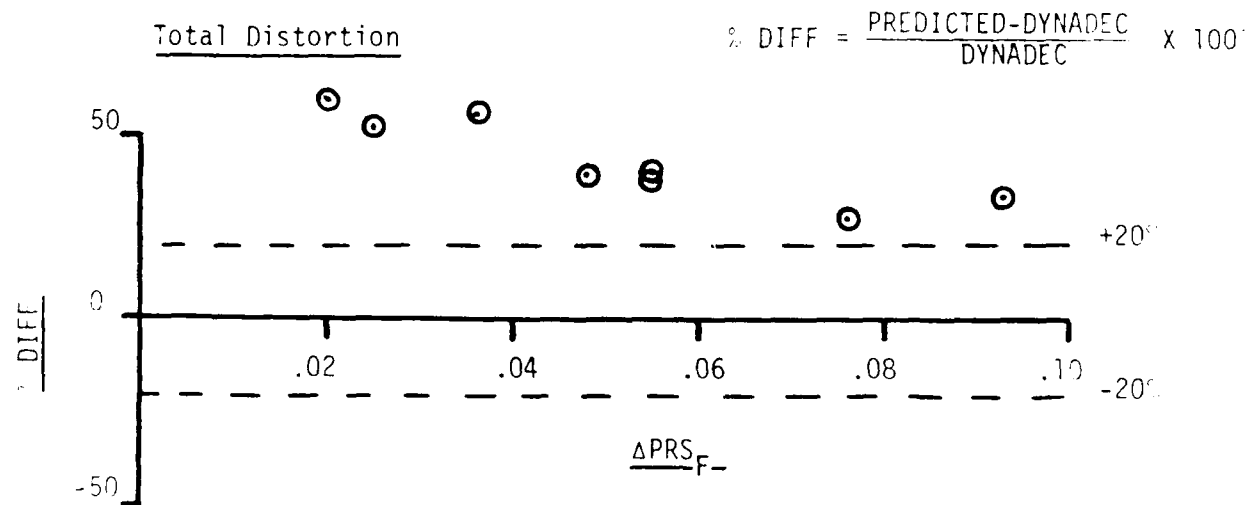


Figure 4 Basic Method (GE_1) - Comparison of Predicted to Measured Distortion

To illustrate the limitations of the basic model, the difference between the predicted and measured peak distortion level as a function of measured distortion level is shown. Next, the average standard deviation of the difference between predicted and measured probe pressure recoveries as a function of turbulence is presented. The $\%RMS_{DIFF}$ for a single case is defined as

$$\%RMS_{DIFF} = \left\{ \frac{1}{n-1} \sum \left[\frac{\Delta P_{T_i}}{P_{T_0}} - \frac{\overline{\Delta P_T}}{P_{T_0}} \right]^2 \right\}^{1/2} \times 100\% \quad (4)$$

where ΔP_T is the difference between a predicted and measured pressure and $\overline{\Delta P_T}$ is the mean difference between the predicted and measured pressures. Finally, the predicted and measured pressure contour maps are shown, including the distortion levels and the histogram of the difference between the predicted and measured probe pressure recoveries.

Figures 4 through 8 present predicted and measured results for the GE₁ engine distortion parameters. The measured peak distortion levels and pressure distortion maps were determined from screened inlet pressure data filtered at a cut-off frequency of 500 HZ. The differences between predicted and measured peak distortion levels are shown in Figure 4. Peak distortion levels are expressed in terms of ΔPRS_F with the circumferential and radial components being IDC_{MAX} and IDR_{MAX} , respectively. The basic model significantly overpredicts ΔPRS_F and IDC_{MAX} . The radial component is more randomly distributed, but with some large differences as well.

In Figure 5, the average standard deviation of the difference in probe pressure recoveries is presented. The difference between predicted and measured pressures increases with increasing average turbulence. Since $\%RMS_{DIFF}$ will vary with different sets of random numbers, several cases were repeated several times using different starting seed values. A linear regression analysis (Reference 15) was then accomplished on the total set of account for differences due the random number process. The resulting regression line and others that follow serve as baselines to show improvements to the model.

Figures 6, 7, and 8 compare the predicted and measured peak distortion maps for three levels of average turbulence. For all three

defined as they are not a part of the input to the statistical prediction method.

Compressor face instrumentation used to measure the time-variant pressures consisted of forty steady-state and high response probes in an eight-rake by five-ring array. The fluctuating pressure data was filtered at 500 HZ and 1000 HZ (-3db) consistent with engine sensitivity, inlet model scale, and available cut-off filter frequencies.

The Pratt & Whitney Aircraft (PWA) K , and the General Electric ΔPRS_F (GE_1) and IDL (GE_2) were the three sets of engine distortion parameters used in the analysis. For the PWA distortion methodology, the total distortion, K_{A_2} , is the sum of the circumferential distortion, K_θ , and the weighted radial, distortion, K_{RA_2} .

$$K_{A_2} = K_\theta + b K_{RA_2} \quad (2)$$

The GE parameters describe either the stall pressure ratio loss, ΔPRS_F , the sum of the loss in fan stall pressure ratio due to circumferential and radial distortion, or the ratio of surge margin required to that available for distortion defined as IDL. Functionally, ΔPRS_F , and IDL can be expressed in terms of the maximum circumferential and radial distortion,

$$\Delta PRS_F, IDL = f (IDC_{MAX}, IDR_{MAX}) \quad (3)$$

Basic Model Results

A common format of comparison between predicted and measured quantities is presented throughout this section and in Section IV. Several measures of goodness are used to assess the capability of the basic and improved models. These measures of goodness were: the difference between the predicted and measured maximum distortion level, the average standard deviation, the distribution, and the range of the difference between predicted and measured pressures, the similarity between the predicted pressure and measured contour maps, and the number of predicted pressures within ± 2 percent of their measured values. Peak distortion pressure contour maps determined with DYNADEC serve as the basis for the measured values.

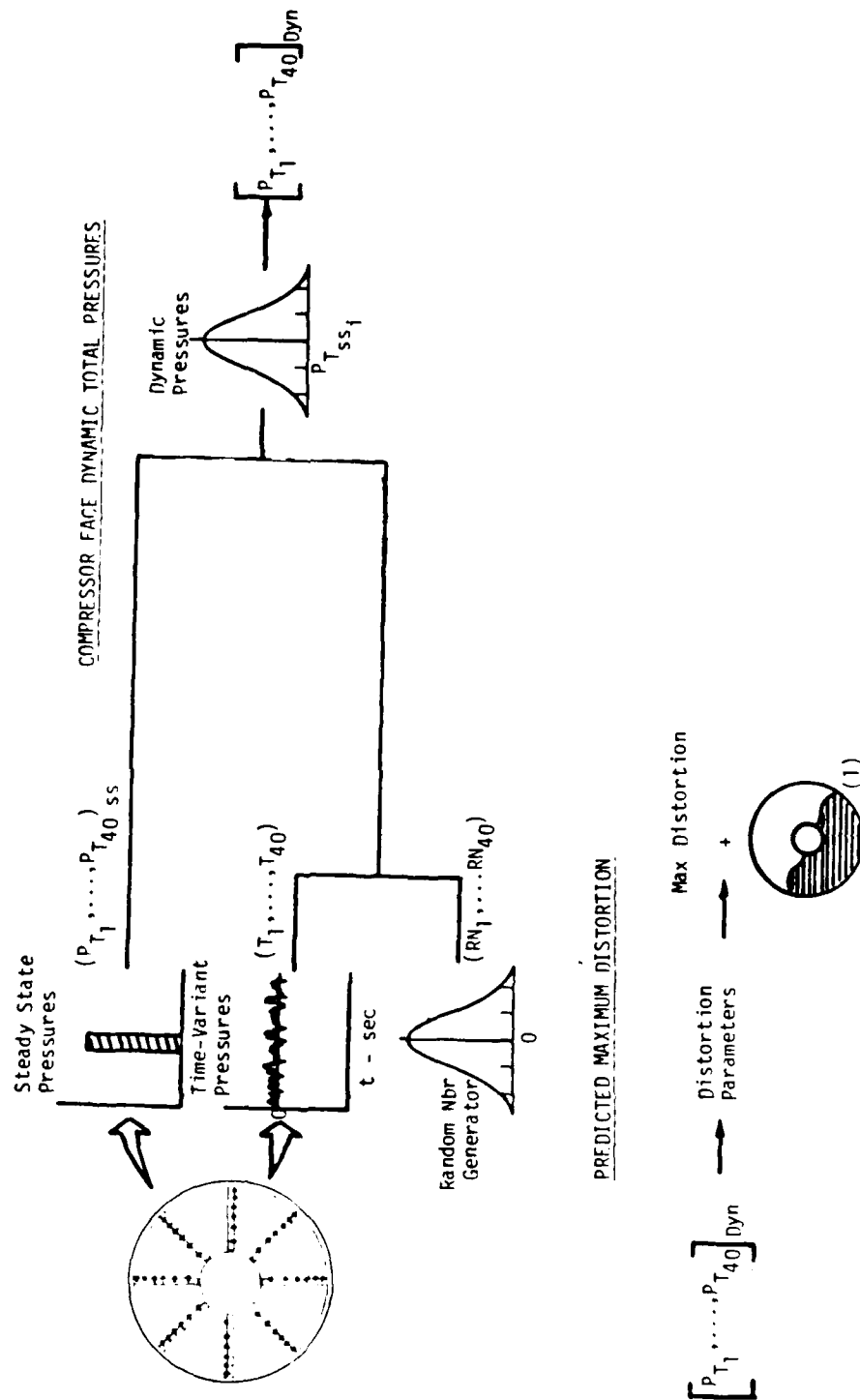


Figure 3 Basic Statistical Prediction Model

SECTION III

BASIC MODEL ANALYSIS

Statistical Prediction Model Description

The basis for the method is that a synthesized fluctuating pressure component can be constructed and added to the steady-state pressure to form the dynamic total pressure. The fluctuating pressure is assumed to be stationary, uncorrelated, and random with a normal distribution.

The synthesized fluctuating pressure can be determined for each probe using a random number generator with a zero mean, and the standard deviation derived from the measured turbulence levels. If the dynamic total pressure is defined in terms of pressure recovery, then for each probe:

$$\left(\frac{P_{Ti}}{P_{To}} \right)_{\text{Dyn}} = \left(\frac{P_{Ti}}{P_{Ts}} \right)_{\text{ss}} + \left(\frac{\Delta P_{T_{\text{RMS}}}}{P_{Ts}} \right)_i \times \left(\frac{P_{Ti}}{P_{To}} \right)_{\text{ss}} \times \text{RN}_i \quad (1)$$

The basic model, Figure 3, consists of two fundamental elements, the generation of the compressor face dynamic total pressures and the determination of the maximum distortion level and pressure contour map. RMS turbulence and random numbers are combined to form the fluctuating pressure components which are added to the steady-state pressures to form the dynamic total pressures. The dynamic total pressures are input to the distortion parameter equations and the level is determined. The pressure contour map is also generated. Forty new random numbers are generated providing a new set of dynamic total pressures which represents data from another equivalent time slice. The distortion level is computed and compared to the current maximum value. The sequence is repeated until a desired sample size is reached.

Inlet Data Base and Engine Distortion Parameters

Forty-nine cases from two sets of inlet data with three sets of engine distortion parameters were used in the investigation. Average compressor face turbulence ranged from approximately .01 to .08. Inlet operating conditions, test conditions, and inlet geometry have not been

A third investigator to report on the development of a statistical synthesis method using a random number generator and local RMS pressure data was Borg (Reference 2). In his method, the normally distributed random numbers were generated by adding twelve independent random numbers from a uniform distribution using the central limit theorem. Briefly, the central limit theorem states that the sums of independent random variables under fairly general conditions will be approximately normally distributed, regardless of the underlying conditions (Reference 14). The RMS pressures were determined using a suitable cut-off filter frequency. Borg used the Pratt & Whitney and Rolls Royce distortion parameters in evaluating his method. Results with the PWA parameters were consistent with that of Stevens and Sanders. One interesting aspect of the study was the use of average RMS pressure values at all probe locations. Since there was no drastic change in the distortion level correlations, Borg concluded that a reduced number of turbulence values could be used if they reflected the average turbulence intensity. No comparisons were made between predicted and measured peak distortion maps.

In summary, the statistical prediction methods were found to provide a reasonable prediction of the maximum distortion level. The methods developed by Motycka, Stevens, and Melick also provided a synthesized pressure distortion map. Each of these methods were found to predict a reasonable distortion map at low-turbulence levels, however, as the turbulence level increased and as the number of measured values of turbulence used in the analysis decreased, the quality of the pressure distortion map deteriorated.

These investigators proposed the use of statistical methods to achieve cost reductions for the analysis of time-variant distortion data from small models with limited instrumentation. Such methods were not intended to supplant the editing systems used for screening inlet distortion data during validation tests of inlet-engine compatibility of aircraft systems.

expected engine sensitivity in determining the probe RMS turbulence levels. Second, no power spectrum shaping is used in the analysis. Large sample sizes are considered necessary to accurately represent dynamic pressure data. For example, if the highest frequency of interest is approximately 1000 HZ, and five or more samples are required per cycle, then some 150,000 samples or time slices are required to analyze an equivalent 30 seconds of data.

Predicted peak distortion levels and pressure contour maps were compared to an F-15 and F-18 inlet data base. Peak distortion levels, based on Pratt & Whitney and General Electric distortion parameters, were approximately 10 percent under and over the measured values, respectively. This result is consistent with Sander's analysis of Motycka's method. Stevens also investigated the use of fewer measured turbulence values to predict the peak distortion levels and found that the results were about the same as when all the measured RMS turbulence values were used. A comparison of predicted versus measured pressure contour maps using both sixteen and forty-eight RMS turbulence values was also accomplished. It was concluded that the pressure contours obtained using the statistical model with forty-eight RMS turbulence values generally agreed well with the measured contours, but for the reduced number of turbulence values, the predicted contours were only representative of the measured contours.

Forner and Manter (Reference 13) used Stevens' method to predict peak distortion levels, based on the Williams Research Corporation distortion parameters, for cruise missile inlet configurations. Comparisons between predicted versus measured peak distortion levels showed that almost all of the data fell within a +10 to -20 percent band. For a number of cases there was poor agreement between the predicted and measured pressure distortion maps. Other patterns were judged to be good on a qualitative basis, but exhibited fairly large differences between individual predicted and measured probe values. The duct flow was known to be highly dynamic with regions of separated flow. Forner and Manter also investigated the use of fewer turbulence measurements and found that four, eight, or twelve values provided as good a prediction of distortion level as with forty turbulence measurements. As fewer measured turbulence values were used, however, fewer predicted patterns agreed with measured patterns.

Motycka's method (Reference 3) consists of determining the mean RMS pressure as a function of frequency, and the power spectral density for each pressure probe. An amplitude probability density curve is generated for each probe from the RMS level assuming a normal distribution. Random numbers are converted to pressures from a cumulative amplitude probability density function determined from the integration of the amplitude probability density curve. The synthesized pressures are scaled to the experimental PSDs with a digital filter and stored. Filter coefficients are determined from an amplitude gain curve formed by dividing the PSD of the test data by the PSD of the random numbers. Therefore, the power spectrum for the synthesized pressures are modified to have the same power spectrum of the experimental data. The resulting equivalent pressure-time traces are then reduced in the same manner as digitized pressure data used in the deterministic method for finding the maximum distortion level and pressure contour map.

Motycka examined a single case, and while there was good agreement between measured and predicted results, he offered no general conclusions regarding the accuracy of the method. Using the extreme value analysis of Reference 12, Motycka concluded that the influence of the filter was to reshape the extreme value distortion versus time relationship. As a consequence, he suggested that the digital filter could be eliminated if the maximum expected value is for a relatively long inlet operating time.

Sanders (Reference 10) evaluated Motycka's method using three distortion factors and four sets of inlet data. There was a tendency to overpredict the maximum distortion level using General Electric (GE) distortion parameters, and a tendency to underpredict the measured values using Pratt & Whitney Aircraft (PWA) and Williams Research Corporation (WRC) distortion parameters. This tendency of underpredicting was believed to be due to an invalid assumption of normality for the pressure data. The prediction of distortion patterns was considered good, but the agreement between measured and predicted maps decreased significantly for turbulence levels greater than .02.

The method developed by Stevens, Spong, and Cliphant (Reference 4) is very similar to that of Motycka, with two differences. First, the pressure data is processed at a cut-off filter frequency consistent with

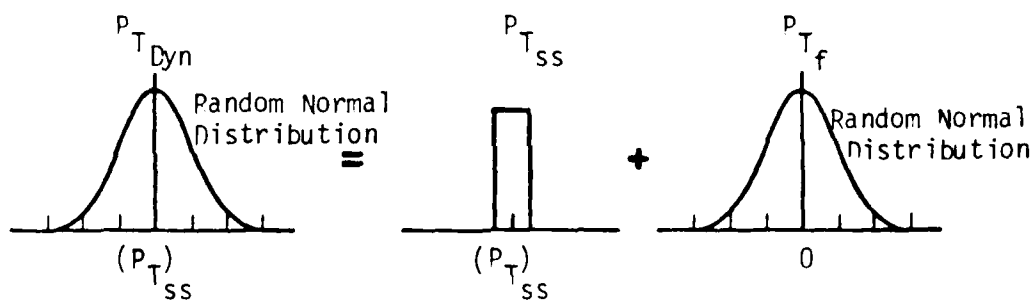


Figure 2 Time Variant Pressure Model

The results indicated that twenty probes yielded essentially the same results as forty probes, with four probes yielding a variation of less than 10 percent compared to a predicted distortion value based on forty probes.

Sanders (Reference 10) provided a comprehensive analysis of Melick's method using three different distortion factor methodologies and four sets of inlet data. One particular distortion parameter was modified by using empirically derived statistics instead of theoretically derived statistics. In general, an excellent correlation was found for the index with the empirically derived statistics, with poor to good agreement for the other distortion factors that were based on the theoretical derived statistics. Comparisons were made of measured and predicted maximum distortion patterns for a narrow range of low-turbulence values ($.012 < T < .023$). Qualitative agreement appeared to range from poor to good for these low-turbulence cases. Schweikhard (Reference 11) also made comparisons of measured data with Melick's method and found much the same results for both the distortion level and pressure distortion pattern.

The next three methods employ a random number process. The fundamental premise of these methods is that a random number process can be used to synthesize the fluctuating component of the dynamic total pressure from the statistical properties of the inlet pressure data. The dynamic total pressure, $P_{T_{Dyn}}$, consists of two components, the steady-state component, $P_{T_{ss}}$, and the fluctuating component, P_{T_f} , such that

$$P_{T_{Dyn}} = P_{T_{ss}} + P_{T_f}$$

where the fluctuating component has a zero mean value. It is assumed that the time-variant pressure data are random, stationary, with a normal distribution. A random number generator with a normal distribution and a zero mean, and the measured standard deviation of pressure are used to form a synthesized fluctuating pressure component. The dynamic pressure model is depicted in Figure 2. The dynamic pressures are then input to a set of distortion parameters and a maximum value is determined.

of a random distribution of discrete vortices being convected downstream by the mean flow and that the effects of a series of vortices can be determined by summing the individual effects of each vortex.

The method assumes that most inlet total pressure fluctuations are normally distributed and that any distortion parameter computed from these pressures will similarly be normal. The vortices in the flow are of arbitrary size, strength, location, and orientation. Vortex size and strength are represented by a Beta distribution, while the location and orientation are assumed to be uniformly distributed. Certain statistical functions are assumed to be related to the physical characteristics of the turbulent flow model. For example, the mean square of the vortex strength is proportional to the root-mean-square of the fluctuations, the mean core size is defined by the frequency of the power spectral density function, and the vortex flux is related to the probability density function.

Through a number of assumptions, the complex statistical and fluid flow relations are simplified to a graphical solution. This graphical approach relates the standard deviation of the distortion parameters to the standard deviation of the pressure fluctuations, to the mean vortex core size, and to the vortex flux. The probability density function of each distortion factor must also be defined, and a Beta density function is constructed to satisfy constraints concerning the shape of the distribution.

To create the instantaneous distortion pattern, a linear vortex is located across the duct between the high- and low-pressure regions of the steady-state distortion pattern. A total pressure increment, due to the total pressure variation within the vortex, is added to each probe pressure value. The strength of the vortex is increased until the predicted instantaneous distortion factor, determined from the graphical solution, is reached.

Comparisons presented by Melick, which were based on two sets of inlet data, showed good agreement with measured results. No comparisons were made between predicted and measured maximum pressure contour maps. The author also examined the effect of using fewer compressor face RMS turbulence measurements.

SECTION 11

BACKGROUND

Several statistical methods have been developed to predict the maximum distortion level, and in some instances, provide a predicted pressure contour map. Those analyses which offer a predicted map capability are discussed here. Two methods that use a form of superposition are addressed first, followed by a discussion of three methods that utilize a random number process.

King, Schuerman, and Muller (Reference 6) reported on a distortion synthesis procedure used to estimate the maximum inlet distortion level associated with "drift" stalls that occurred during an inlet-engine test. The procedure consists of defining a reference 180° segment (based on the steady-state pressure contour map) defined as the segment with the minimum steady-state total pressure average. The steady-state pressure contour map is intensified by subtracting total pressure increments from the steady-state probe pressures within the reference 180° segment and by adding increments to the probe pressures outside the reference segment. The total pressure increment is defined as the sum of the root-mean-square (RMS) of the total pressure fluctuations for a given probe and the average RMS for all the probes contained within the associated 180° segment. The pressure increment is multiplied by a coefficient determined by the extreme value extrapolation method of Jacocks and Kneile (Reference 7). Briefly, Jacocks' method assumes that a short time segment of distortion data can be used to statistically predict the maximum distortion level corresponding to any time period of inlet operation. King concluded that there was good agreement between the synthesized and measured distortion with a tendency to overpredict the maximum distortion level. Unfortunately, no comparisons were made between the intensified and measured pressure contour maps for the maximum distortion levels.

Melick's analytical model (References 8 and 9) has a statistical basis that is intended to provide both an understanding and quantitative description of unsteady inlet flow. A solution to the one-dimensional, time-dependent, Navier-Stokes equation is used to describe the flow field of an isolated vortex. It is hypothesized that the flow field consists

pressure to the steady-state total pressure). In spite of these results, the approach of using random numbers to generate a synthesized pressure distortion map remained promising if improvements could be made to the method.

In Section III, a description of the basic statistical prediction model is presented. The inlet data base and the engine distortion parameters used to determine maximum distortion levels are described. Comparisons between the model and DYNADEC analysis results are presented to show the limitations of the method in predicting the maximum distortion level and pressure contour map over a range of inlet distortion and turbulence levels. It is generally assumed that inlet total pressures are normally distributed and uncorrelated. Previous studies (References 2 and 5) have investigated and supported the assumption of normality and therefore will not be addressed. The assumption that the pressures are uncorrelated is examined to assess its importance to the method. Because the power spectrum of the pressures used in a distortion analysis exhibits a decreasing amplitude with increasing frequency due to turbulent mixing and filtering to define engine sensitivity, an additional constraint is imposed on the statistical model. Two digital filters are described that shape the power spectral density (PSD) of the random numbers set to approximate the PSD of inlet pressure data.

Section IV focuses on the revised statistical prediction model that incorporates the two digital filters described in Section III. Comparisons between predicted and measured maximum distortion levels and pressure contour maps are presented to demonstrate the applicability of the model. A map averaging approach is then described that offers a substantial improvement in the quality of the pressure contour map. This study also investigates the use of a reduced number of measured RMS turbulence values in the analysis. Results are presented based on using eight turbulence values.

Section V presents a summary and conclusions of the investigation.

models in large facilities, and the extensive instrumentation and data processing requirements. Thus smaller models, with less instrumentation and less data processing requirements, are being considered for use in smaller facilities. In addition, there has been an effort to develop analytical models which are based on a more simplified data processing approach to supplement the analog screening process described above.

A number of technical needs can be fulfilled by having an analytical model that synthesizes time-variant distortion. Such a tool would be useful in the inlet preliminary design and development phases. The availability of such a model could provide on-line prediction capability during wind tunnel tests, allow the prediction of peak distortion based on a limited amount of pressure instrumentation, and provide space at the compressor face plane to measure other flow quality parameters. Such a method, however, must provide the pressure contour pattern as well as the maximum distortion level, be accurate at high-turbulence levels, and be economical relative to the testing with full dynamic instrumentation.

In recent years various inlet flow distortion analyses have been proposed which use statistics. These methods use either the distortion parameter or the pressure statistical properties to predict the maximum distortion level. Some of these methods include a synthesis of the pressure distortion pattern. Distortion pattern synthesis has been accomplished by the intensification of the steady-state pattern and by the use of a random number process. These synthesis methods are described in Section II.

It is the use of the random number process, coupled with the inlet pressure statistical properties that is the subject of this report. This approach has been examined previously by three investigators (References 2, 3, 4). Because of the potential of these methods, a model similar to that described by Stevens (Reference 4) was used in comparison with several inlet distortion data sets. The initial results appeared to validate the model, particularly in terms of the predicted peak distortion level. As cases with increasing average inlet turbulence were investigated and as fewer RMS turbulence measurements were used in the analysis, the quality of the predicted maps deteriorated. (Turbulence is defined as the ratio of the standard deviation or RMS of the time-variant

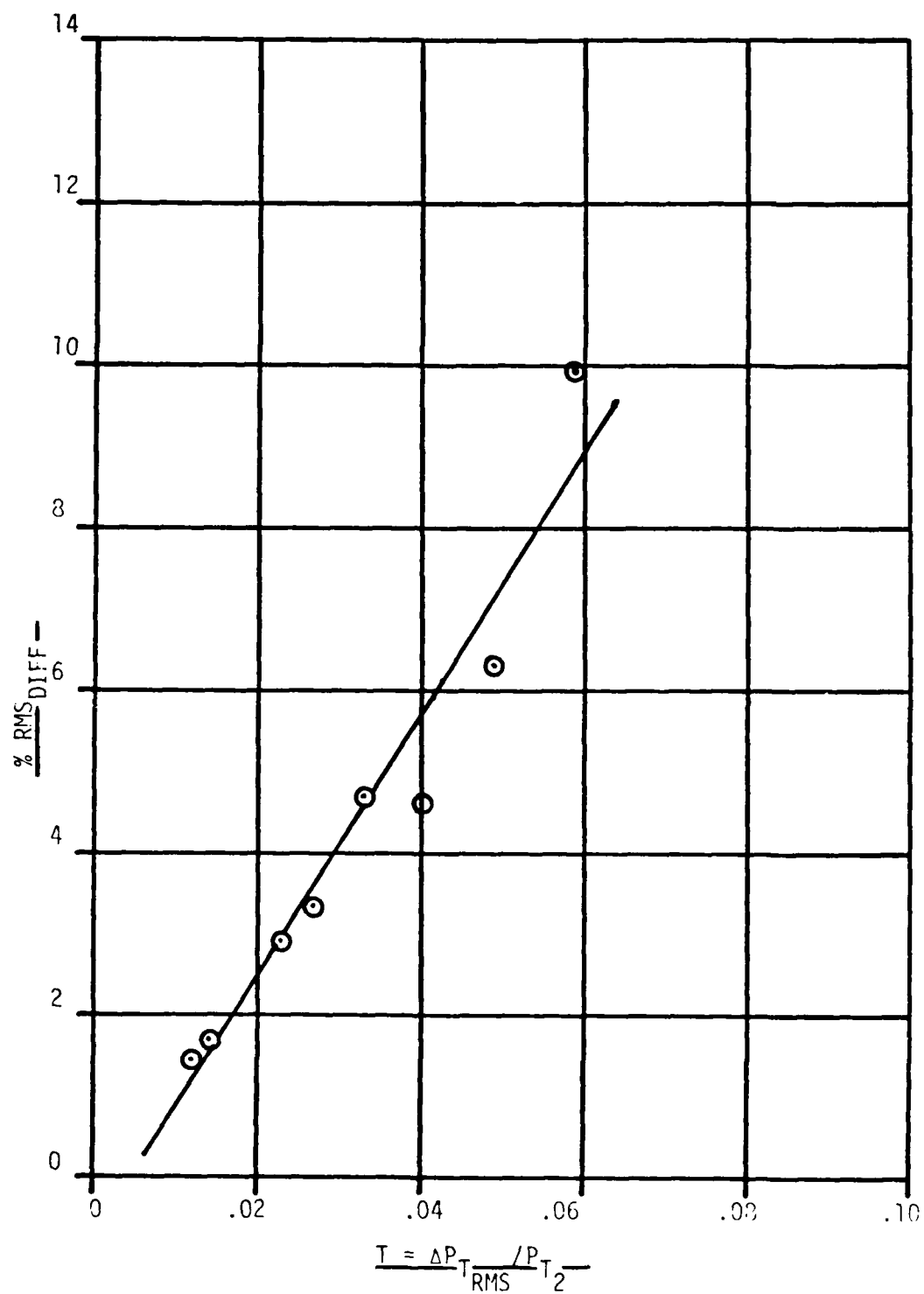
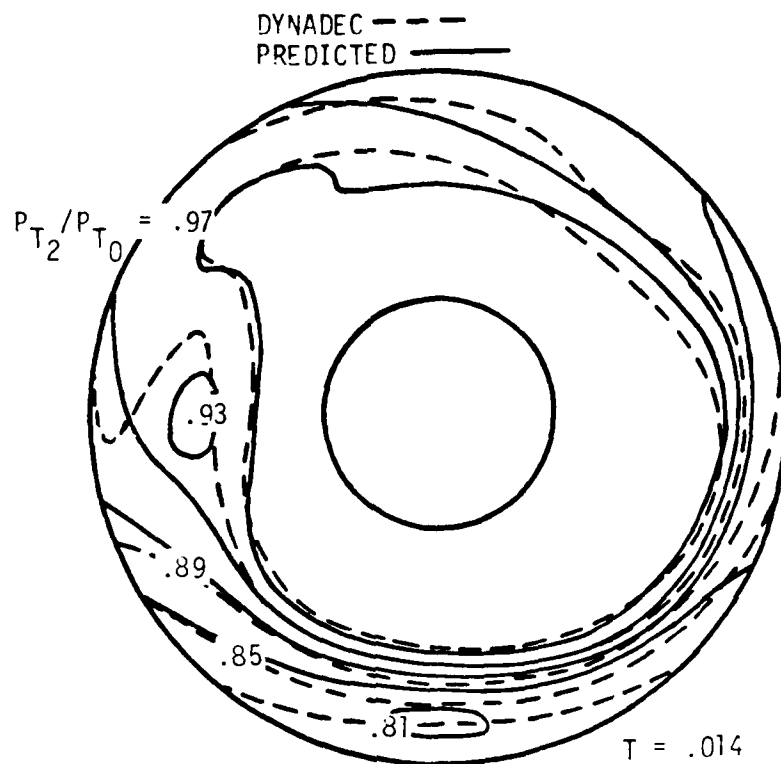


Figure 5 Basic Method (GF_1) - Percent RMS Difference



	<u>DYNADec</u>	<u>PREDICTED</u>
ΔPRS_F	.020	.032
IDC_{MAX}	.094	.117
IDR_{MAX}	.063	.067

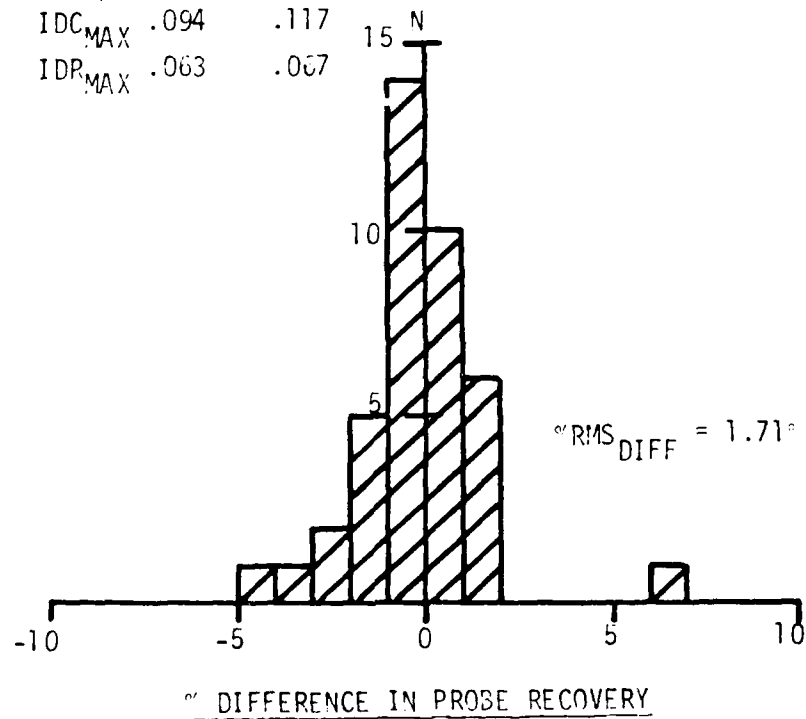
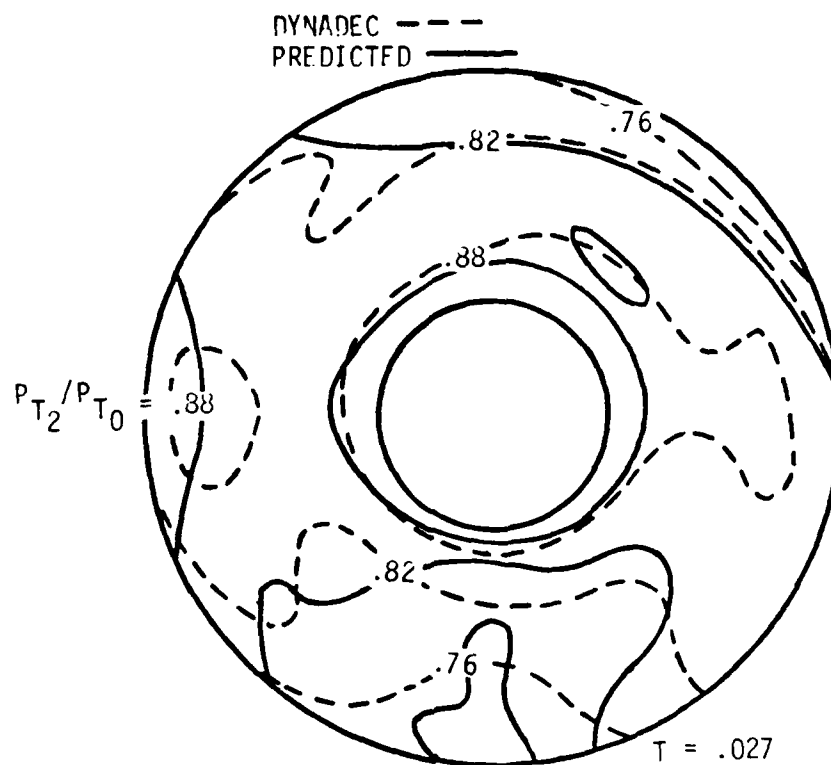


Figure 6 Basic Method (GF_1) - Pressure Contour Map and Histogram, Low Turbulence



	<u>DYNADEC</u>	<u>PREDICTED</u>
ΔPRS_F	.048	.067
IDC_{MAX}	.127	.090
IDR_{MAX}	.033	.018

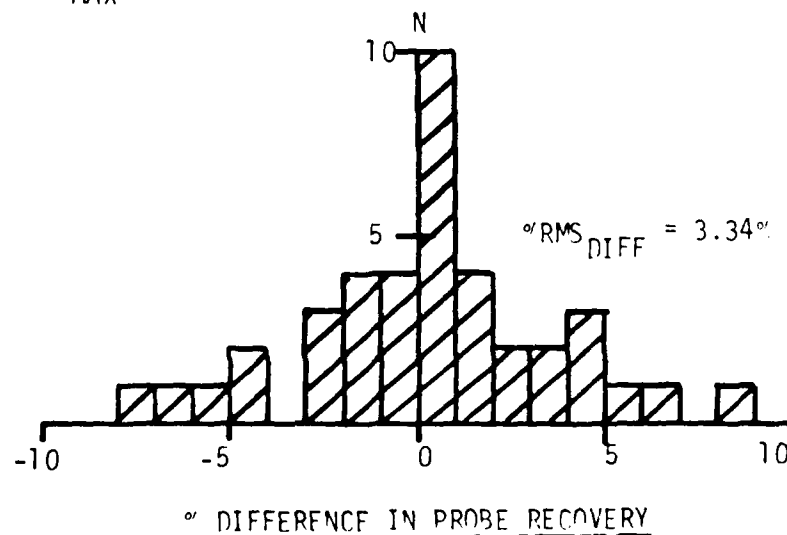


Figure 7 Basic Method (GF₁) - Pressure Contour Map and Histogram, Moderate Turbulence

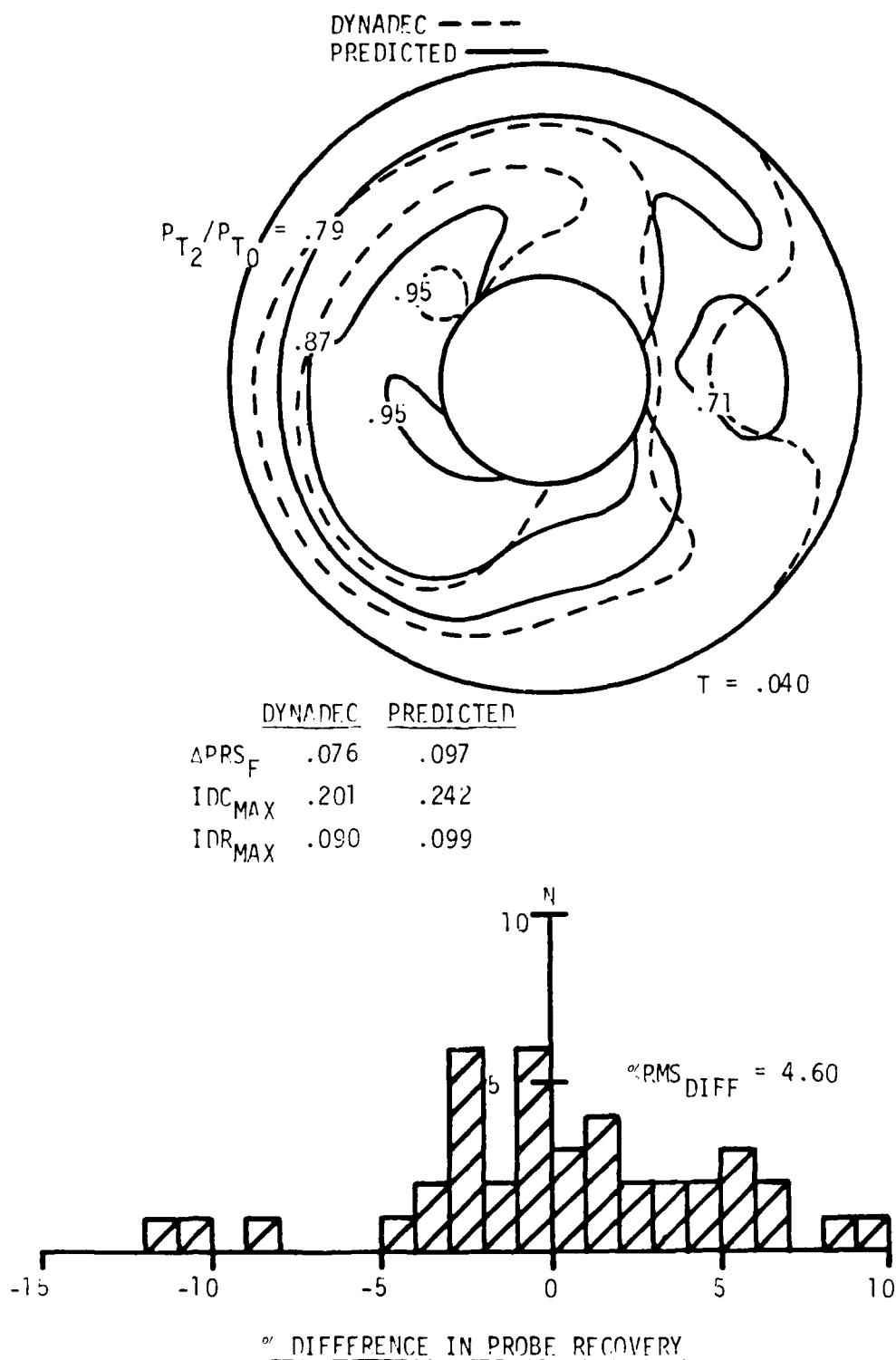


Figure 8 Basic Method (GE_1) - Pressure Contour Map and Histogram, High Turbulence

cases, the predicted maximum distortion (ΔPRS_F) levels are greater than the measured values including the low-turbulence case ($T = .014$), where there is good agreement between the predicted and measured pressure contours. As turbulence increases, there is more disparity between the predicted and measured distortion maps. The histograms indicate a decreasing concentration of probes centered about the zero difference in predicted versus measured pressure recovery with a wider variation in that difference. For example, only fifteen probes have predicted pressures within ± 2 percent of their measured values for the high-turbulence case ($T = .040$) compared to twenty-two probes within that band for the moderate-turbulence case ($T = .027$). Further, there is a 22 percent variation in the pressure recovery difference for the high-turbulence case compared to a range of 17 percent for the moderate-turbulence case.

The capability of the basic model using the PWA distortion parameters is illustrated in Figures 9 through 13. A cut-off filter frequency of 1000 HZ was used to filter the pressure data. The differences between the predicted and measured total distortion, along with its components are shown in Figure 9. The predicted values of K_{A_2} fall within a ± 20 percent band, showing a tendency to overpredict the measured peak distortion levels at low distortion levels and underpredict at higher distortion levels. K_θ shows a similar trend since it constitutes a substantial portion of the total distortion level. The radial distortion component, K_{RA_2} exhibits a substantial variation with differences as large as 50 percent.

Figure 10 presents the $\%RMS_{DIFF}$ as a function of average turbulence. As before, the data points represent the cases presented in the previous figure while the linear regression line is based on the repetition of several cases repeated several times using different sets of random numbers. The increased slope of the regression line, compared to the slope of the regression line in Figure 5, reflects a greater difference between predicted and measured pressures and is attributed to filtering the pressure data at a higher cut-off frequency.

Comparisons between the predicted and DYNADEC generated pressure contour maps are shown in Figures 11, 12, and 13. For the low-turbulence case, Figure 11, there is reasonable agreement between the two maps with most of the disparity in the contour shapes between the eight and eleven

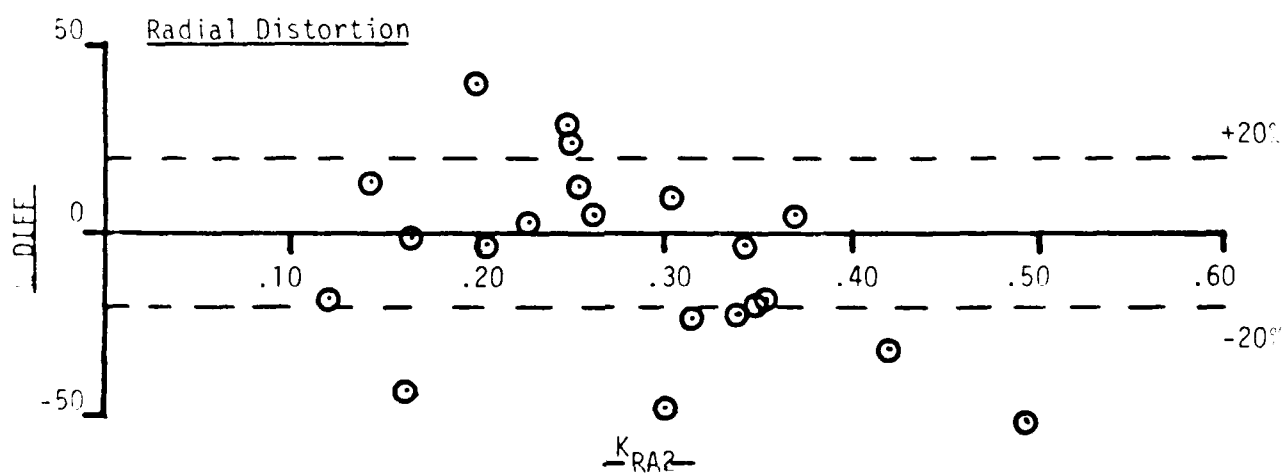
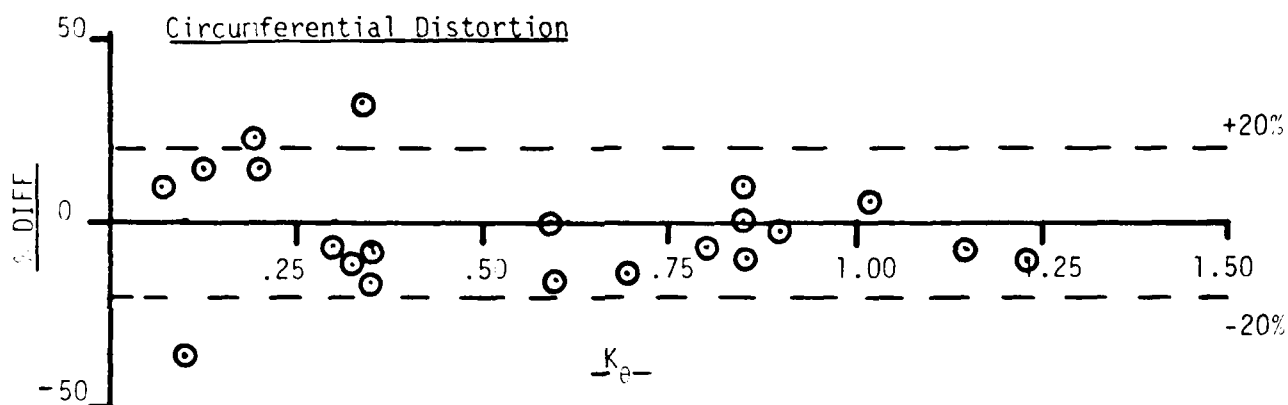
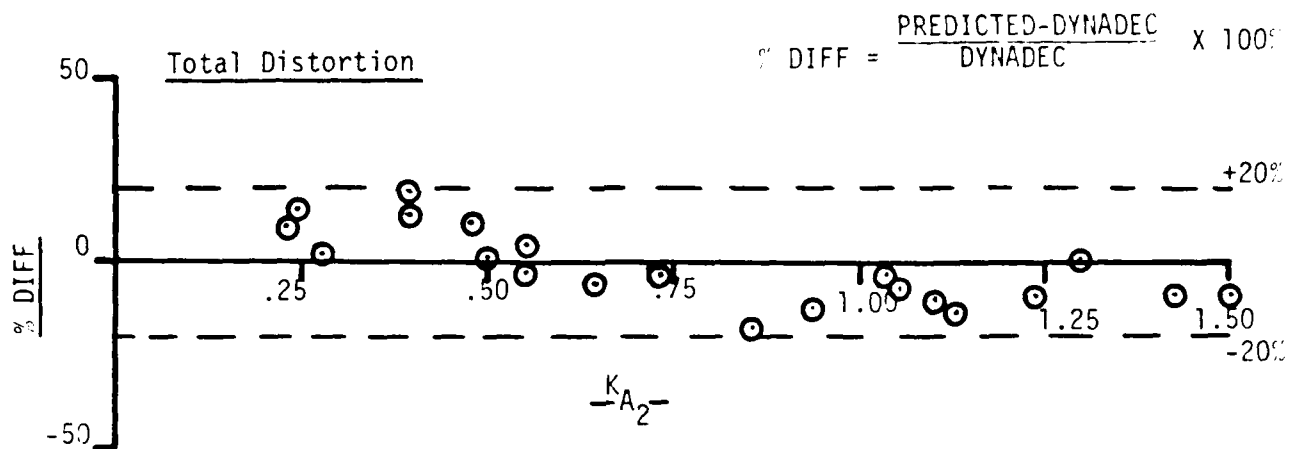


Figure 9 Basic Method (PIA) - Comparison of Predicted to Measured Distortion

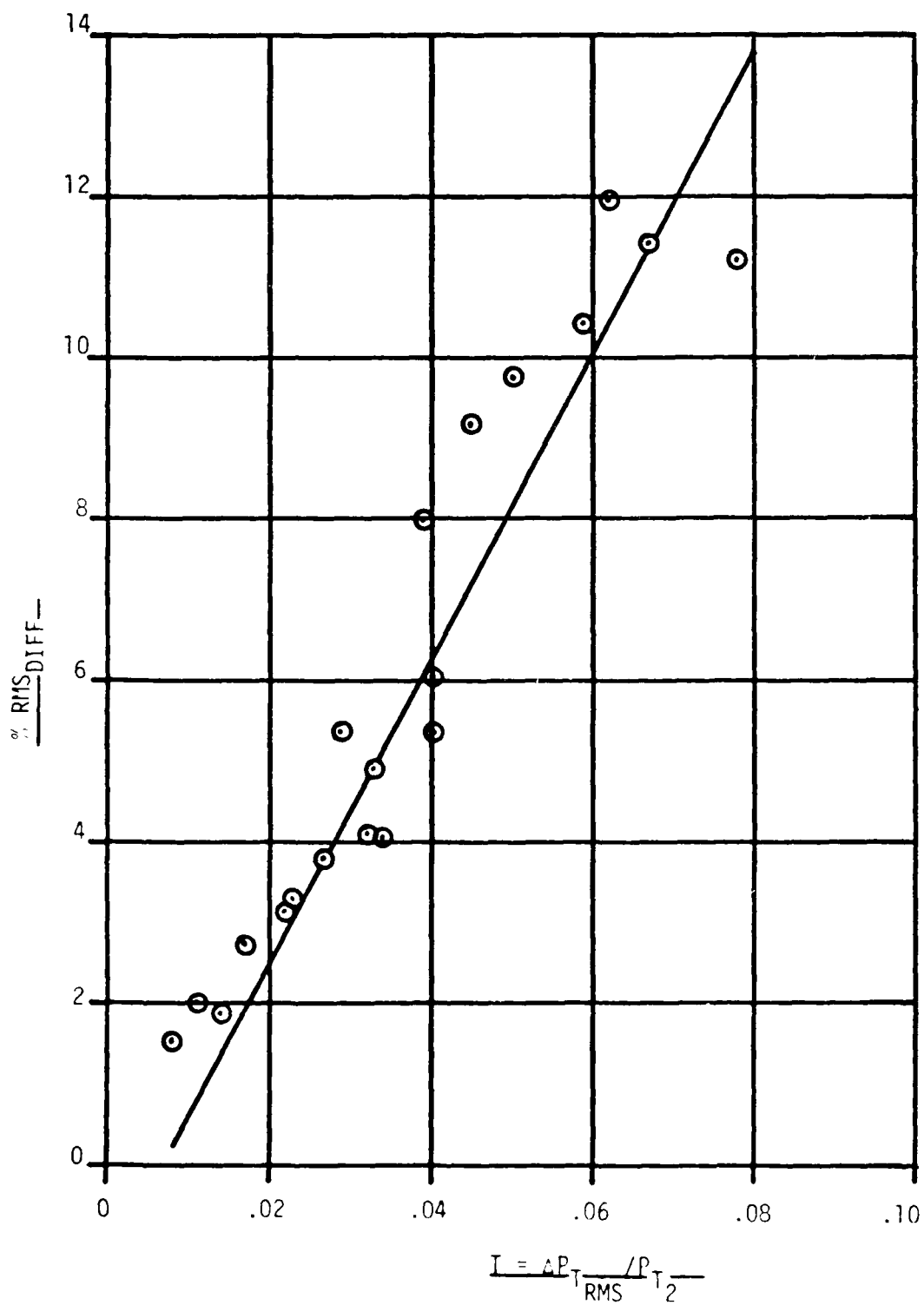
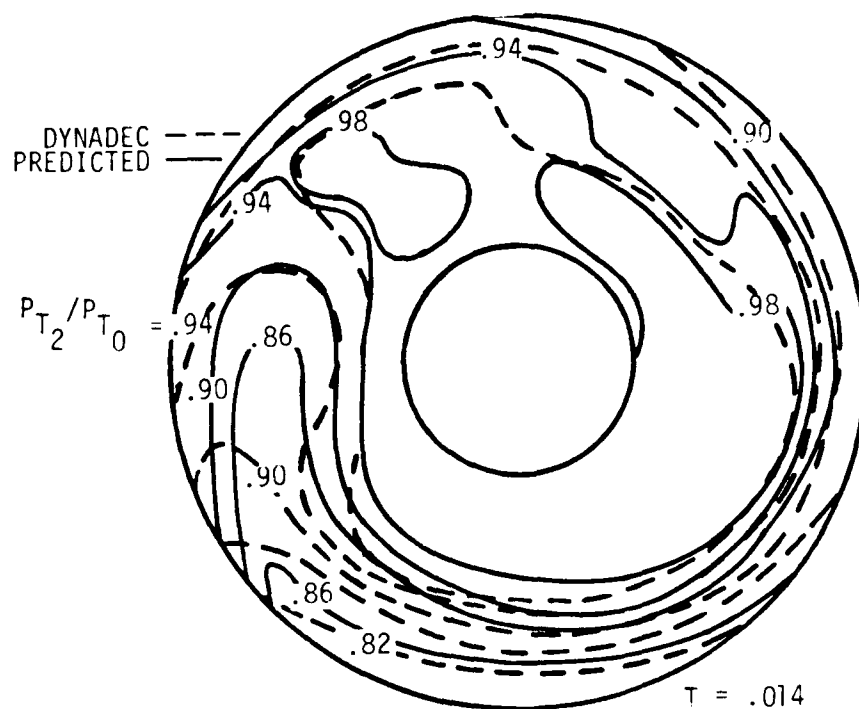


Figure 10 Basic Method (PWA) - Percent RMS Difference



	PREDICTED	DYNADec
K_{A2}	.243	.279
K_{θ}	.124	.144
K_{RA2}	.143	.163

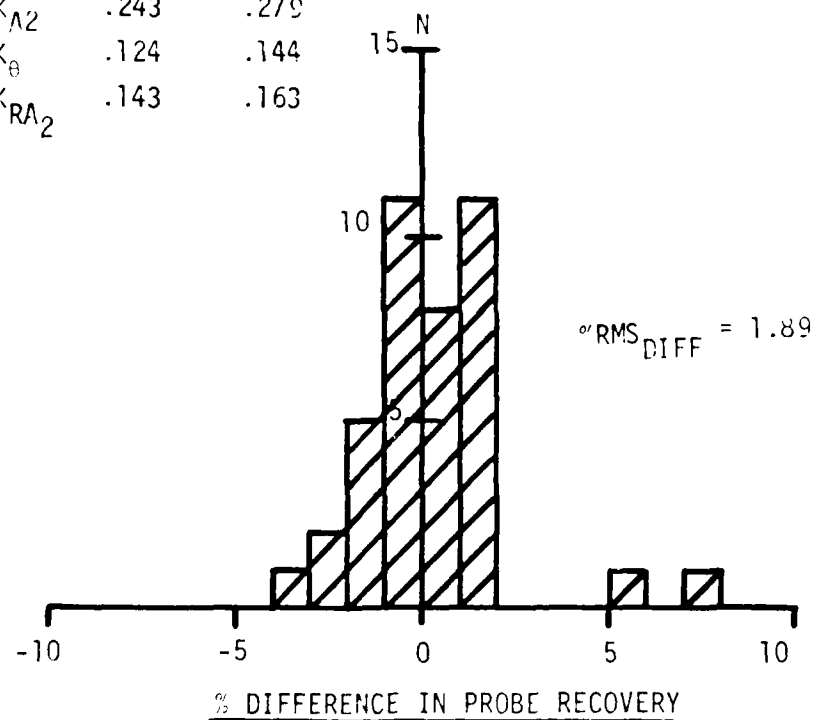


Figure 11 Basic Method (PWA) - Pressure Contour Map and Histogram, Low Turbulence

o'clock positions. Thirty-five of the predicted pressure recoveries are within ± 2 percent of their measured values. The predicted contour maps for the moderate- and high-turbulence cases, Figures 12 and 13, bear little resemblance to the measured contour maps, despite the fact that the predicted distortion levels are in good agreement with the measured peak values. The histograms show the same trend as before, as turbulence increases, there is a flattening and spreading of the distribution of the difference between predicted and measured pressures. For the moderate-turbulence ($T = .027$) case, twenty probes agree within ± 2 percent of their measured values with a range of 19 percent in the difference between predicted and measured recoveries. The number of probes agreeing to within ± 2 percent decreased to twelve while the range increased to 30 percent for the high-turbulence case ($T = .040$).

Figures 14 through 18 present a set of comparisons for the second set of GE engine distortion parameters (GE_2). Inlet pressure data was filtered at a cut-off filter frequency of 500 HZ. The differences between predicted and measured values of IDL, IDC_{MAX} , and IDR_{MAX} are shown in Figure 14. Predicted values of IDL vary from essentially no difference to values in excess of 50 percent from measured values. The circumferential distortion exhibits a similar behavior as it is the dominate term of the total distortion. The radial distortion is randomly distributed with a wide variation from -25 to +60 percent of the measured values.

The average standard deviation of the difference in probe recoveries for this data set is shown in Figure 15. As before, the linear regression line is based on repeating several cases several times to account for variations due to the random number process. The resulting slope of the regression line is similar to that of the GE_1 distortion parameter set, Figure 5, where the pressure data was filtered at 500 HZ.

A comparison of predicted and measured pressure contours are shown in Figures 16, 17, and 18. With some exception, the predicted and measured contour lines for the low-turbulence case, Figure 16, show good agreement with each other. Twenty-seven probes agree to within ± 2 percent of their measured pressures. The range of the difference is 11 percent. For the moderate-turbulence case, Figure 17, the predicted and

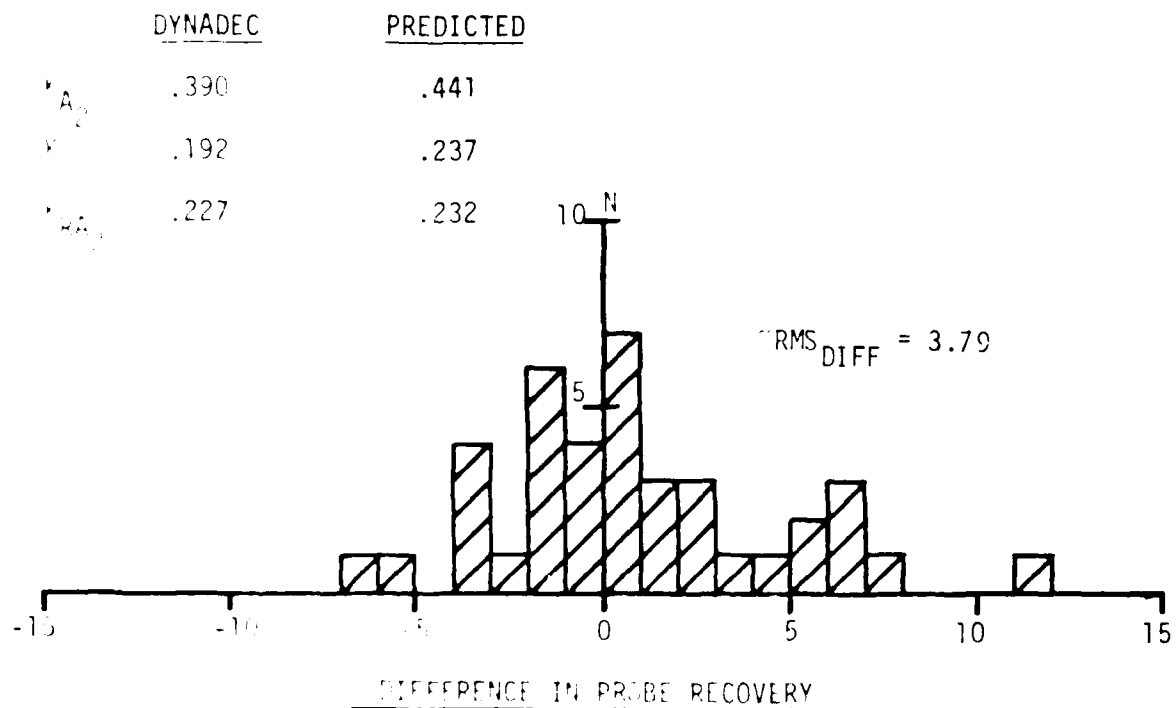
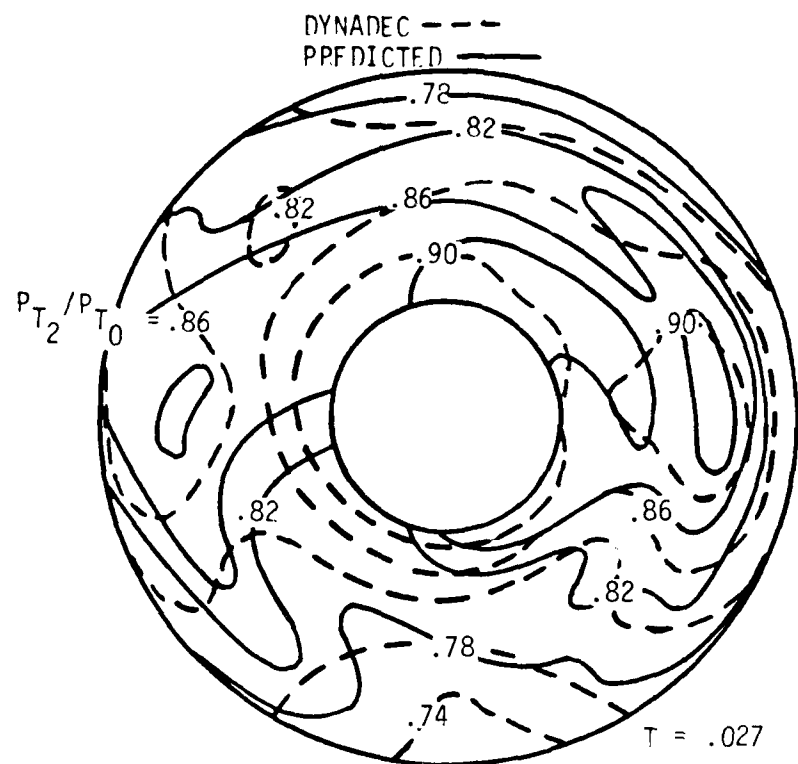
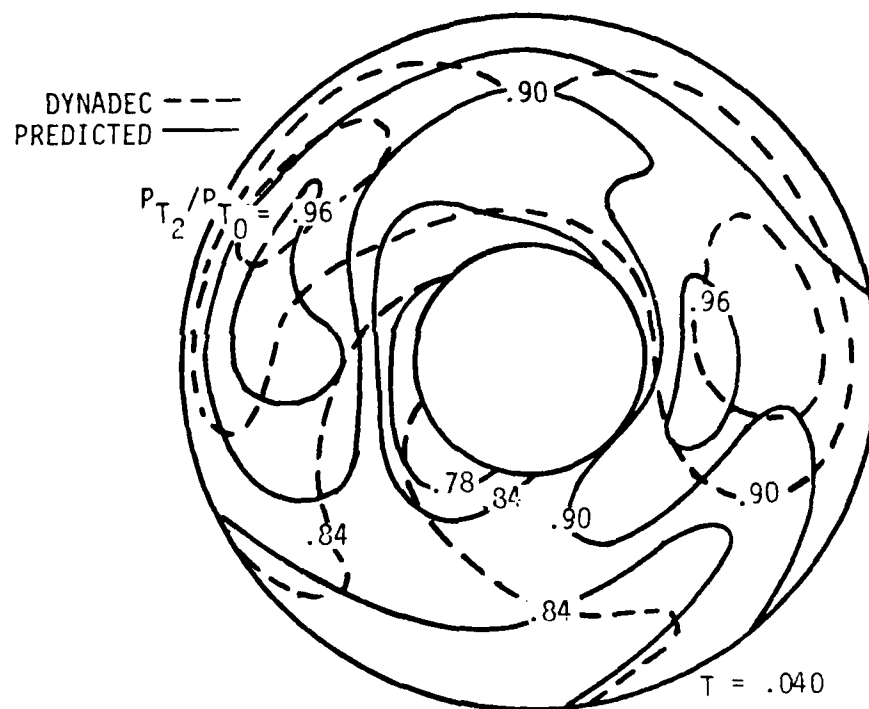


Figure 10 Basic Method (PWA) - Pressure Contour Map and Histogram,
Mach 0.3 Turbulence



	<u>DYNADEC</u>	<u>PREDICTED</u>
K_{A2}	.643	.601
K_{θ}	.353	.297
K_{RA2}	.370	.388

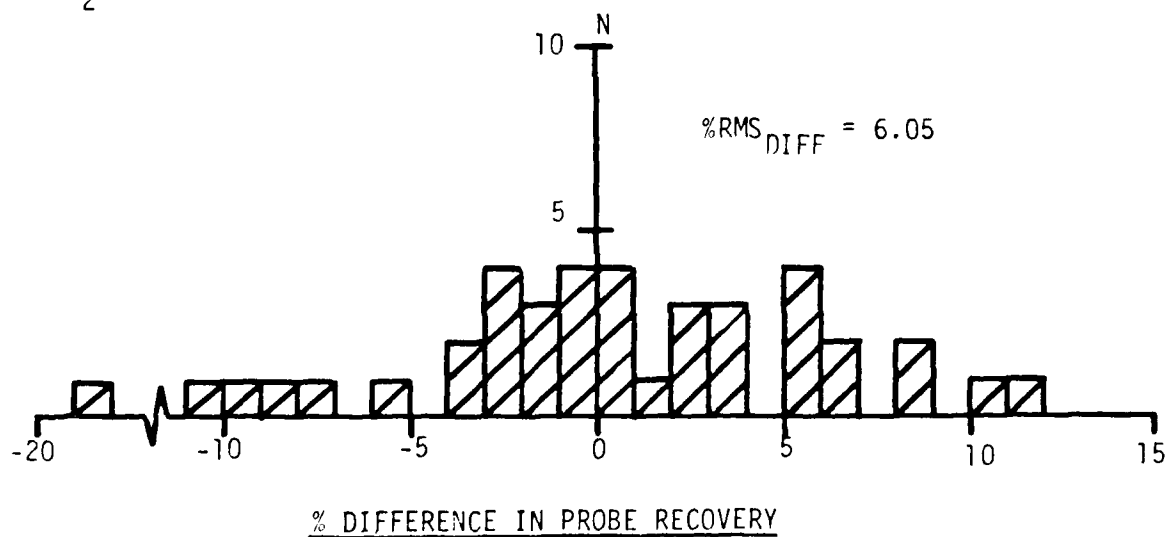


Figure 13 Basic Method (PWA) - Pressure Contour Map and Histogram,
 High Turbulence

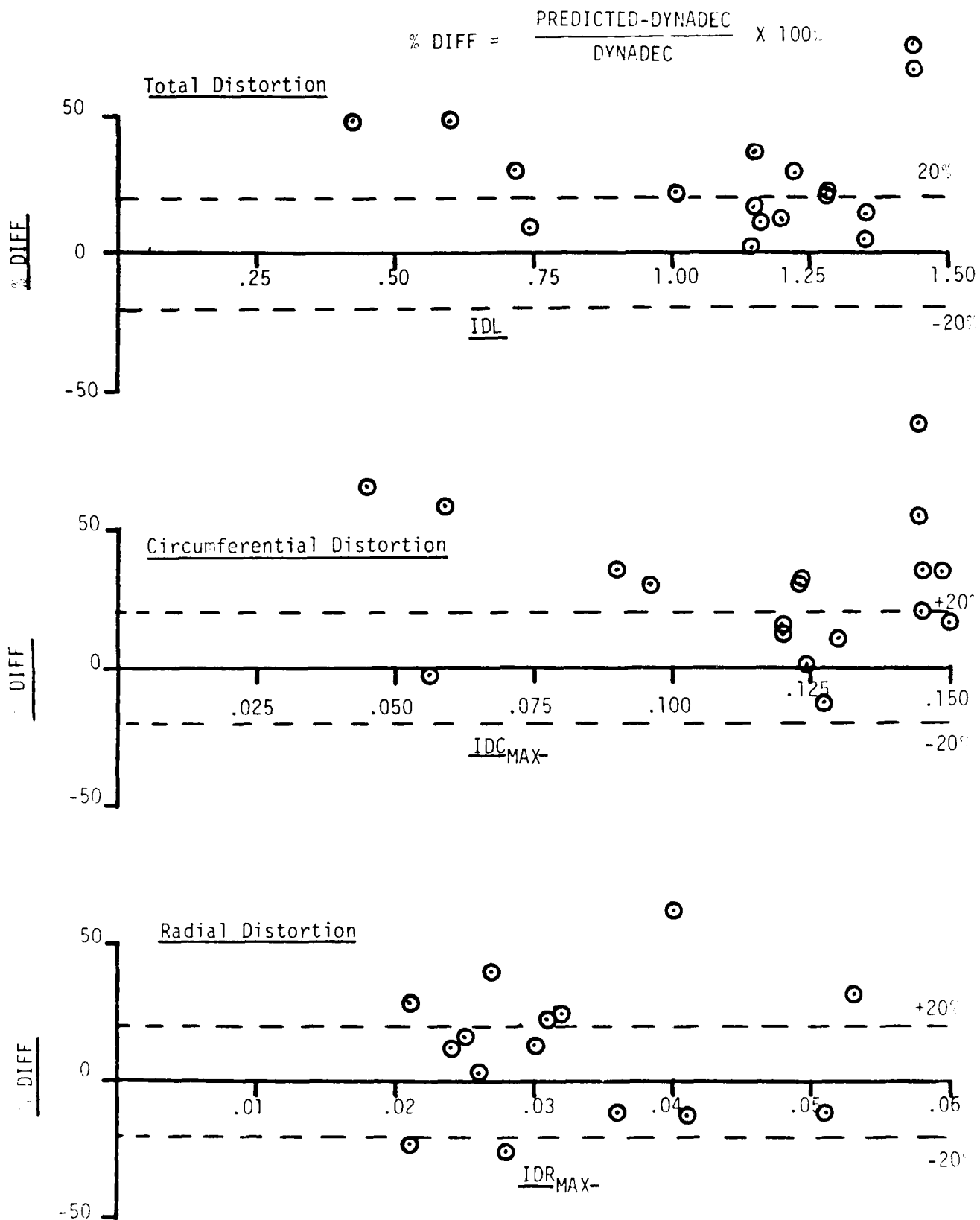


Figure 14 Basic Method (GF_2) - Comparison of Predicted to Measured Distortion

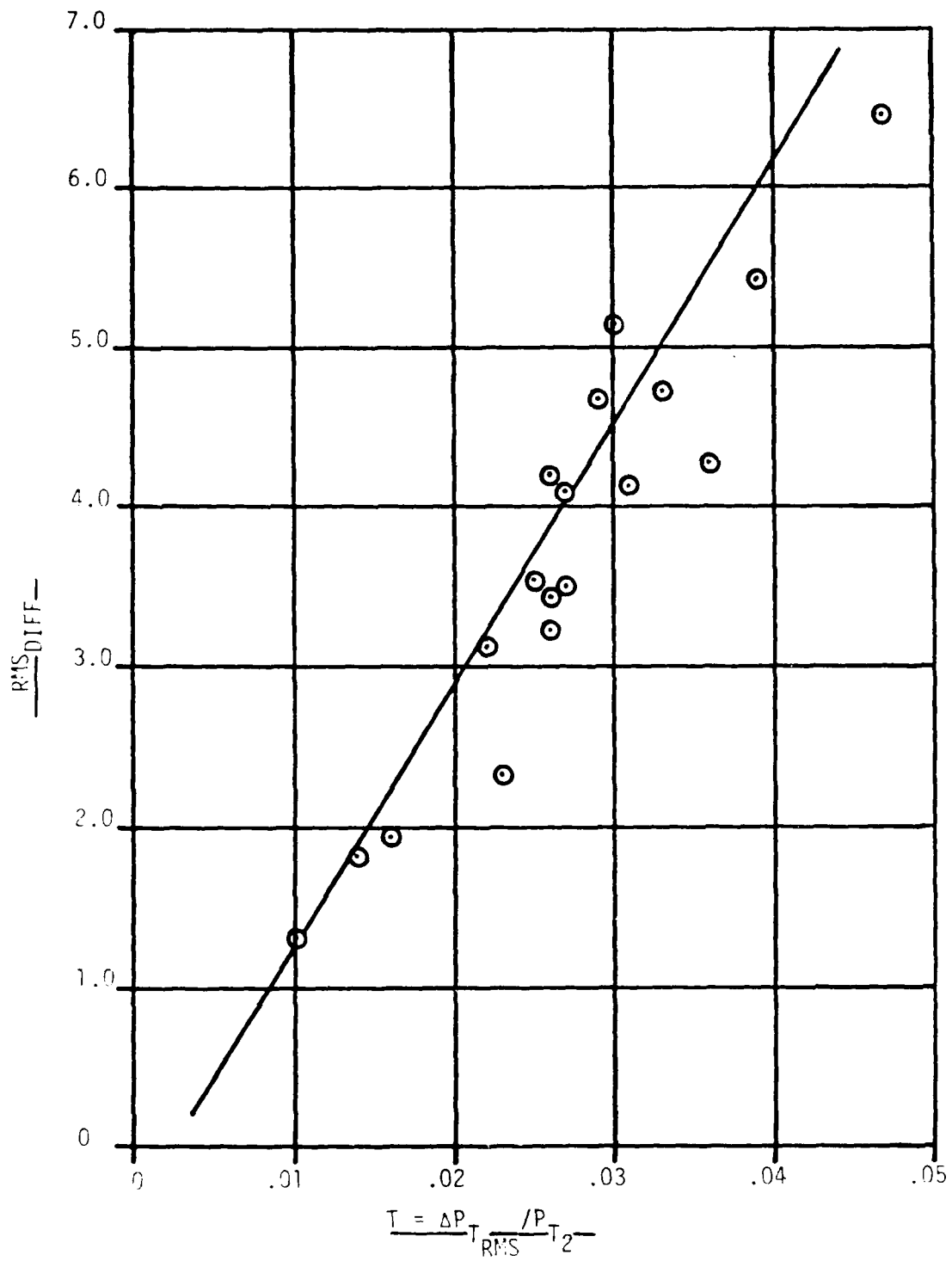


Figure 15 Basic Method (GF_2) - Percent RMS Difference

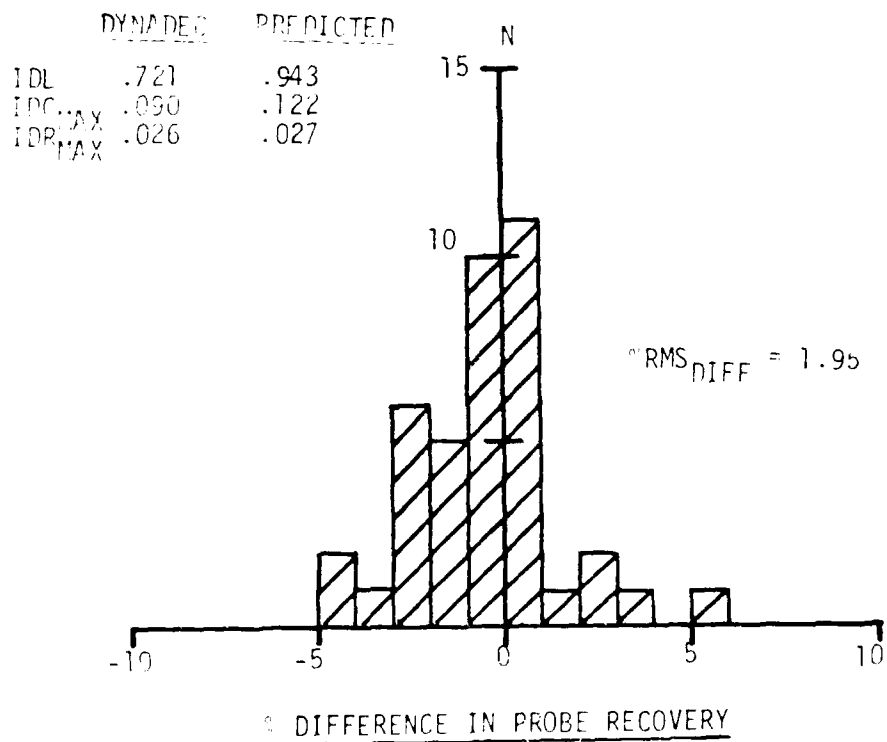
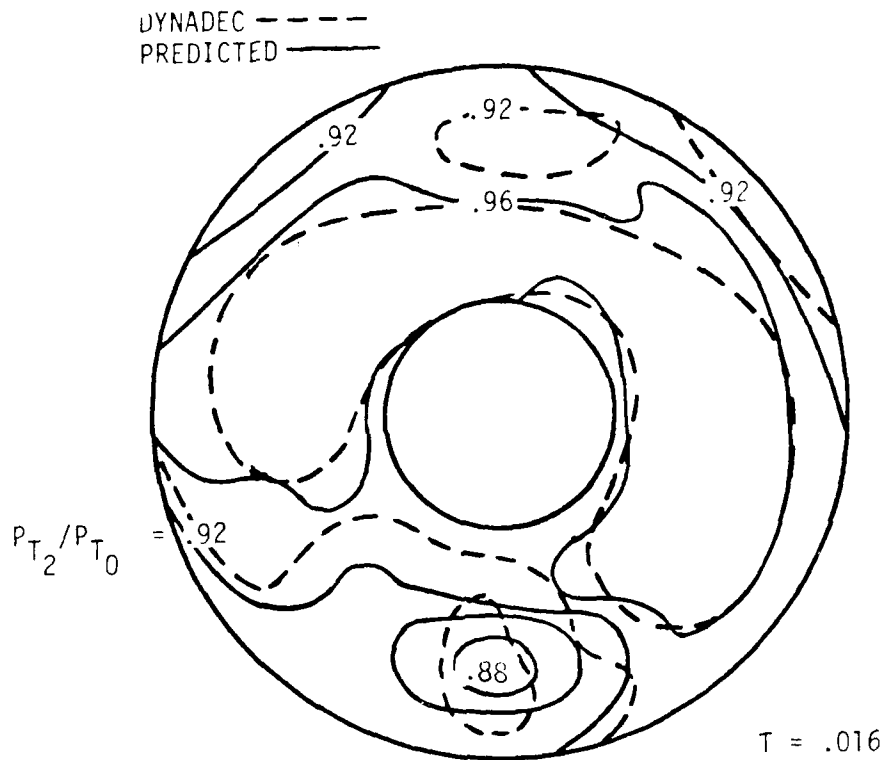


Figure 16 Basic Method (GF_2) - Pressure Contour Map and Histogram, Low Turbulence

of filter is

$$Y_n = h_0 X_n + \sum_{k=1}^M [h_k (X_{n-k} + X_{n+k})] \quad (10)$$

A filter with three coefficients was selected to minimize model points in the power spectrum. Generalized power spectral density shapes for a random number set filtered with the non-recursive filter are illustrated in Figure 26. As the values of h_k increase and h_0 decrease, the spectrum exhibits a progressively steeper roll-off characteristic. The influence of this filter on the predicted maximum distortion level and pressure contour map is also determined by the engine sensitivity cut-off filter frequency. If the cut-off frequency is in the lower portion of the spectrum, where it is essentially flat, the effect of the non-recursive filter is very small. Thus, the non-recursive filter has a secondary effect on the predicted maximum distortion level for small values of h_k and lower cut-off filter frequencies.

The filter used to describe engine sensitivity has the greatest effect on predicted levels of distortion. Engine manufacturers have specified three or four-pole linear-phase (Bessel) and constant-amplitude (Butterworth) filters to describe critical engine frequencies (Reference 20). Butterworth filters exhibit a sharper roll-off characteristic beyond the cut-off frequency while Bessel filters minimize in-phase relationships with frequency. Three-pole Butterworth filters are used to filter the pressure data used in the DYNADEC analysis.

A recursive filter has been developed to represent a three-pole analog Butterworth filter. Whereas the output of a non-recursive filter is a function of the input only, the recursive filter output is a function of previous output as well as input. This recursive filter (Reference 21) uses a bilinear transformation of a continuous filter function, defined as

$$S = \frac{Z-1}{Z+1} \quad (11)$$

where S is a complex variable and Z is a rational function that maps the imaginary axis of the S -plane onto the unit circle of the Z -plane. The desired digital filter is obtained by substituting the bilinear transform into the analog transfer function, $H(S)$, which for a three-pole

correlation is seen to have an overall lower level compared to the previous two figures due to the relatively low-turbulence levels in the low pressure regions.

These examples show the complexity of describing the turbulent flow in terms of a correlation coefficient. Obviously, it is not appropriate to apply the model to those conditions where a discrete frequency exists, such as inlet buzz, duct resonance, or any other in or out-of-phase oscillation. These conditions can not be adequately described with only the steady-state and RMS pressures. A statistically significant level of correlation ($\rho_{ij} > .3$) has been shown to exist for adjacent probes on a rake, in particular, those located near the outer wall. In the absence of any flow oscillations, it appears that the assumption that the pressures are uncorrelated is not a necessary condition for the model to be valid.

Digital Filter Development

The power spectral density of inlet pressure data used in a dynamic distortion analysis has two features. First, the spectrum exhibits a decreasing amplitude with increasing frequency as more energy is usually present at lower frequencies. Second, the spectrum has a sharp roll-off above some frequency due to the use of a filter defining engine sensitivity. Digital filters have therefore been added to the basic prediction model to impose the additional constraint that the power spectral density for the generated random numbers will have a shape approximating that of inlet pressure data.

A normally distributed, uncorrelated set of random numbers is equivalent to white noise which has a flat power spectrum. The PSD function for low-pass white noise is defined as

$$G_x(f) = a, 0 < f < B; \text{ otherwise zero} \quad (9)$$

A non-recursive filter is used to satisfy the general observation that more energy is contained in the lower portion of the spectrum. Non-recursive filters represent a data averaging technique that uses variable weighting coefficients. The formula (Reference 6) for this type

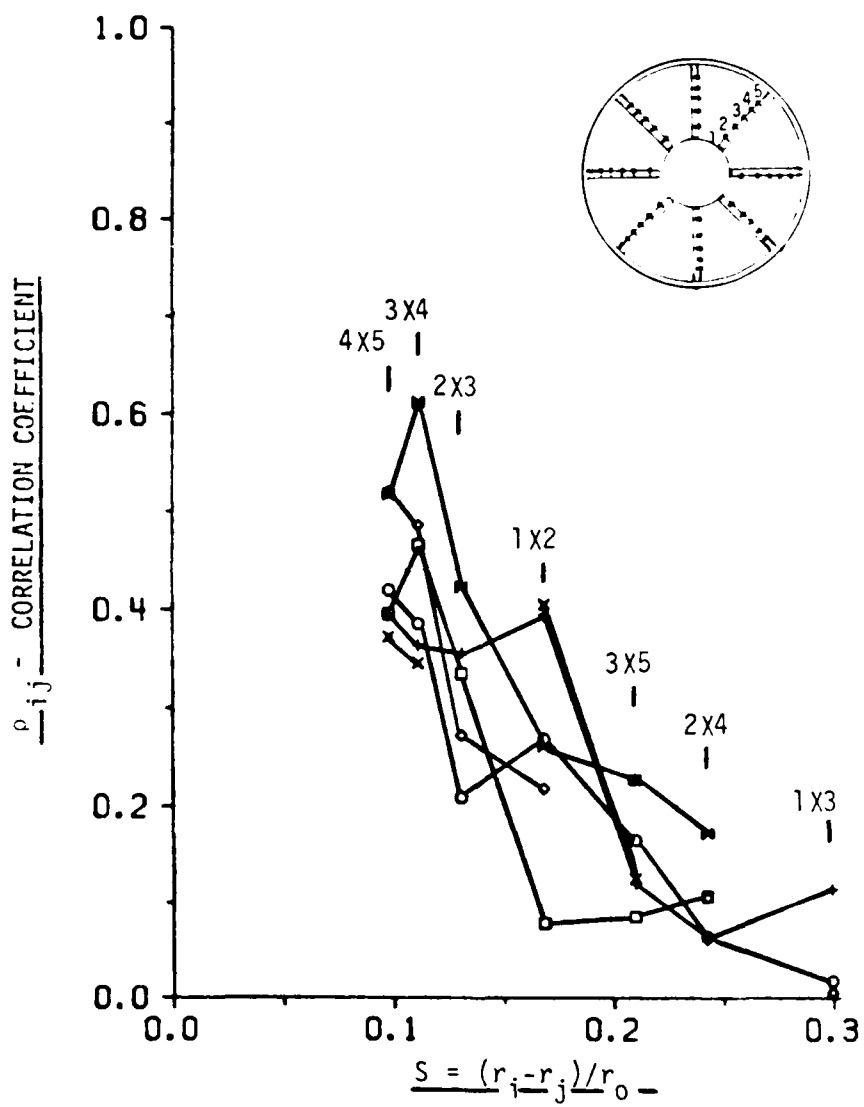


Figure 25 Probe-to-Probe Cross Correlation

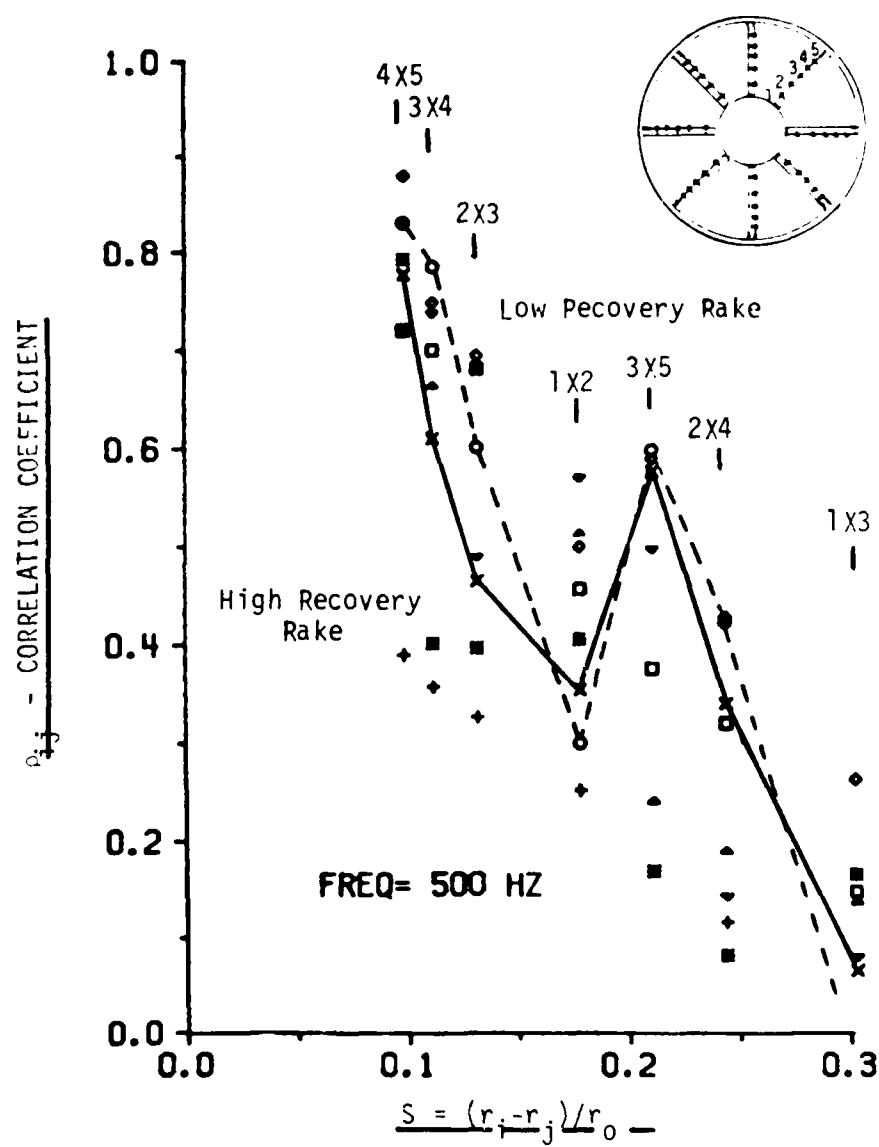


Figure 24 Probe-to-Probe Cross Correlation

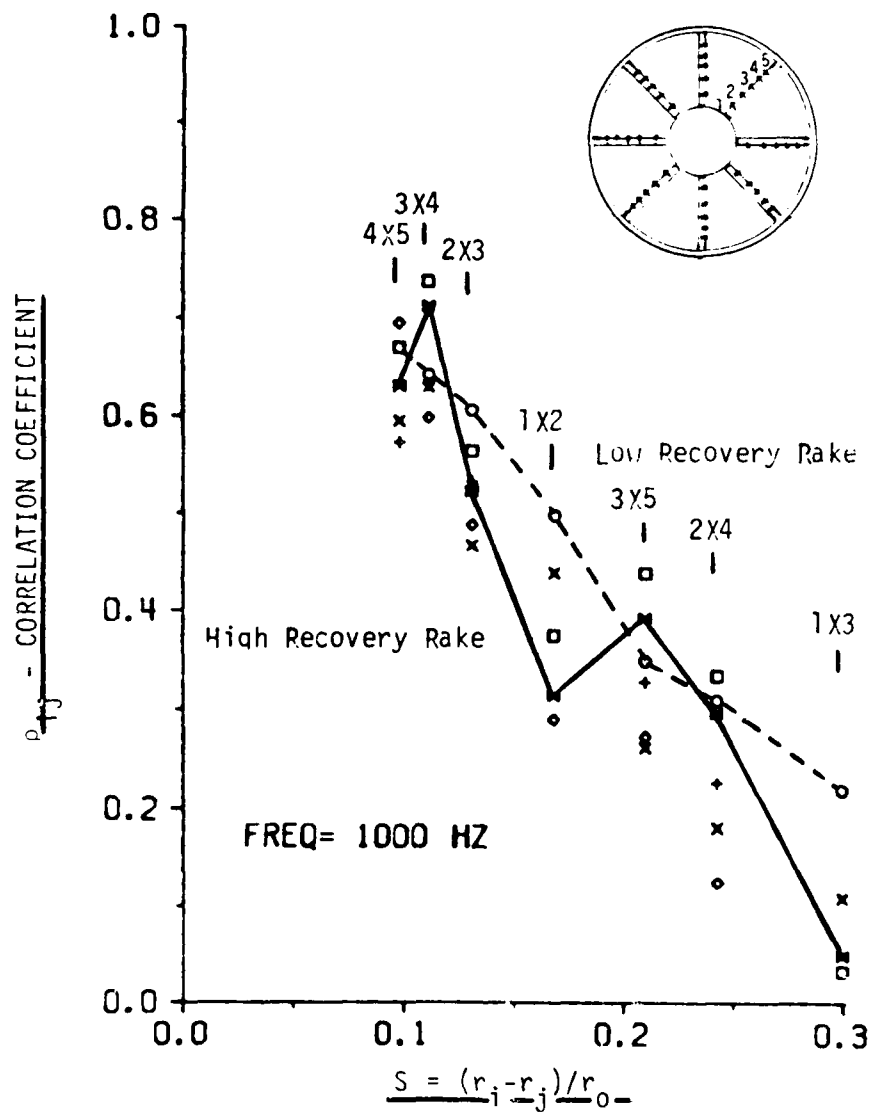


Figure 23 Probe-to-Probe Cross Correlation

cut-off filter frequency. The more closely spaced probes near the outer duct wall exhibit a high correlation level with the level decreasing rapidly as probes become progressively further apart (probes located near the hub or two non-adjacent probes). The correlation is also a function of cut-off filter frequency. As cut-off frequency decreases, the correlation coefficient increases.

Figure 23 presents the correlation coefficient for probes along several rakes for a circumferential distortion pattern. As with the results presented in the previous figure, the level of correlation decreases with increasing distance between probes. There is no systematic trend in the correlation level for probes located progressively between the high and low pressure rakes. In addition, the range of the correlation level for the various rakes appears to be within the scatter of the correlation for the high- and low-pressure regions denoted by Mace and Sedlock (Reference 18).

The correlation for another circumferential distortion pattern is presented in Figure 24. In addition to a wide variation in the coefficient for a given probe-to-probe spacing, the correlation exhibits a "sawtooth" characteristic. This "sawtooth" behavior illustrates that the correlation is a function of other variables as well as distance. In a study by Martin (Reference 5), for example, the cross-correlation and phase angle showed significant differences between adjacent compressor face probes. To explain the behavior of the cross-correlation function, a turbulent zone concept was proposed to describe the boundary layer/shock wave mechanisms present in the flow. Other mechanisms that would affect the correlation function are boundary layer separation and the interaction between shock waves. For the correlation to be only a function of distance, the turbulent flow must be isotropic, or at least locally isotropic, that is, the decay in turbulence has no preference for any specific direction (Reference 19). Such conditions can be approximated behind a grid with no pressure distortion present. Thus, the "sawtooth" behavior of the correlation is more likely representative of inlet diffuser flow.

Figure 25 presents the correlation for probes located on rakes in the low pressure region from three radial distortion patterns. The

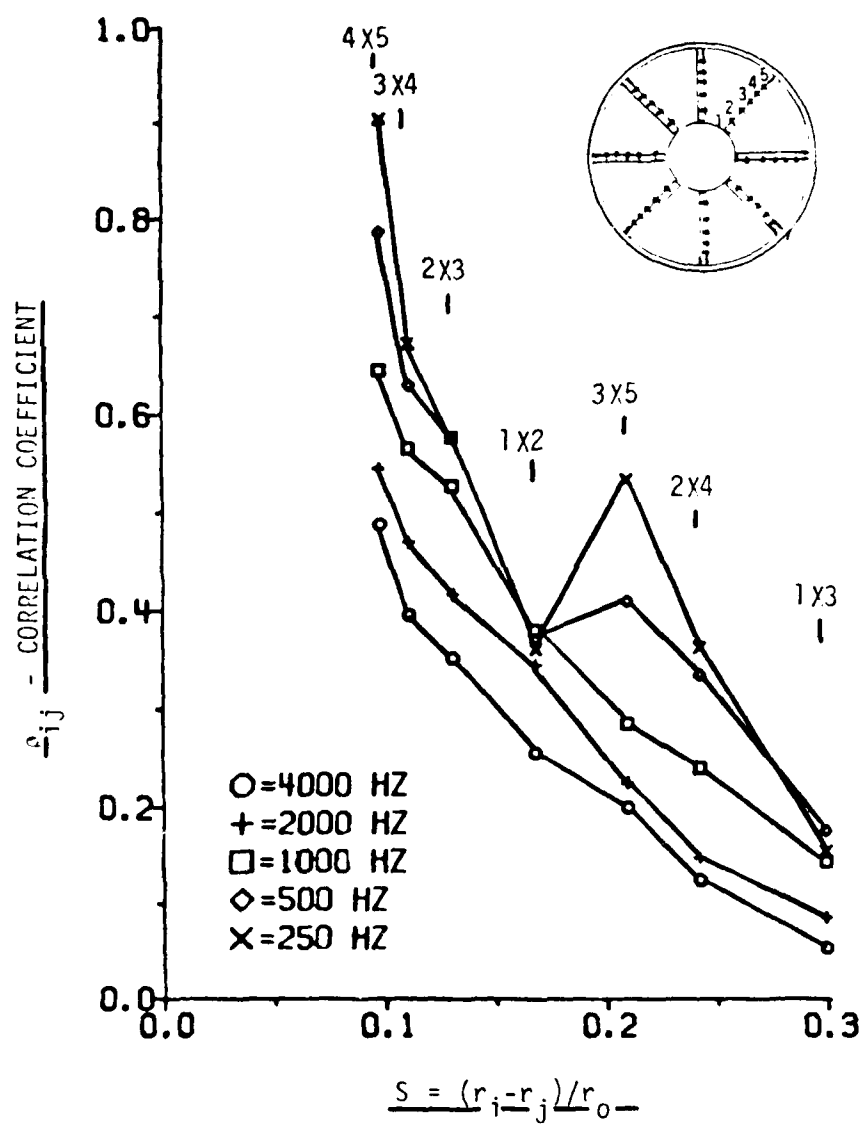


Figure 22 Probe-to-Probe Cross Correlation

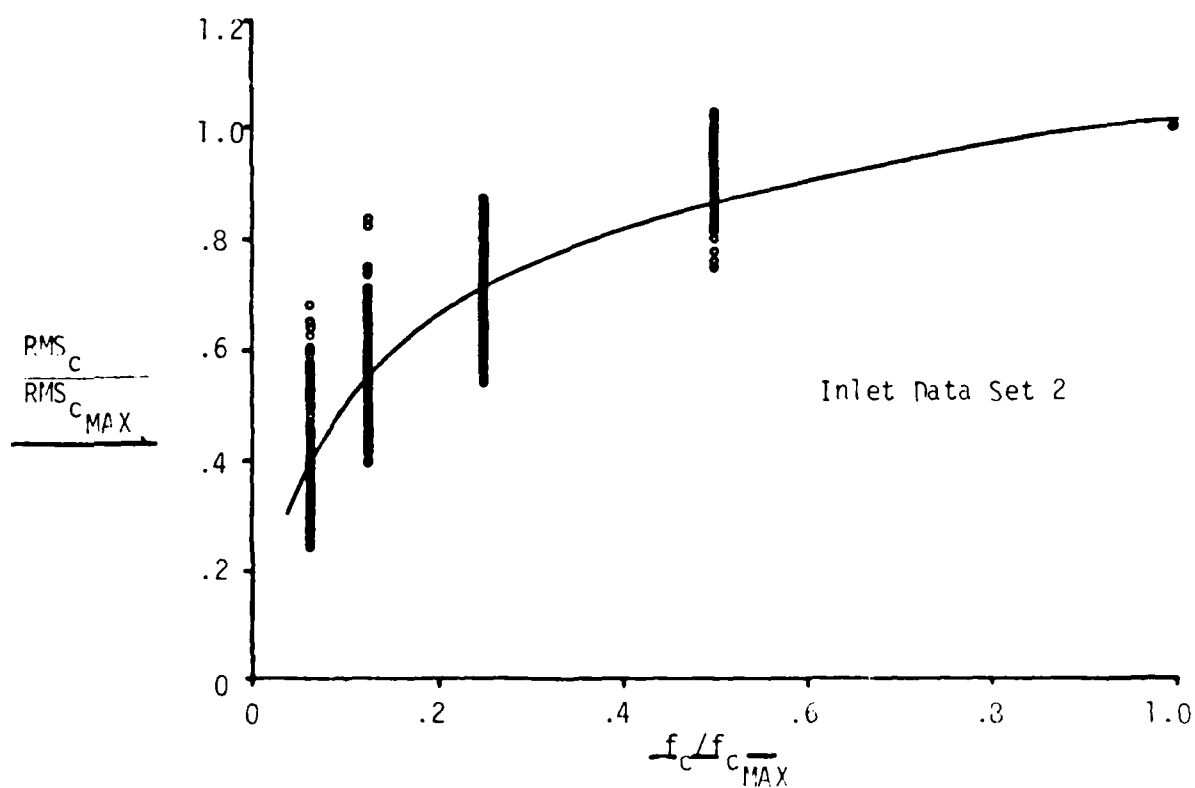
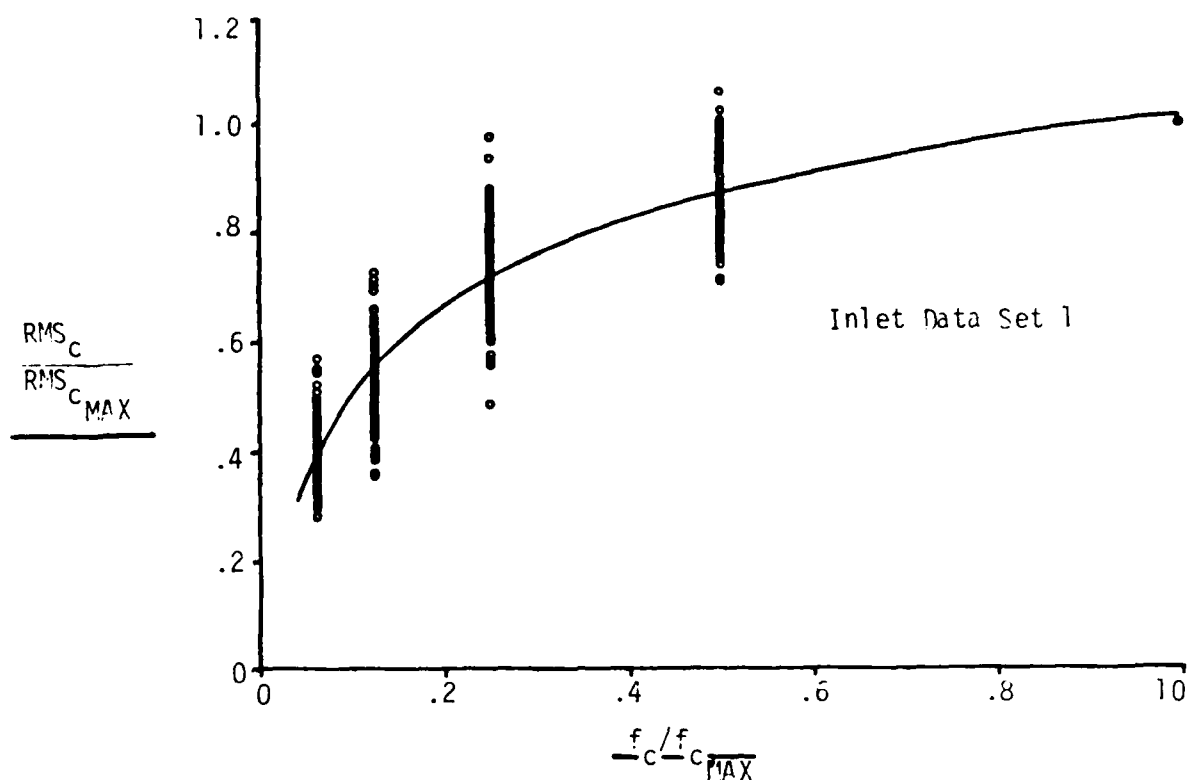


Figure 21 RMS Pressure - Frequency Correlation

correlation between probes located along a rake. The cross-correlation function is obtained by averaging the product of two random pressure-time histories over a statistically significant time period. The cross-correlation function for two laterally spaced probes is

$$R_{xy} = \frac{1}{T} \int_0^T x(t)y(t)dt \quad (5)$$

The correlation coefficient is defined as

$$\rho_{ij}(t) = \frac{R_{xy}}{\Delta P_{T(RMS)}(x) \Delta P_{T(RMS)}(y)} \quad (6)$$

where $\Delta P_{T(RMS)}$ is the standard deviation of a time-variant pressure. Filtered time-variant pressure data were input to these equations which were programmed on an analog computer. The data was filtered at cut-off frequencies of $125 \text{ Hz} \times 2^N$, where $N = 0, 1, \dots, 5$, to determine the effect of frequency on the RMS pressure and the correlation coefficient.

Figure 21 presents the variation in RMS pressure as a function of frequency for two inlet data sets. The RMS pressures for each probe for all the cases used in the investigation are included in this figure. The RMS pressures were non-dimensionalized by the maximum RMS pressure at the maximum frequency. A logarithmic transformation (Reference 15) of the form

$$Y = \beta_0 + \beta_1 X' + \epsilon \quad \text{where } X' = \log_{10} X \quad (7)$$

was used to fit a regression curve to the data. The regression equations for both data sets are virtually identical and therefore described by a single expression

$$\frac{RMS_C}{RMS_{MAX}} = 1.020 + .520 \log_{10} \left(\frac{f_C}{f_{C_{MAX}}} \right) \quad (8)$$

Some of the correlation results obtained are presented in the figures that follow. Figure 22 presents the correlation coefficient, ρ_{ij} , as a function of the distance between probes along a rake and

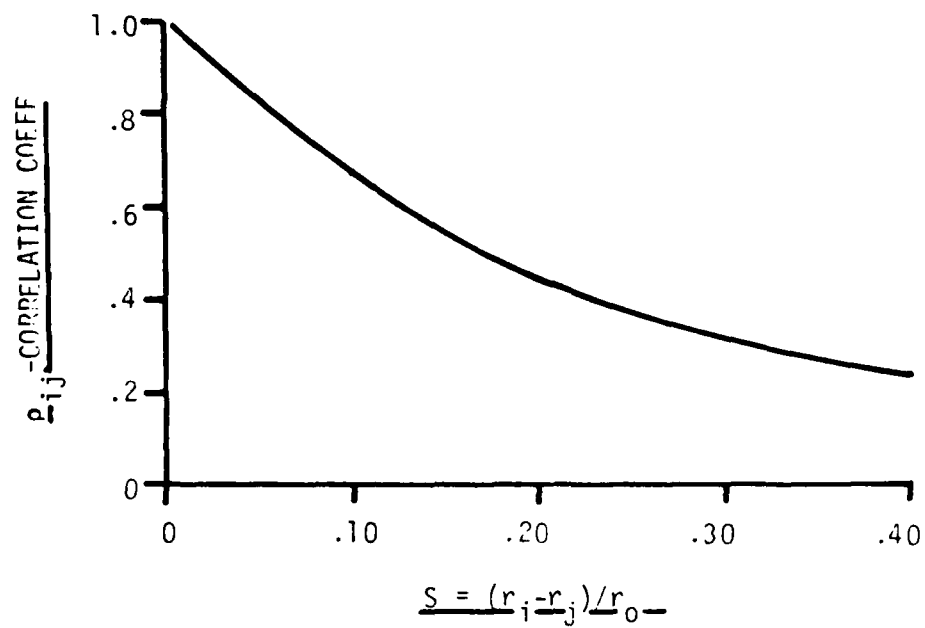


Figure 19 Probe-to-Probe Cross Correlation

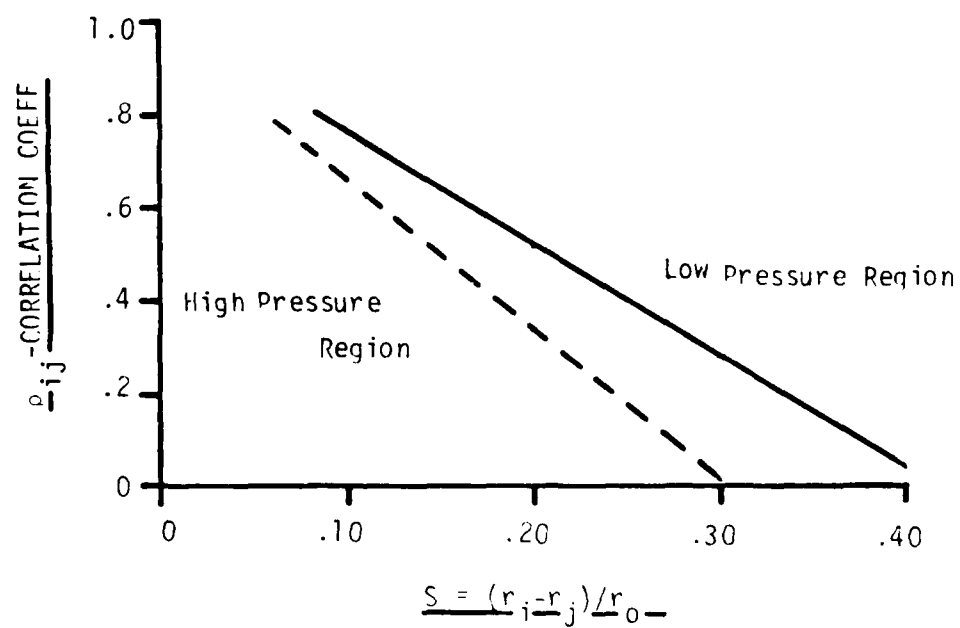


Figure 20 Probe-to-Probe Cross Correlation

the probes are more than 10 percent of the duct radius apart. The correlation on which Motycka based his conclusion is shown in Figure 19 and is based on pressure measurements taken behind a turbulence generator with grill, pipe, and egg crate devices positioned between the generator and the engine compressor face (Reference 16). The correlation was developed to indicate the scale of the turbulence eddies generated by the different devices. For a typical spacing between probes (20 percent of the duct radius), the correlation coefficient has an approximate value of five-tenths. Motycka pointed out that a high correlation would exist across the engine face under the conditions of inlet buzz and duct resonance. In those instances, the engine reaction to the discrete frequency would be evaluated separately.

Borg (Reference 2) also cautioned against applying the prediction model to low mass flow conditions where inlet buzz may exist, but presented no data in support of the assumption that the pressures are uncorrelated.

Crites and Heckart (Reference 17), reviewing model scale and transducer spacing requirements, discussed the need to have the distance between probes sufficiently small to allow an accurate interpolation of time-variant pressure data. The correlation fields of two probes would therefore have to overlap at a statistically significant value, implied to be three-tenths.

Mace and Sedlock (Reference 18) explored the use of a spatial correlation coefficient for estimating the time-variant pressure at some point between two laterally spaced pressure probes. The spatial correlation, shown in Figure 20, was used in a set of regression equations to estimate the pressure fluctuations. Analysis showed that the waveform of the estimated pressure fluctuations were representative of the frequency and amplitude characteristics of the measured pressure waveform at that location. It was concluded that adjacent high-response probes on a rake exhibited a statistically significant correlation. A comparison of the correlation developed by Mace and Sedlock with that presented by Motycka show the correlations to be of comparable magnitude.

As part of this investigation, a correlation study was accomplished with a portion of the inlet pressure data to determine the level of

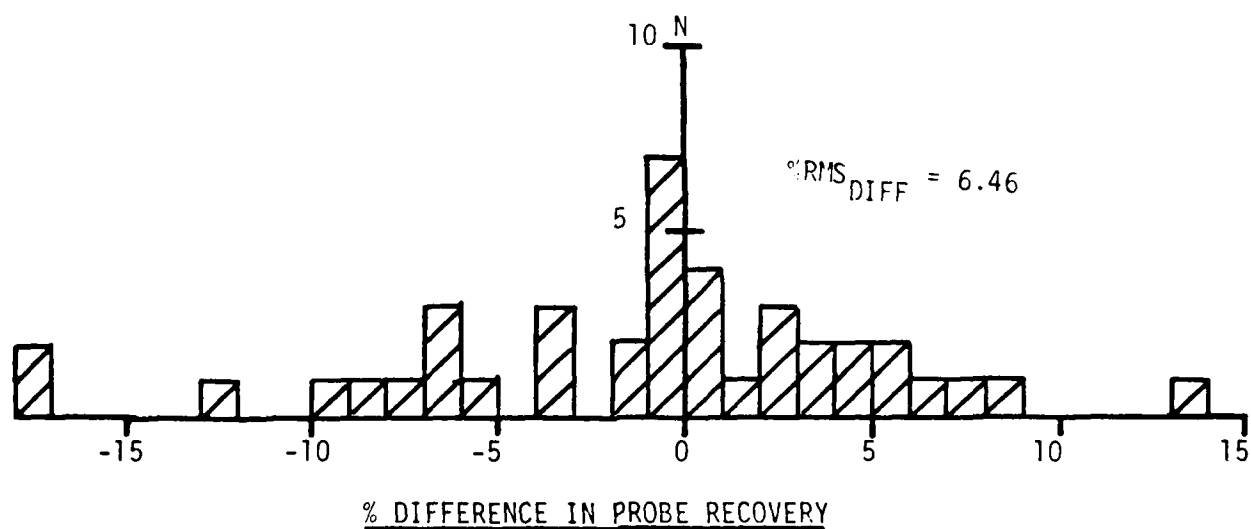
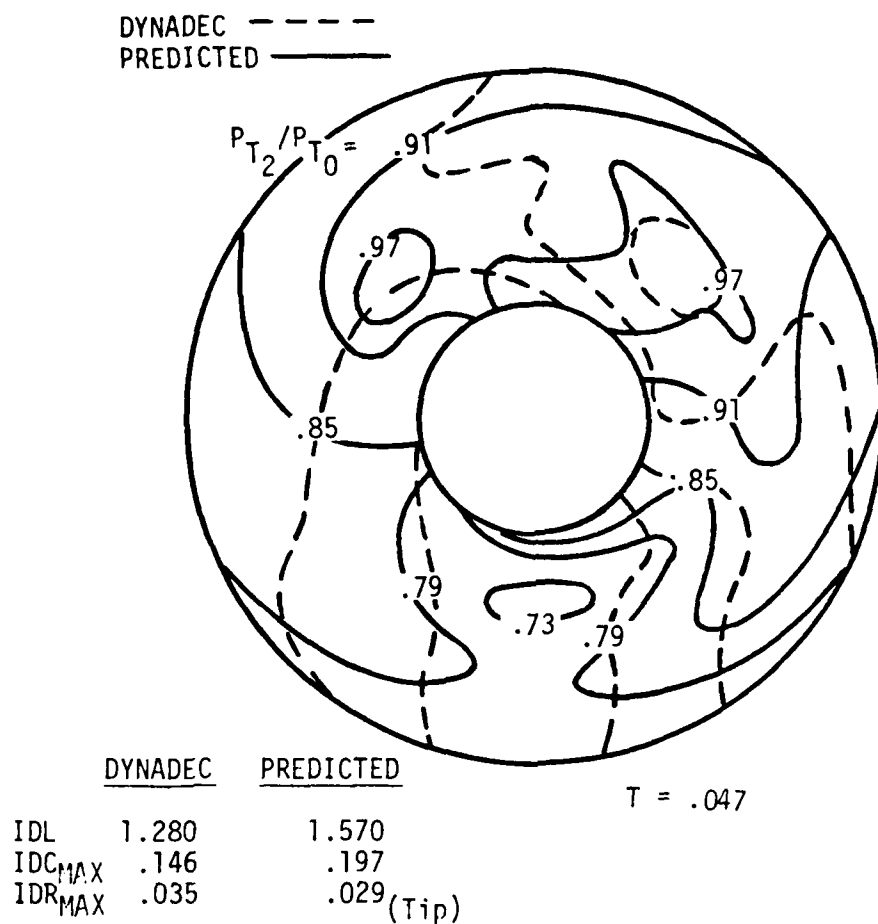


Figure 18 Basic Method (GE₂) - Pressure Contour Map and Histogram,
 High Turbulence

measured maps exhibit good similarity, but the number of probes within ± 2 percent of their measured values has decreased to eighteen and the range of the difference has increased to 18 percent. For the high-turbulence case ($T = .047$) shown in Figure 18, there is no similarity between the predicted and measured contour maps. Only fourteen probes are within ± 2 percent of their measured values while the range has increased to 32 percent.

In summary, it appears that a statistical prediction model's ability to accurately predict the maximum distortion level may have little to do with providing an accurate distortion map. A distortion parameter can provide some averaging that minimizes the effect of the differences between predicted and measured probe recoveries. For example, the PWA circumferential distortion parameter, K_θ , uses a Fourier curve fit of the pressure distribution about a ring, and consequently may be less affected by errors in pressure values. On the other hand, the GE circumferential distortion parameter, IDC, uses the low recovery probe value in defining the distortion level. If that minimum value is in error, it has a significant effect on the prediction of total distortion.

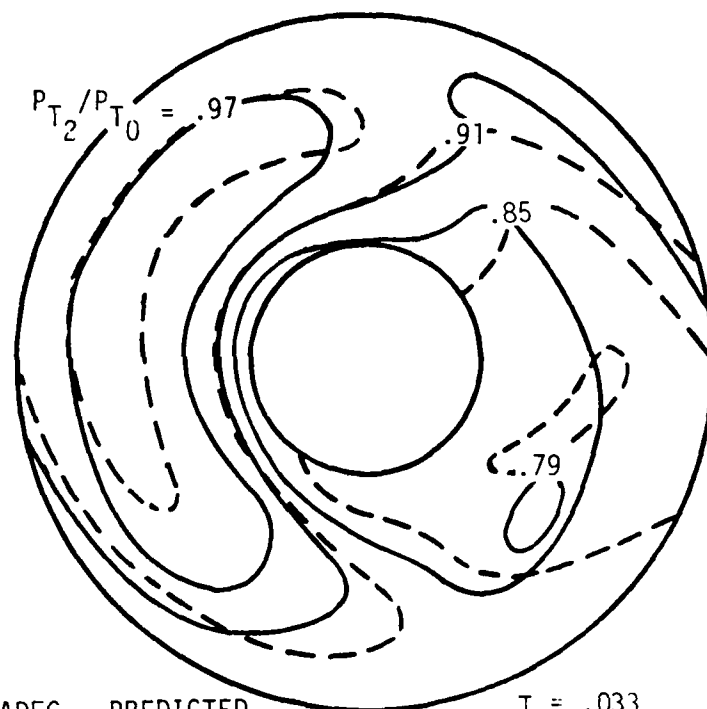
Histograms for the forty-nine cases investigated have shown that as turbulence increases, there is a flattening and spreading of the distribution with large differences between predicted and measured probe pressures.

Correlation Analysis

An assumption of the basic statistical prediction model is that the individual compressor face pressures are uncorrelated. If this assumption is true, then the pressure fluctuations at one location have no bearing upon the pressure fluctuations at another location and cannot be used to predict anything about the pressures at that point. However, previous investigations (References 5, 17, and 18) have shown that a statistically significant level of correlation can exist between two laterally spaced, adjacent probes. The assumption that the pressures are uncorrelated was therefore examined to determine its relative importance to the model.

Motycka (Reference 3) presented data to show that the correlation between adjacent probes is generally low (less than 60 percent) because

DYNADEC ---
 PREDICTED —



	<u>DYNADEC</u>	<u>PREDICTED</u>
IDL	1.222	1.579
IDC MAX	.130	.144
IDR MAX	.040	.065

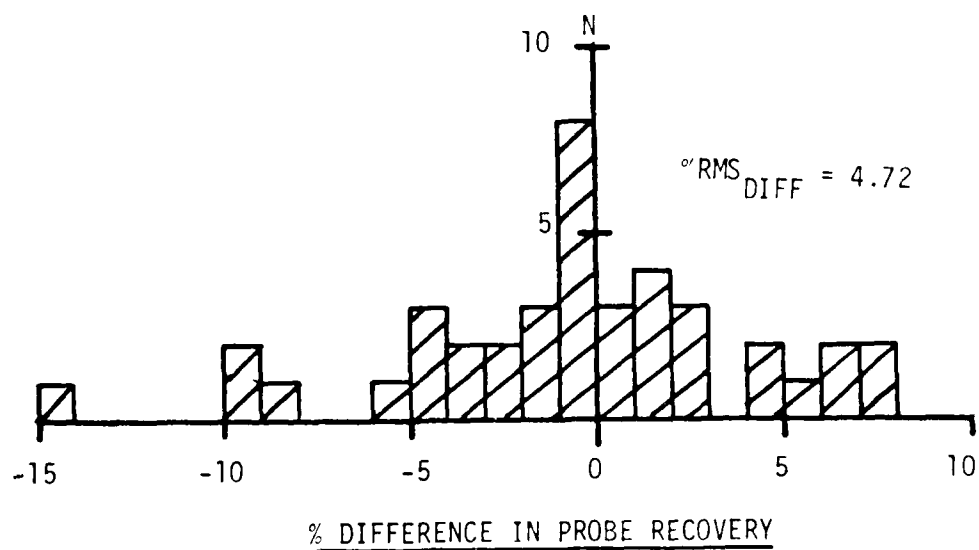


Figure 17 Basic Method (GE_2) - Pressure Contour Map and Histogram,
 Moderate Turbulence

Butterworth filter is

$$H(S) = \frac{\omega_A^3}{S^3 + 2S^2\omega_A + 2S\omega_A^2 + \omega_A^3} \quad (12)$$

where ω_A is an analog frequency variable defined as

$$\omega_A = \tan \frac{\pi f_c}{\text{sampling rate}} \quad (13)$$

Expanding the equation, and combining certain terms defined as:

$$\begin{aligned} A_0 &= \omega_A^3 + 2\omega_A^2 + 2\omega_A + 1 \\ A_1 &= -3\omega_A^3 - 2\omega_A^2 + 2\omega_A + 3 \\ A_2 &= -3\omega_A^3 + 2\omega_A^2 + 2\omega_A - 3 \\ A_3 &= -\omega_A^3 + 2\omega_A^2 - 2\omega_A + 1 \end{aligned} \quad (14)$$

the following coefficients can then be defined:

$$\begin{aligned} B_0 &= B_3 = \omega_A^3/A_0 \\ B_1 &= B_2 = 3\omega_A^3/A_0 \\ C_1 &= A_1/A_0; C_2 = A_2/A_0; C_3 = A_3/A_0 \end{aligned} \quad (15)$$

Then, the filter output becomes,

$$Y_0 = B_0X_i + B_1Z^{-1}X_i + B_2Z^{-2}X_i + B_3Z^{-3}X_i + C_1Z^{-1}Y_0 + C_2Z^{-2}Y_0 + C_3Z^{-3}Y_0 \quad (16)$$

where X_i , $Z^{-1}X_i$, $Z^{-2}X_i$, $Z^{-3}X_i$ are the current and past three input values of X_i , respectively, and $Z^{-1}Y_0$, $Z^{-2}Y_0$ and $Z^{-3}Y_0$ are the past three output values.

By defining the Butterworth filter in this manner, the coefficients can be determined by specifying the cut-off frequency and sampling rate. Based on experience, the sampling rate should be at least four times the cut-off filter frequency as lower sampling rates were found to introduce instabilities in the filter algorithm. Figure 27 presents an example of the smoothed power spectral density for a random number set filtered at a cut-off frequency of 500 HZ.

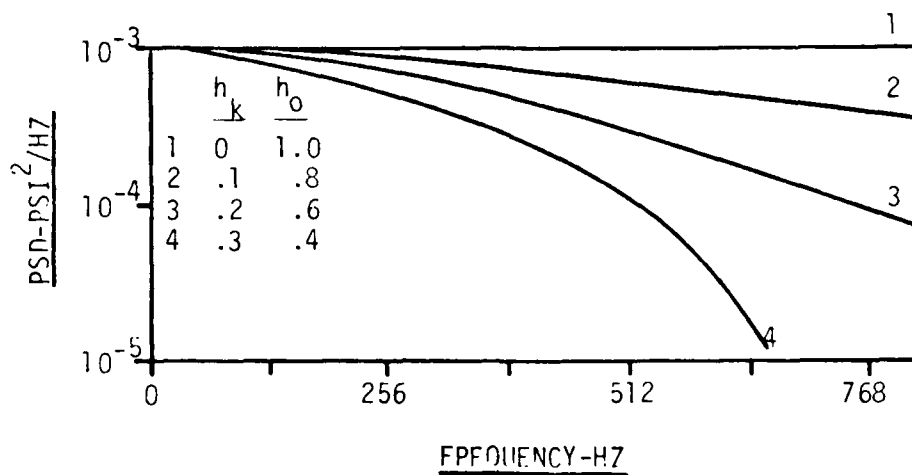


Figure 26 Generalized Random Number PSD with Non-Recursive Filter

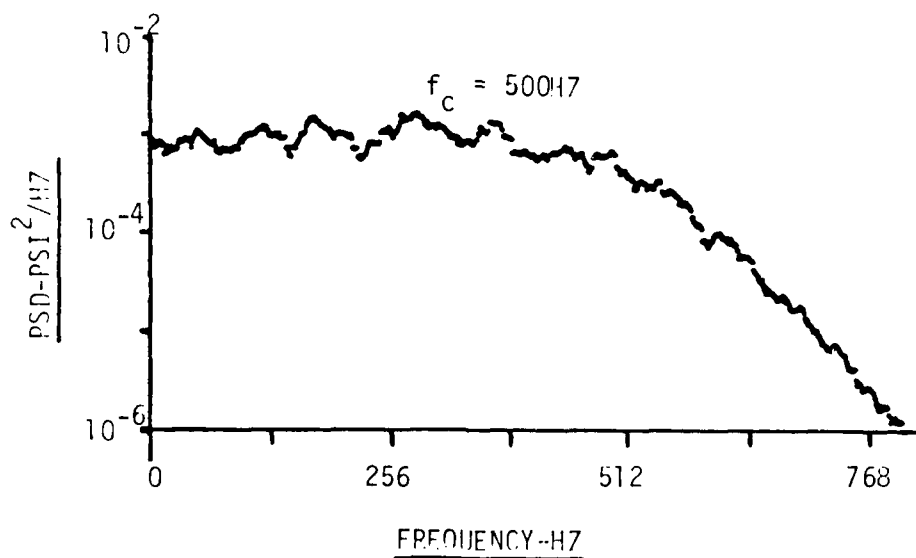


Figure 27 Random Number PSD with Recursive Filter

The problem is magnified in implementing these two digital filters because there are forty independent synthesized pressure signals to be developed. Rather than create forty long strings of synthesized pressures, a moving window concept and several small arrays are used to store current and past input and output filter values. A two step process is used, an initialization phase to start the filter process, and a run phase to filter the synthesized pressures. The following is a brief description of the arrays used in the filter process:

<u>Step</u>	<u>Operation</u>
1	Build an array (RANO) of 120 random numbers, RANO = A(I), I = 1,120
2	Build an array (RAN) of forty random numbers, RAN = B(I), I = 1,40
3	Shift RANO one place to the left and replace each third value from the RAN array, RANO = A(2), A(3), B(1), A(5), A(6), B(2),..., A(119), A(120), B(40)
4	Filter the RANO array using the non-recursive filter and create an array (PA40H) of forty values, PA40H = C(1), C(2),..., C(40) where: $C(1) = h_k A(2) + h_o A(3) + h_k B(1)$ $C(2) = h_k A(5) + h_o A(6) + h_k B(2)$ $C(40) = h_k A(119) + h_o A(120) + h_k B(40)$
5	Shift an array (PA120), initially filled with zeros, one place to the left and replace each third value with a value from the PA40H array, PA120 = 0, 0, C(1), 0, 0, C(2),..., 0, 0, C(40)

Steps 2 through 5 are repeated three times during the initialization phase. The RAN array is filled with a new set of random numbers with each iteration.

At the end of the initialization phase, the PA120 array has been filled with the output of the PA40H array (the non-recursive filter output). The 120 numbers in the PA120 array consist of forty independent sets of three numbers that represent three samples of each synthesized pressure. The first two samples are past non-recursive filter values while the third sample is the current value. The current value is determined from the past two values from RAN0 and a new random number from RAN.

In the run phase, steps 2 through 5 are continued to generate the forty filtered (non-recursive) synthesized pressure samples. The Butterworth filters are then activated. Two additional arrays are employed, an array which holds the current forty values and another array which contains forty sets of the past three output values of the Butterworth filters. By manipulating these arrays in the same manner as described above, the Butterworth filter can be programmed using a relatively small amount of storage.

SECTION IV

IMPROVED MODEL ANALYSIS

This chapter begins by describing the improved statistical prediction model that includes the two digital filters described in Section III. Predictions from this model are compared to the same inlet distortion data used to examine the capabilities of the basic model. A map averaging concept is described which offers a substantial improvement in the quality of the predicted pressure distortion maps. Finally, the results using eight measured RMS turbulence values in the analysis are presented.

Improved Statistical Prediction Model Description

A schematic of the improved model is shown in Figure 28. The method consists of three elements; the generation of the compressor face dynamic total pressures, the determination of the maximum distortion level and pressure contour map, and the map averaging method that provides the most probable maximum distortion level and pressure contour map. A more detailed discussion of map averaging is presented later.

The RMS turbulence and random numbers are combined, as was done in the basic method. However, these synthesized pressure signals are now input into the two digital filters added to the basic model. The first filter is the non-recursive filter that provides a slight roll-off characteristic over the entire power spectrum and the second filter, the recursive filter, accounts for engine sensitivity. The second filter's output is the filtered synthesized fluctuating pressure component that is added to the steady-state pressure to form the dynamic total pressure. The dynamic total pressures are input to the distortion parameter equation where the distortion level is determined. Forty new random numbers are generated, providing forty dynamic pressures for another equivalent time slice. The distortion level is then computed and compared to the current maximum value. The larger value is retained, including the pressures for the distortion map. The sequence is repeated until the desired sample size is reached which is based on cut-off filter frequency. The solution is restarted with another set of random numbers, another maximum

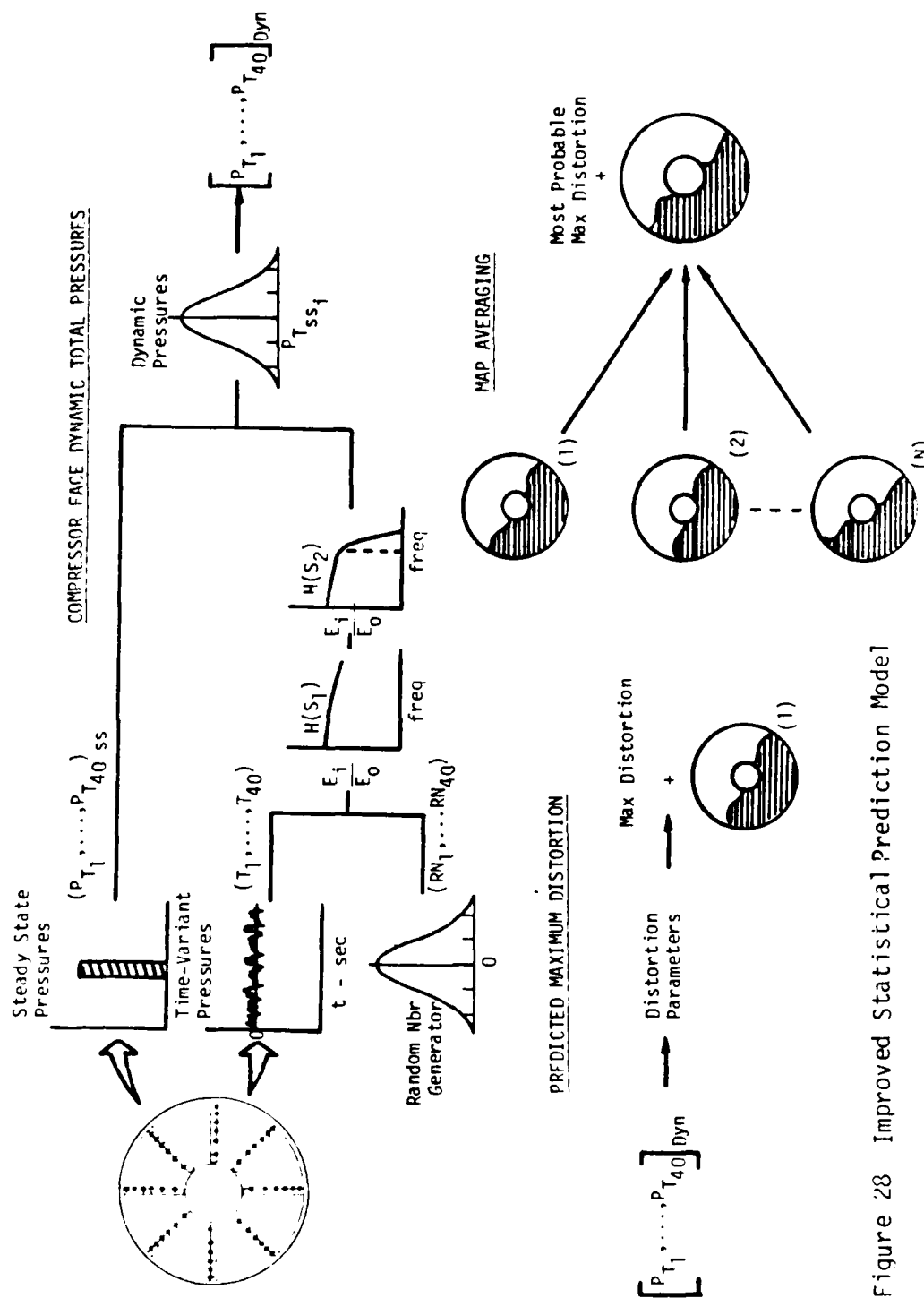


Figure 28 Improved Statistical Prediction Model

distortion map is generated, and the sequence is repeated several times. The pressure recoveries of each probe for all the generated maximum distortion maps are averaged to develop the most probable maximum distortion map.

Prediction Model with Filtering

The same set of comparisons is used to demonstrate the capabilities of the model. To reiterate, the differences between the predicted and measured distortion levels are presented as a function of measured distortion. Next, the standard deviation of the difference between predicted and measured probe pressure recovery is examined. Then, a comparison is made between the predicted and measured pressure contour maps, including the histogram depicting the distribution of the difference in probe recovery. An additional figure is presented to further illustrate the difference between the improved and basic prediction models. A histogram is presented showing the distribution of probe recovery difference based on the average of several solutions for the particular example.

The improved model's capabilities are illustrated first without map averaging to show the benefits of filtering the synthesized pressures to account for engine sensitivity. For the cases presented, the non-recursive filter is not included in the model for two reasons; first, the cut-off filter frequency ($f_c = 500$ HZ) used in conjunction with the GE distortion parameters is in the flat portion of the shaped spectrum, and second, the basic and improved models with the PWA parameters tend to underpredict the peak distortion level at higher distortion levels.

Figure 29 presents the differences between the predicted and measured peak distortion levels, including the circumferential and radial distortion components, using the GE₁ engine distortion parameters. The synthesized pressures have been filtered at a cut-off filter frequency of 500 HZ. Recalling that the basic method substantially overpredicted the peak ΔPRS_F (Figure 4), including the circumferential and radial components, the results from the improved model with filtering show significantly better agreement with all the measured components of the distortion. The average difference for ΔPRS_F is approximately -2.1

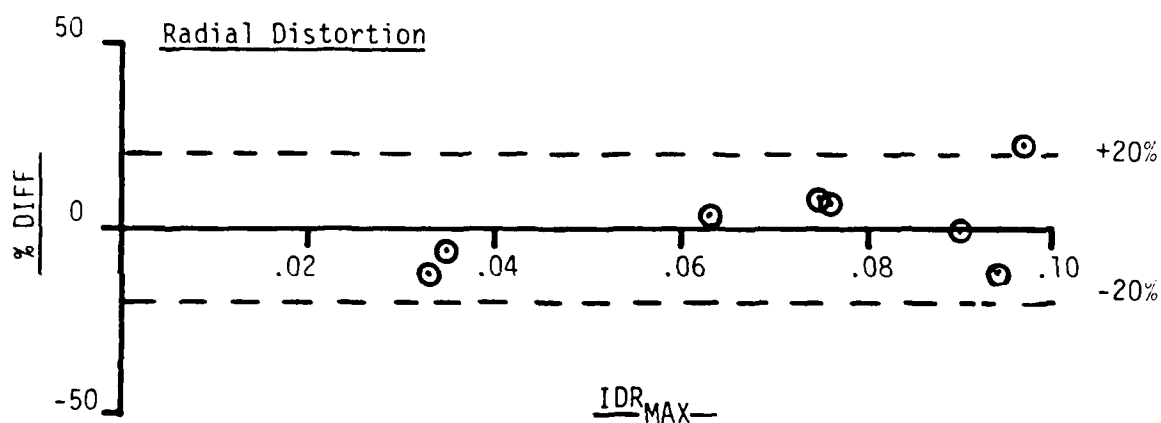
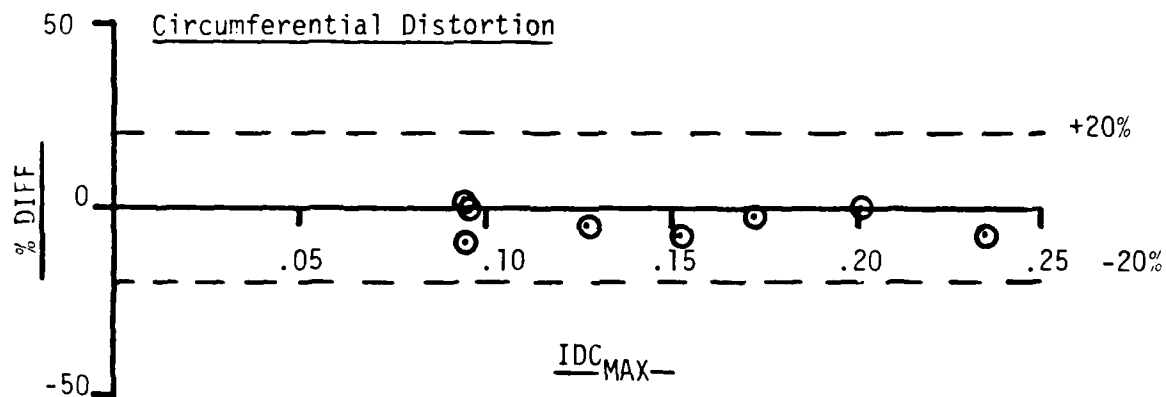
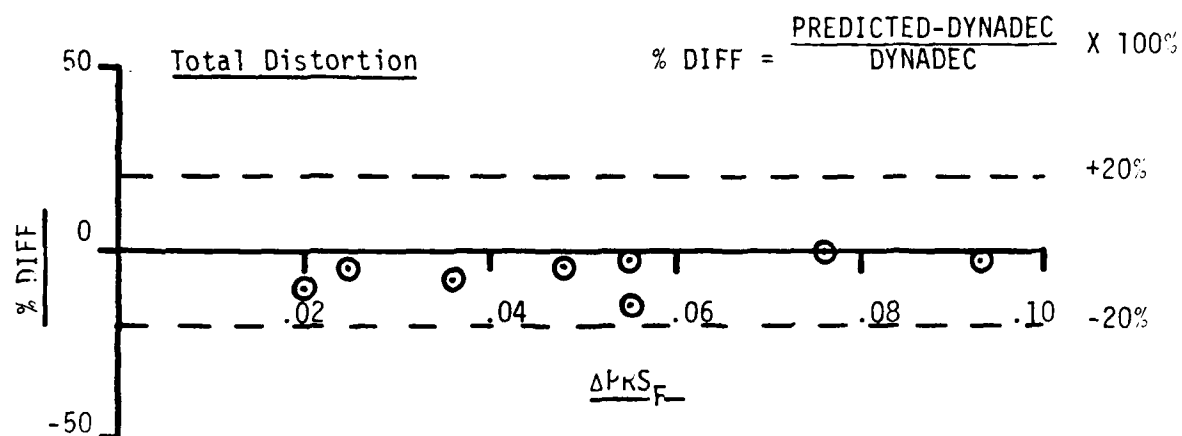


Figure 29 Improved Method (GF_1) - Comparison of Predicted to Measured Distortion (Filtered)

percent with a standard deviation of about 7.5 percent. The average difference and standard deviation for IDC_{MAX} and IDR_{MAX} are -3.5 and 4.2 percent, and 1.4 and 11.6 percent, respectively.

The improvement to the model is further emphasized in the difference between the regression lines for the basic and improved models shown in Figure 30. The data points, shown in the figure, are the same cases presented in the previous figure with the regression lines also based on repeating several of those cases several times to account for variations due to the random number process. Filtering the synthesized pressures has reduced the percent RMS difference in probe pressure recovery from 25 to 40 percent at the high- and low-turbulence levels, respectively.

Figures 31, 32, and 33 present the predicted and measured pressure contour maps for the low, moderate, and high-turbulence cases (GE_1) presented earlier. For the low-turbulence case, Figure 31, there is an improved definition of the predicted pressure contours. There is excellent agreement between the predicted and measured distortion components. The percent RMS difference has been reduced by 30 percent to a value of 1.20. A more dramatic improvement between the predicted and measured distortion maps for the moderate-turbulence case can be seen in Figure 32. Substantial agreement exists between the pressure contours and between the predicted and measured distortion levels. The histogram shows a tighter distribution about the zero difference in probe recovery with the range of the difference having decreased from 17 (basic) to 12 percent (improved). The RMS difference is 2.63%, a reduction amounting to 21 percent. Similar results are achieved for the high-turbulence case, Figure 33. With the exception of the recovery contours of .95, the predicted and measured contours show very good agreement. Predicted and measured distortion levels are identical. The $\%RMS_{DIFF}$ decreased from 4.60 percent to 3.24 percent, the range decreased from 22 to 16 percent, and the number of predicted pressures agreeing within ± 2 percent of their measured values increased from fifteen to twenty-two in number, compared to basic model results.

Figure 34 presents the average distributions of probe recovery difference of several solutions for the three cases just presented. The results show a substantial improvement to the model with filtering.

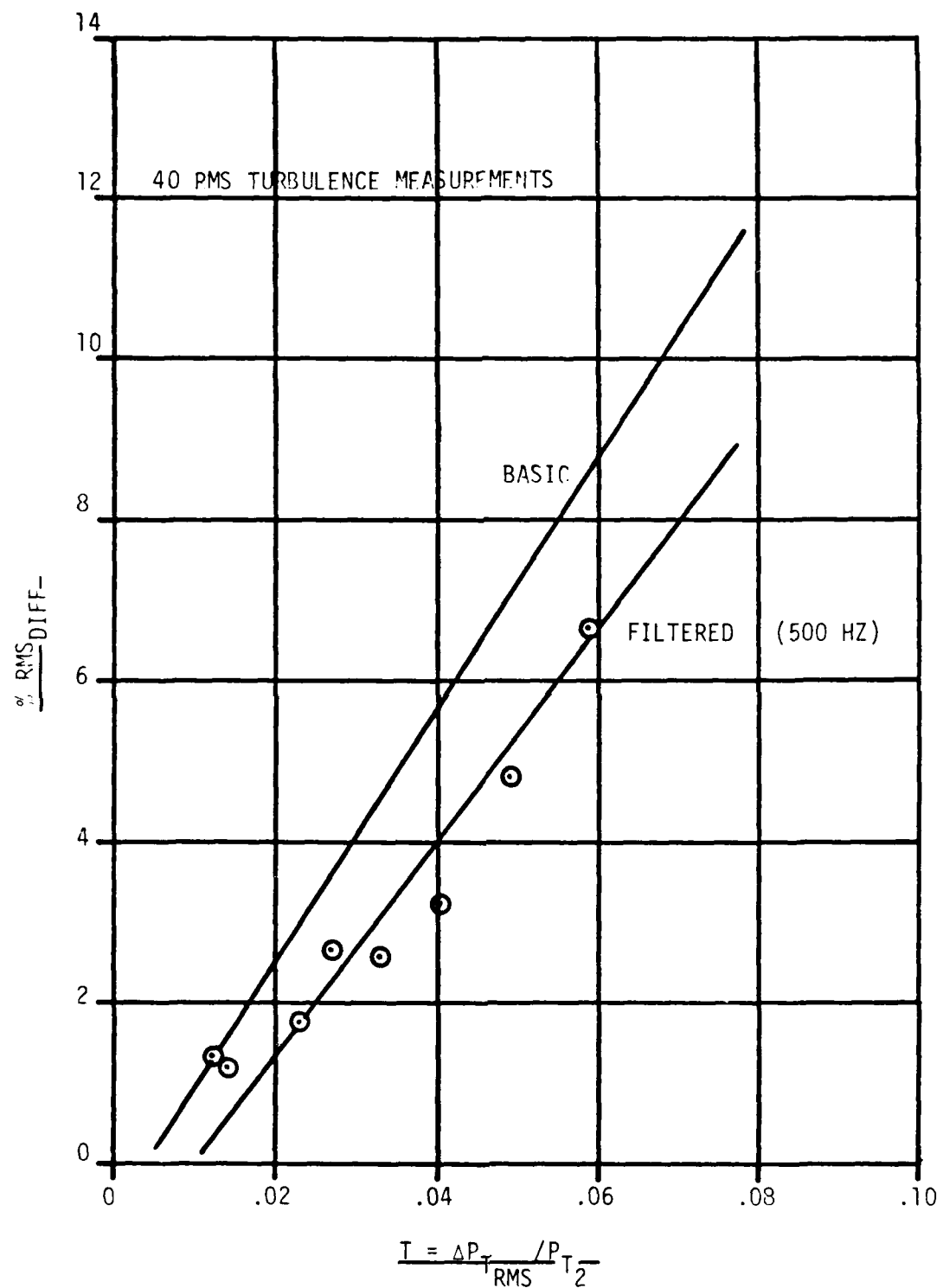
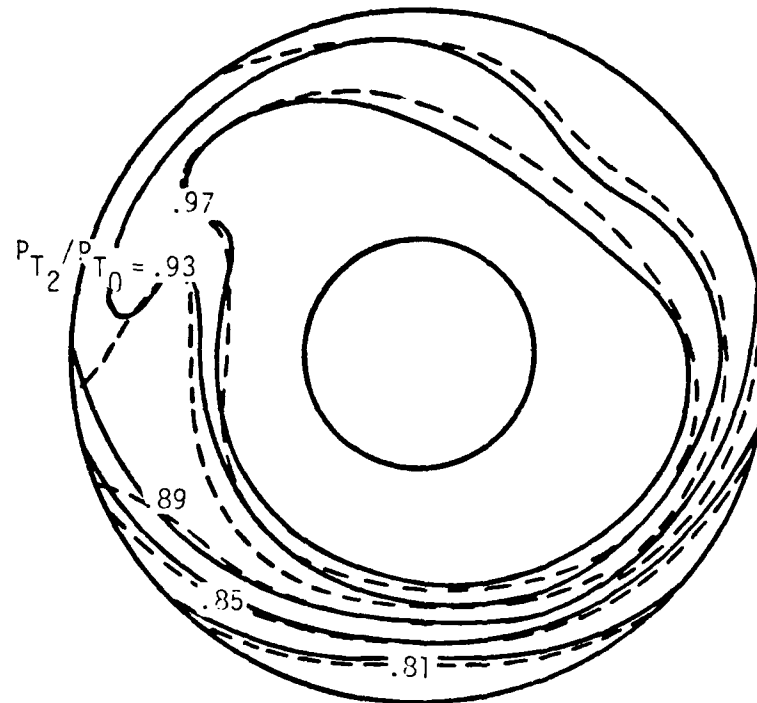


Figure 30 Improved Method (GF_1) - Percent RMS Difference

DYNADEC - - -
 PREDICTED ———



$T = .014$

	<u>DYNADEC</u>	<u>PREDICTED</u>
ΔPRS_F	.020	.022
IDC_{MAX}	.094	.096
IDR_{MAX}	.063	.065

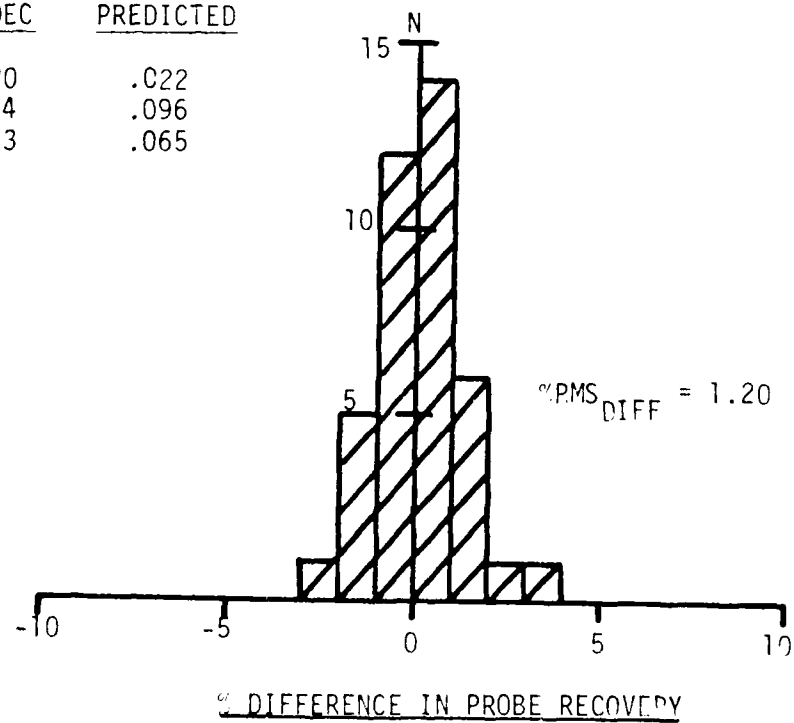
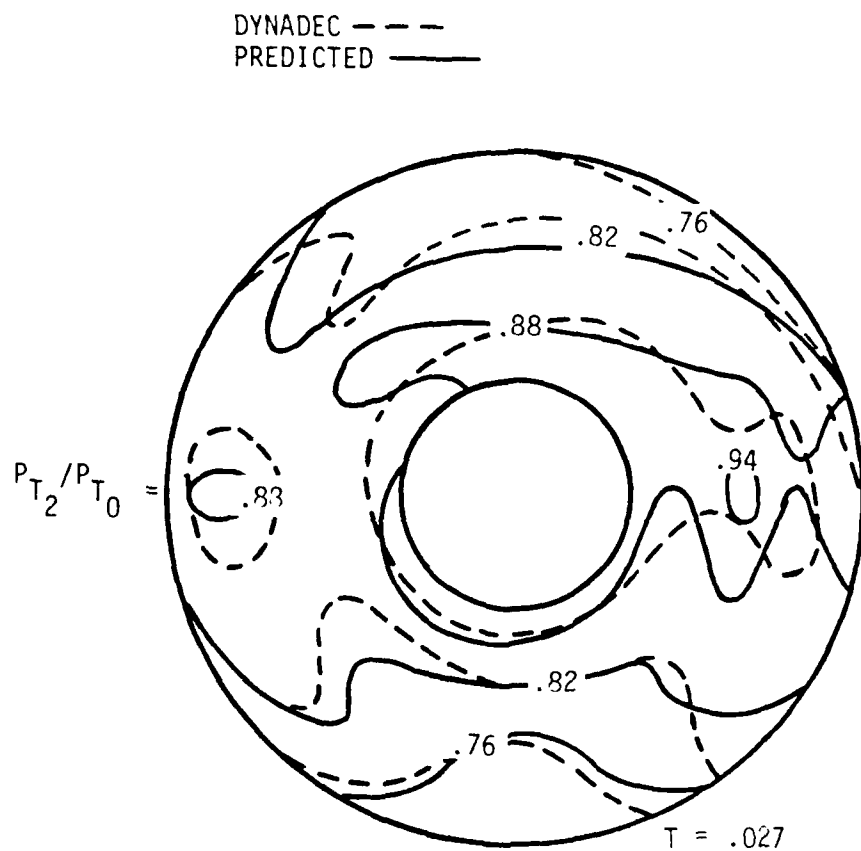


Figure 31 Improved Method (GF_1) - Pressure Contour Map and Histogram, Low Turbulence (Filtered)



	<u>DYNADec</u>	<u>PREDICTED</u>
ΔPPS_F	.048	.046
IDC_{MAX}	.127	.121
IDR_{MAX}	.033	.029

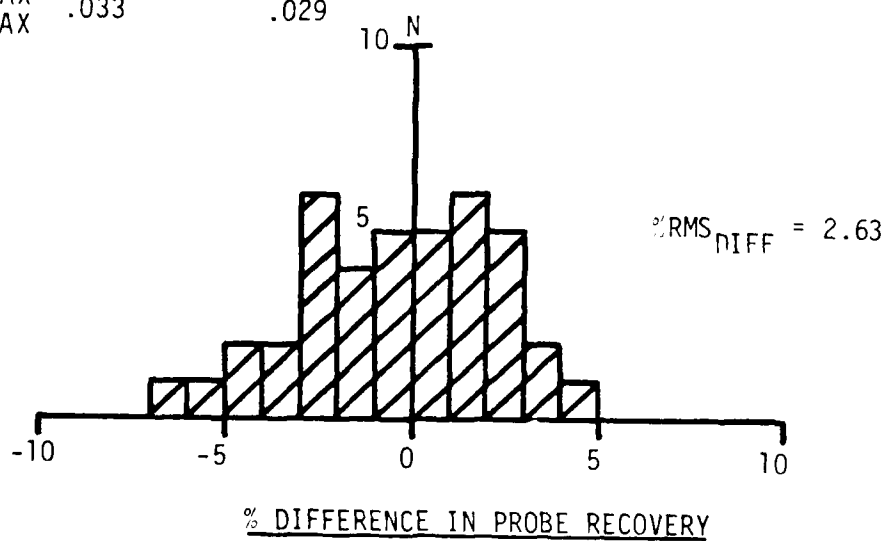
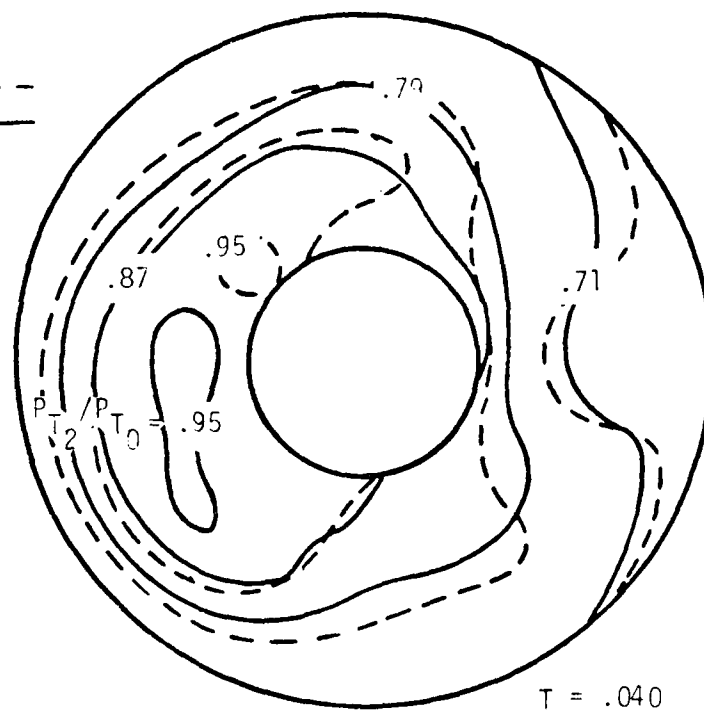


Figure 32 Improved Method (GF_1) - Pressure Contour Map and Histogram, Moderate Turbulence (Filtered)

DYNADEC - - - -
 PREDICTED ———



	<u>DYNADEC</u>	<u>PREDICTED</u>
ΔPRS_F	.076	.076
IDC_{MAX}	.201	.201
IDP_{MAX}	.090	.090

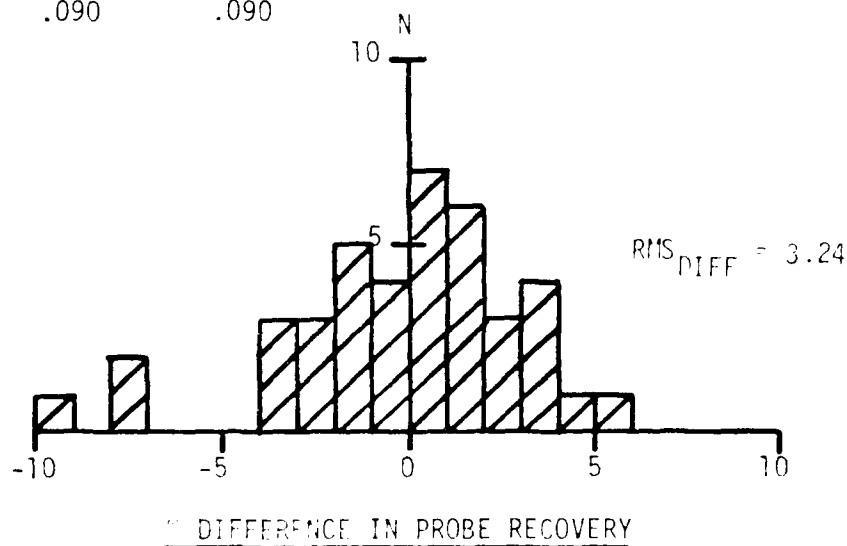


Figure 33 Improved Method (GF_1) - Pressure Contour Map and Histogram, High Turbulence (Filtered)

$f_c = 50017$

BASIC
FILTERED

$T = .014$

$T = .027$

$T = .040$

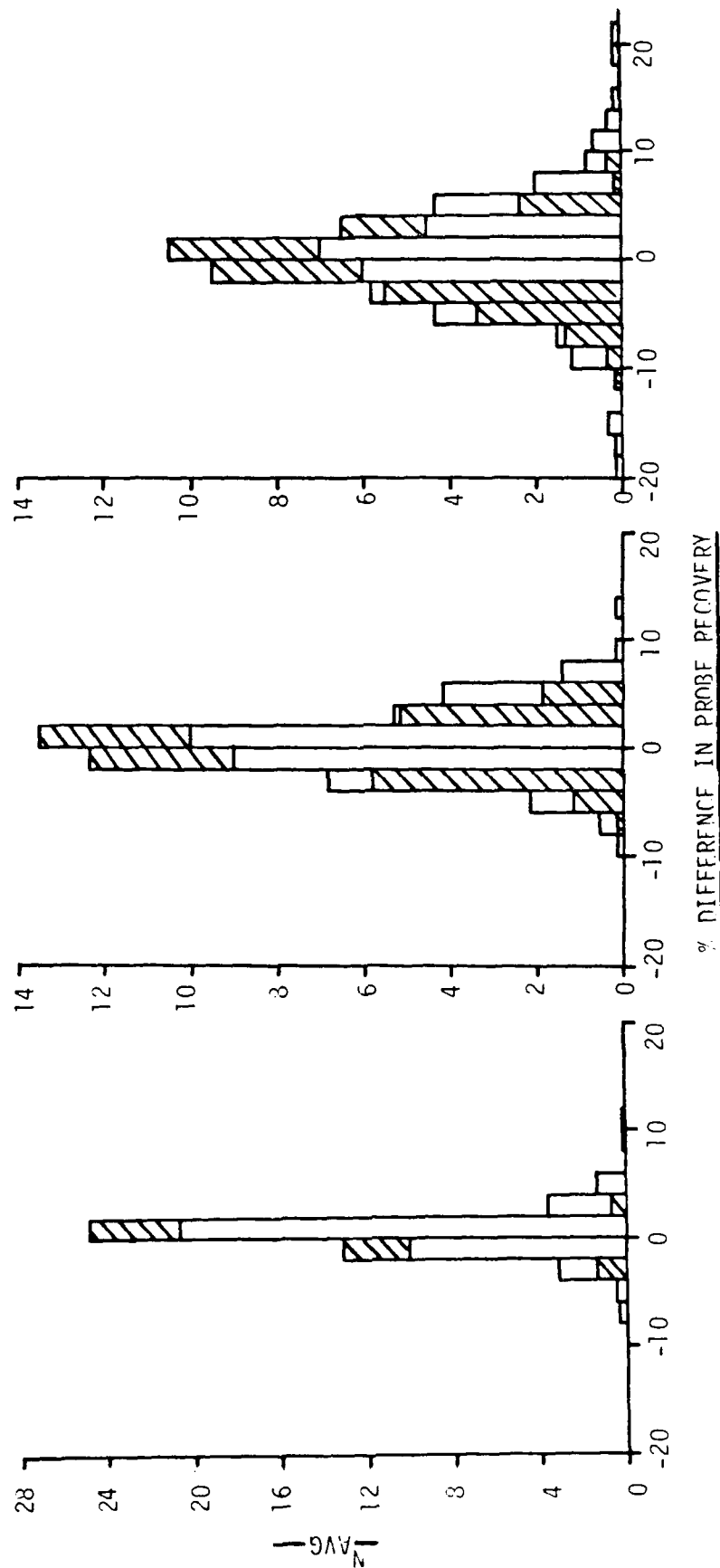
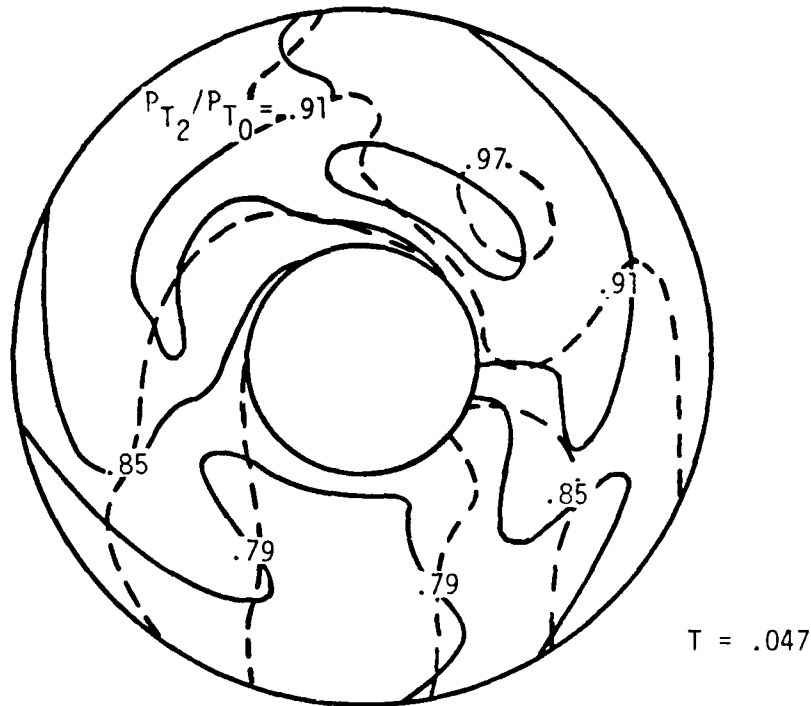


Figure 34 Distribution of probe Recovery difference (GE_1)

DYNADEC ---
 PREDICTED —



	<u>DYNADEC</u>	<u>PREDICTED</u>
IDL	1.280	1.230
IDC MAX	.146	.158
IDR MAX	.035	.003

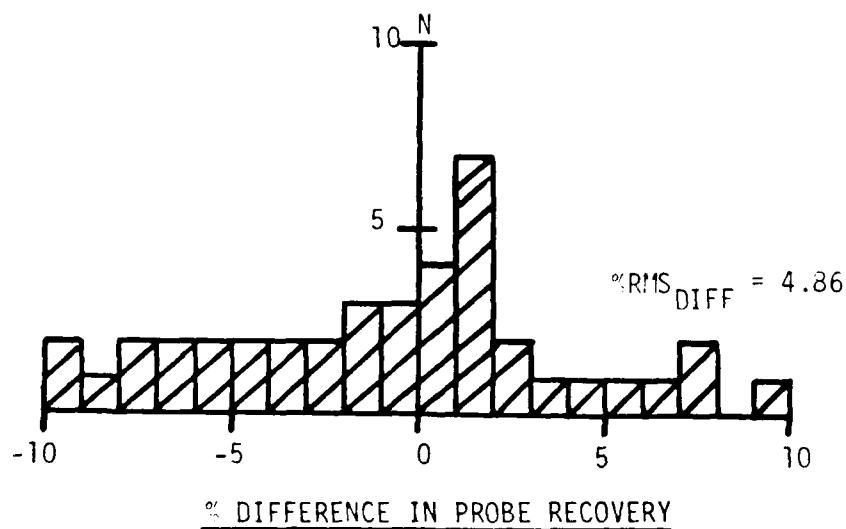
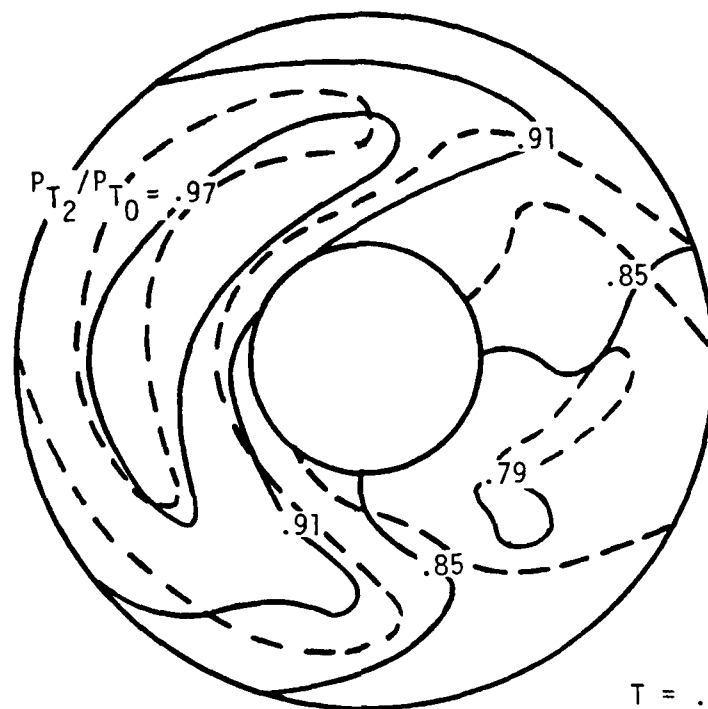


Figure 45 Improved Method (GE_2) - Pressure Contour Map and Histogram, High Turbulence (Filtered)

DYNADEC - - - -
 PREDICTED ———



	<u>DYNADEC</u>	<u>PREDICTED</u>
IDL	1.222	1.175
IDC _{MAX}	.130	.146
IDR _{MAX}	.040	.014

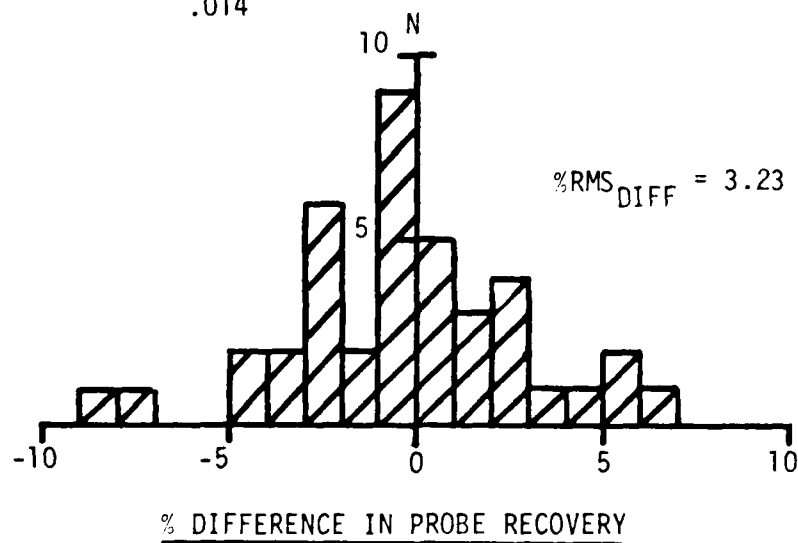
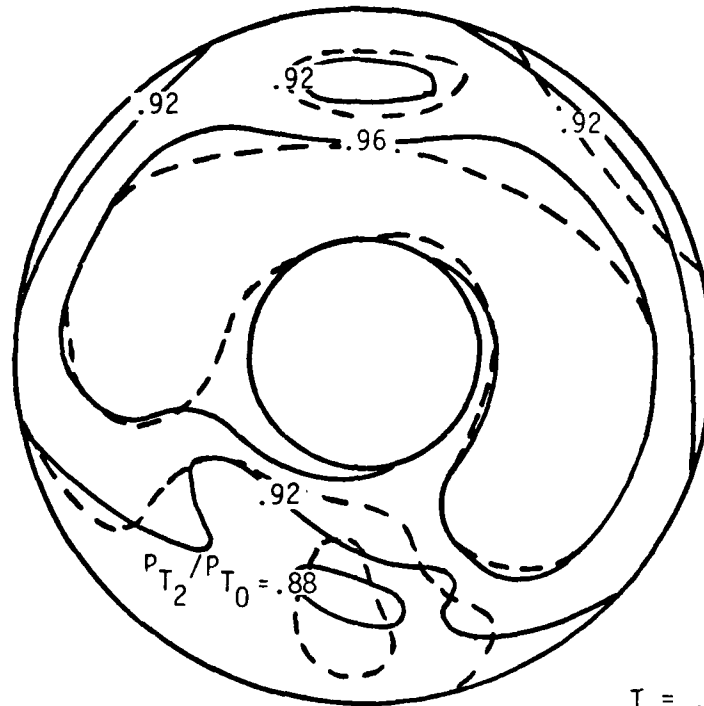


Figure 44 Improved Method (GE_2) - Pressure Contour Map and Histogram, Moderate Turbulence (Filtered)

DYNADEC - - - -
 PREDICTED - - - -



$T = .016$

	<u>DYNADEC</u>	<u>PREDICTED</u>
IDL	.721	.800
IDC MAX	.090	.102
IDR MAX	.026	.027

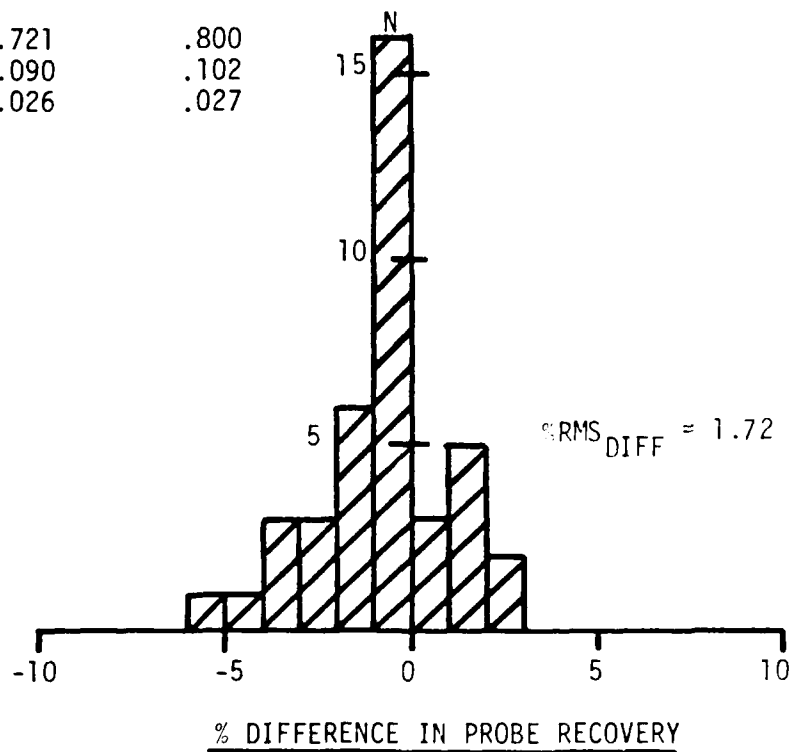


Figure 43 Improved Method (GF_0) - Pressure Contour Map and Histogram, Low Turbulence (Filtered)

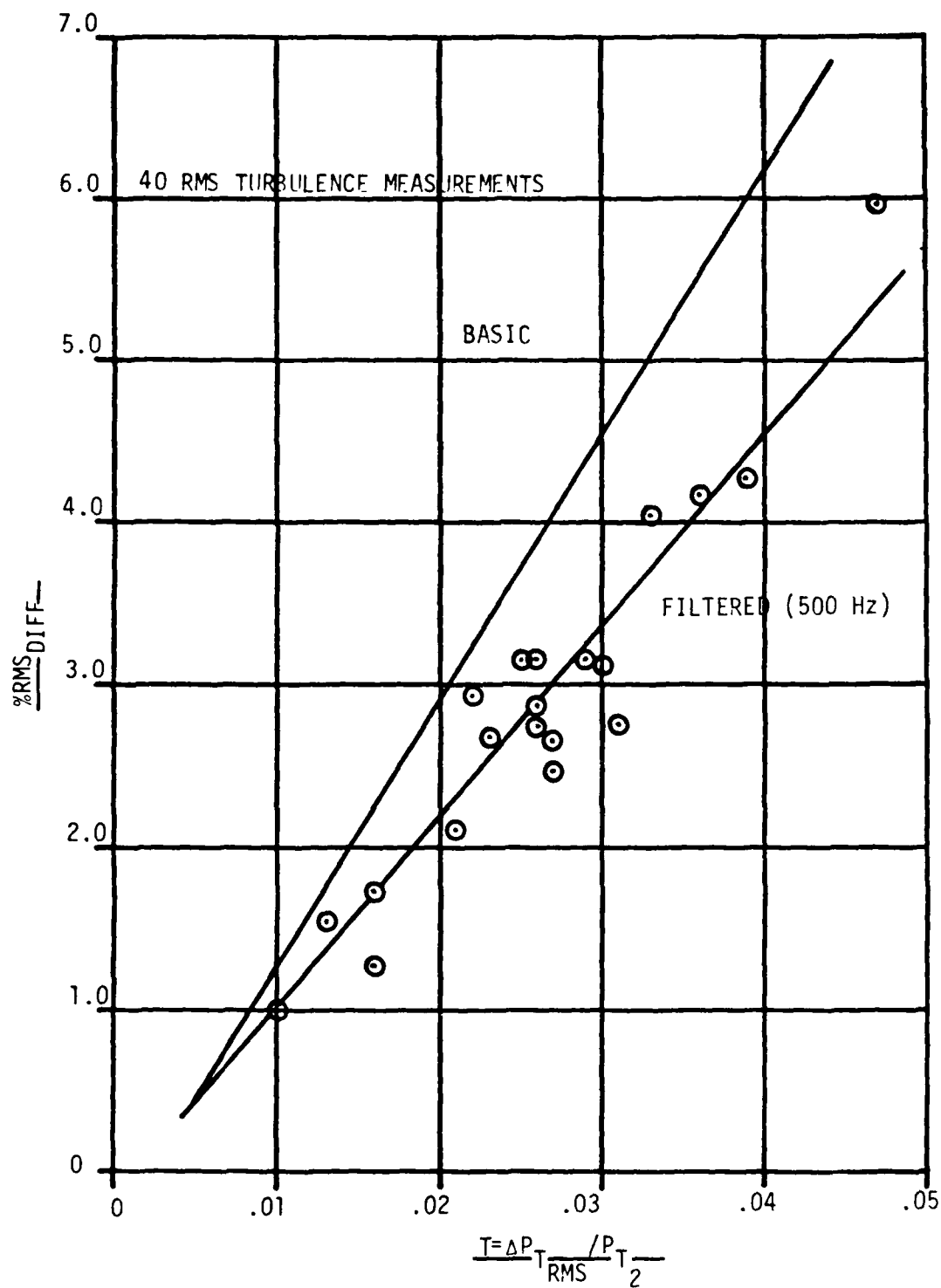


Figure 42 Improved Method (GF_2) - Percent RMS Difference, (Filtered)

average differences amounting to -1.9 percent and a standard deviation of 24.7 percent. While the standard deviation appears large, the levels of radial distortion are small emphasizing the relative differences between the predicted and measured values of IDR_{MAX} .

A comparison of the percent RMS difference in probe pressure recovery for the improved and basic methods is shown in Figure 42. As with the other distortion parameters, filtering has a very beneficial effect of reducing the difference between predicted and measured pressures. The reduction in $\%RMS_{DIFF}$ between the two models varies from no difference at very low-turbulence levels to approximately 25 percent at high-turbulence levels.

Pressure contour maps and histograms for the three levels of turbulence previously presented are shown in Figures 43, 44, and 45. For the low-turbulence case presented in Figure 43, there is excellent agreement between the predicted and measured distortion maps. The predicted level of IDL is approximately 10 percent greater than the measured peak IDL, however, the differences between the predicted and measured circumferential and radial distortion components are very small. It is how those elements are combined that contributes to the difference between the predicted and measured value of IDL. Thirty-three predicted pressures are within ± 2 percent of their measured values and the $\%RMS_{DIFF}$ is 1.72, a decrease of 12 percent over the results with the basic method. The improvement to the predicted distortion map for the moderate-turbulence case, Figure 44, appears to be only somewhat improved over the results attained with the basic model. However, an examination of the histogram shows that the range of the difference in probe pressure recovery decreased from 22 to 15 percent with a resultant decrease in $\%RMS_{DIFF}$ of approximately 32 percent. The high-turbulence case is shown in Figure 45. Again, there is an improvement over what was predicted with the basic model, attaining substantial improvements in the predicted distortion levels, the reduction in the range of the difference and percent RMS difference in probe recovery. However, as was the case with the PWA high-turbulence example, there appears to be an upper limit for applying the improved model with filtering.

The average distribution of the difference in probe recovery is presented in Figure 46. The distributions for the three turbulence

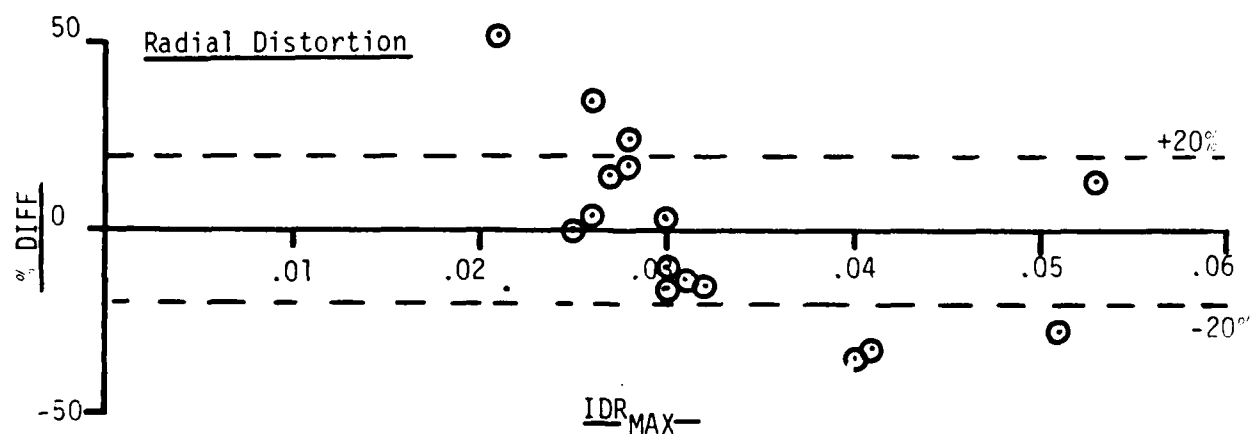
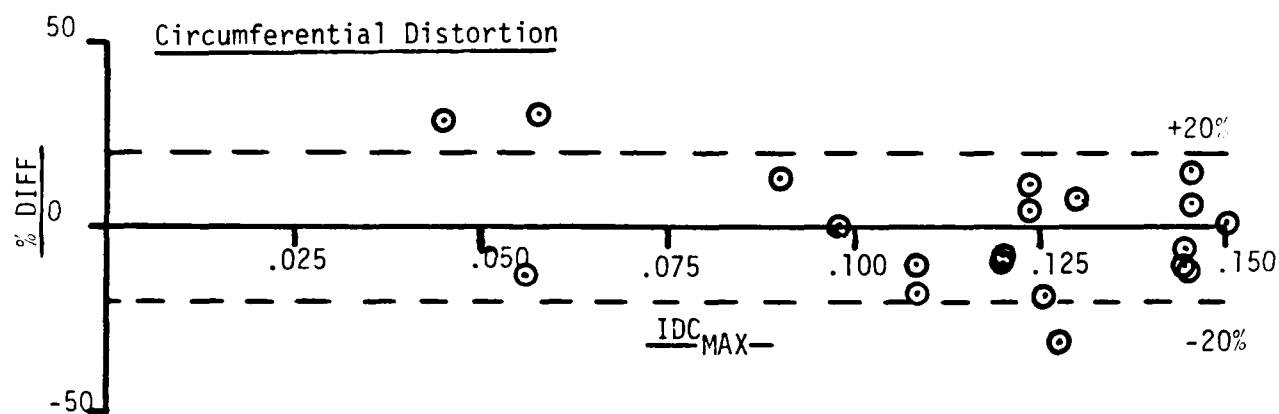
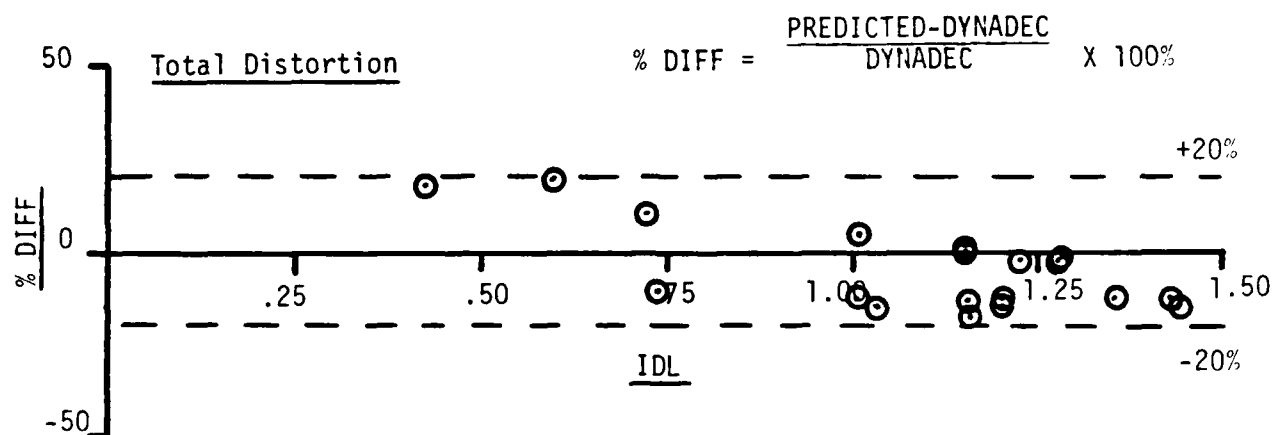


Figure 41 Improved Method (GF_2) - Comparison of Predicted to Measured Distortion, (Filtered)

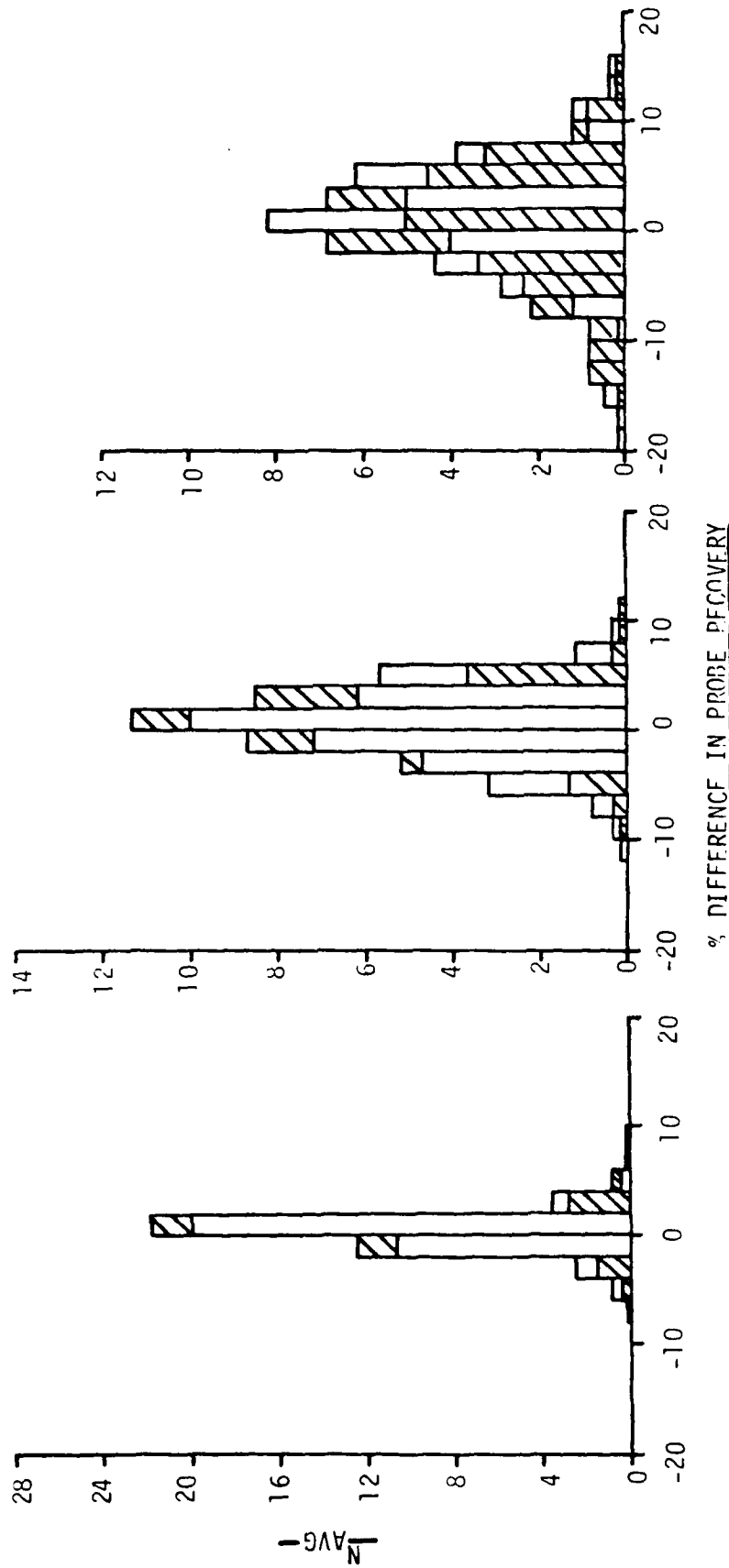


Figure 40 nistribution of probe Recovery Difference (p4A)

DYNADEC ---
 PREDICTED —

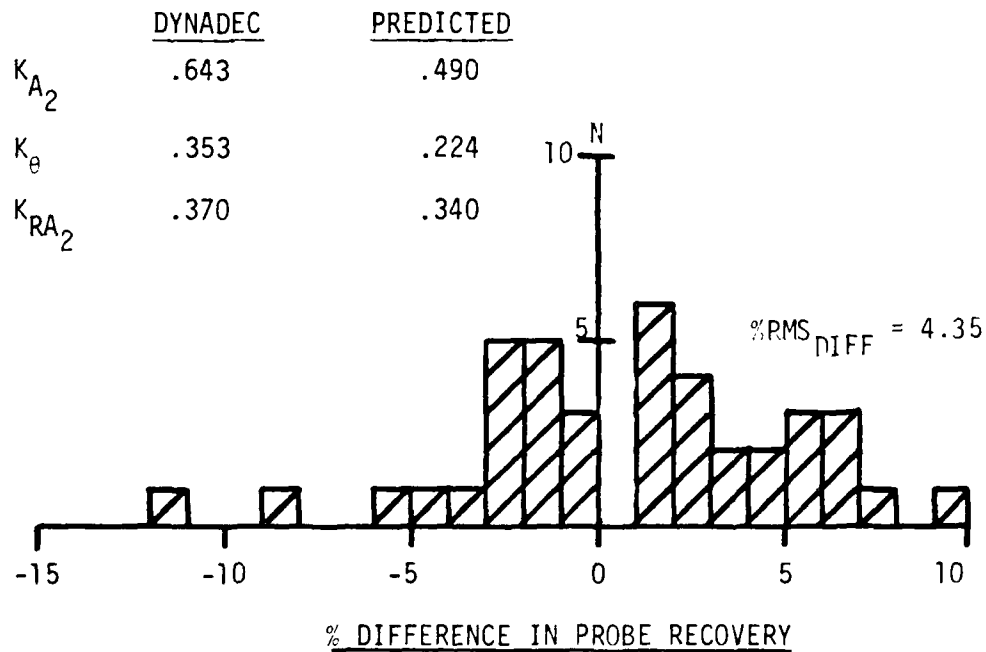
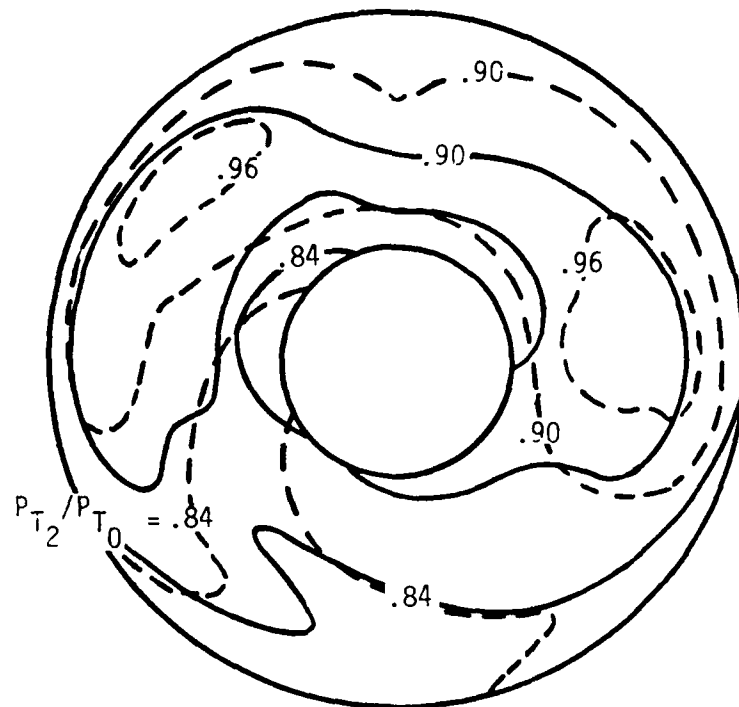
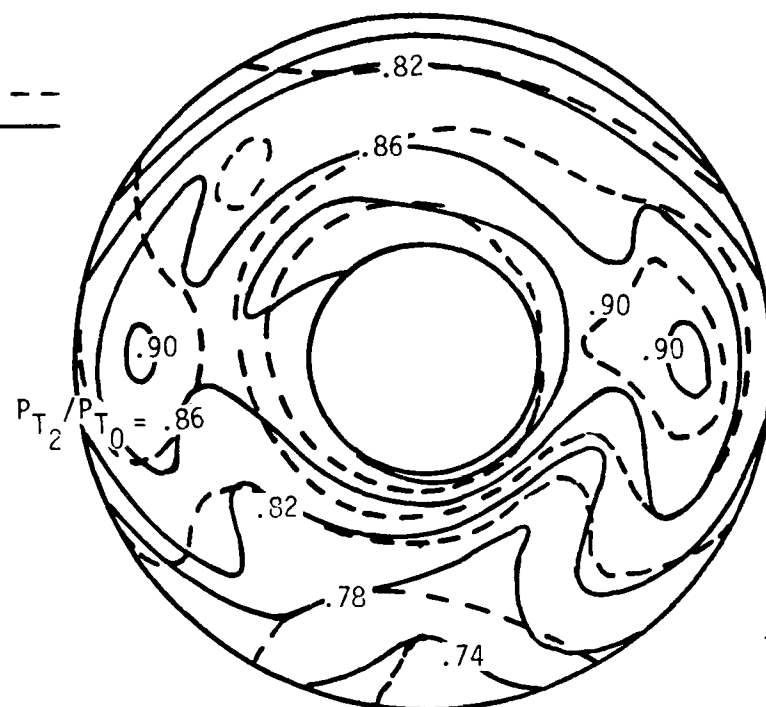


Figure 39 Improved Method (PWA) - Pressure Contour Map,
 High Turbulence (Filtered)

DYNADEC - - -
 PREDICTED ———



	<u>DYNADEC</u>	<u>PREDICTED</u>
K_{A2}	.390	.394
K_{u1}	.192	.199
K_{RA2}	.227	.223

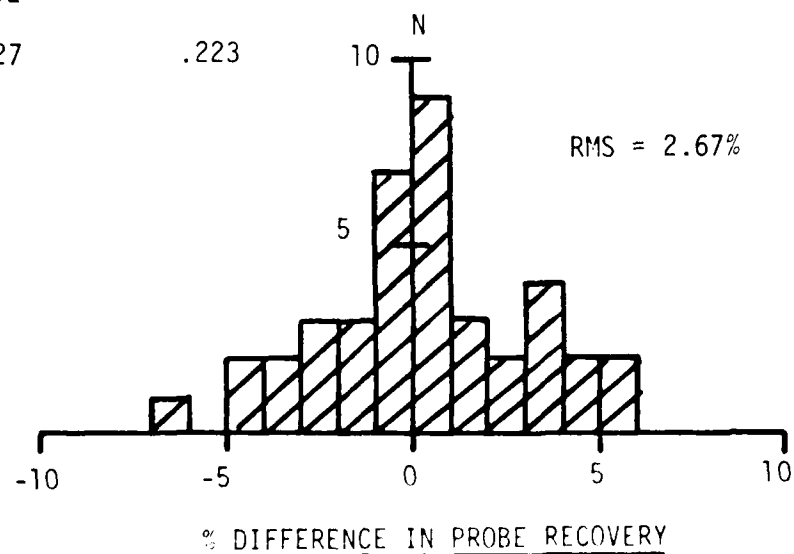


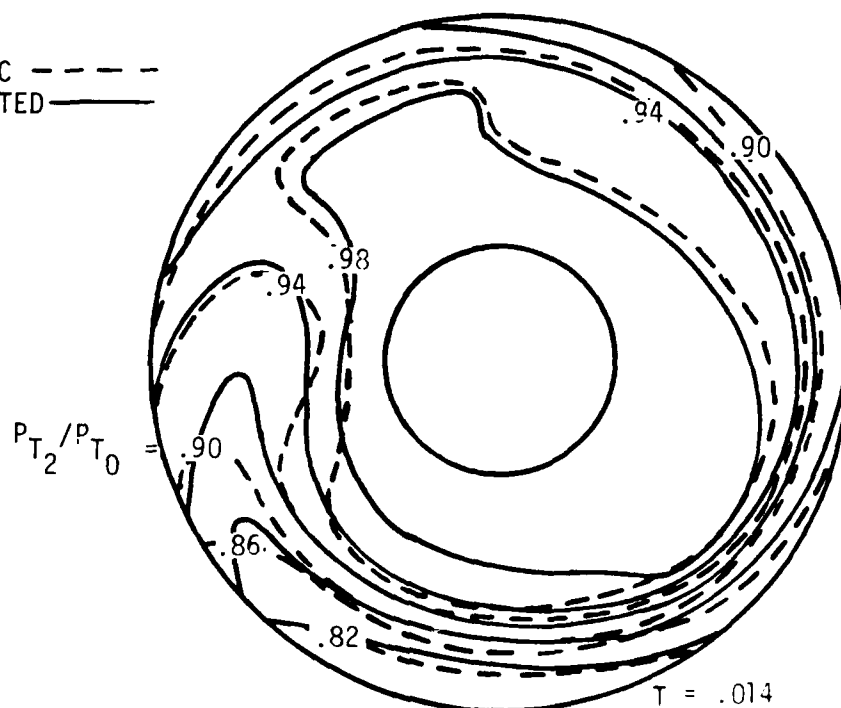
Figure 38 Improved Method (PWA) - Pressure contour Map and Histogram, Moderate Turbulence (Filtered)

distortion map for the moderate-turbulence case, Figure 38, shows very good agreement with the measured distortion map. Other than the obvious difference in the nine to eleven o'clock position, there is good agreement between predicted and measured contours. While the number of probe recoveries agreeing within ± 2 percent is just slightly greater than that for the results with the basic model, there is a substantial reduction in $\%RMS_{DIFF}$ (30 percent) reflecting a narrower range in the difference in probe recovery (12 versus 17 percent). Finally the high-turbulence case ($T = .040$) is presented in Figure 39. Although the predicted and measured distortion maps are in better agreement, compared to the basic model results, there are nevertheless significant differences between the two maps. A reduction in $\%RMS_{DIFF}$ of 28 percent was attained over the basic model, but the relatively small number of predicted pressures agreeing within ± 2 percent of their measured values obviously is a factor in the disparity between the predicted and measured maps. Thus, the combination of high average value of turbulence ($T = .040$) and high cut-off frequency (1000 HZ) may represent an upper limit in applying the improved model.

The average distributions of the difference in probe pressure recovery for these three cases are shown in Figure 40. The most notable gains are at the low- and moderate-turbulence levels with only small improvements in the distribution for the high-turbulence case. A comparison of this distribution with the distribution for the high-turbulence case presented in Figure 34 shows the relatively small number of pressures within ± 2 percent of their measured values.

Figures 41 through 46 illustrate the improved method's capabilities with the GE_2 distortion parameters. The synthesized pressures were filtered at a cut-off filter frequency of 500 HZ. The differences between predicted and measured peak distortion levels are shown in Figure 41. In contrast to the basic method which predicted total and circumferential distortion levels significantly greater than the measured values, the improved method predicts levels that are in substantial agreement with the measured values. The average difference between predicted and measured values of IDL is -5.1 percent with a standard deviation of 11.3 percent. For IDC_{MAX} , the average difference is -.1 percent with a standard deviation of 15.5 percent. The large variation in the radial distortion component has been substantially reduced as well with the

DYNADEC - - - -
 PREDICTED - - - -



	<u>DYNADEC</u>	<u>PREDICTED</u>
K_{A2}	.243	.255
K_{θ}	.124	.130
K_{RA2}	.143	.150

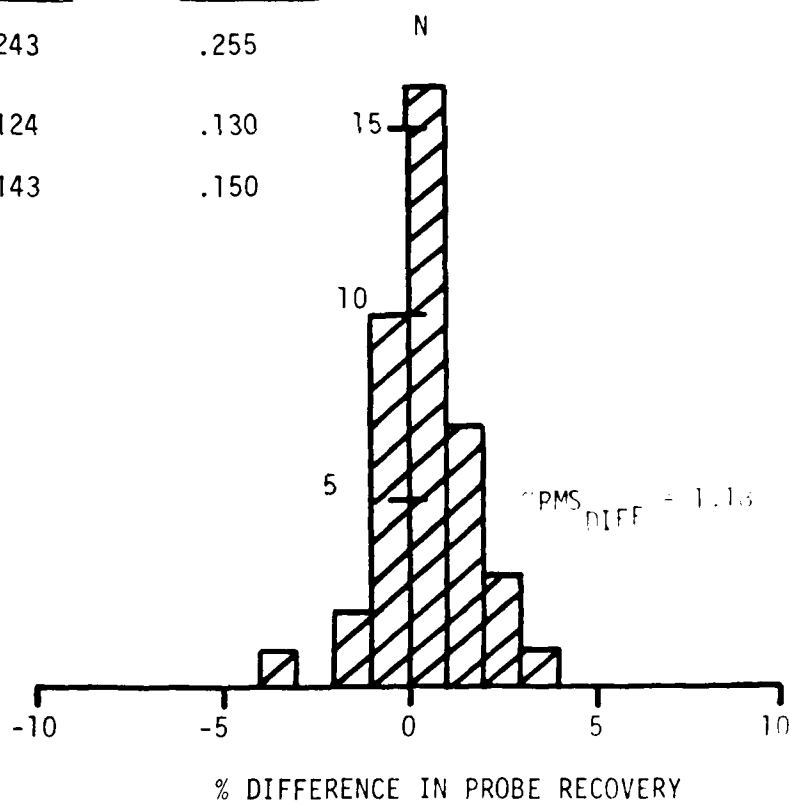


Figure 37 Improved Method (PVA) - Pressure Contour Map and Histogram, Low Turbulence (Filtered)

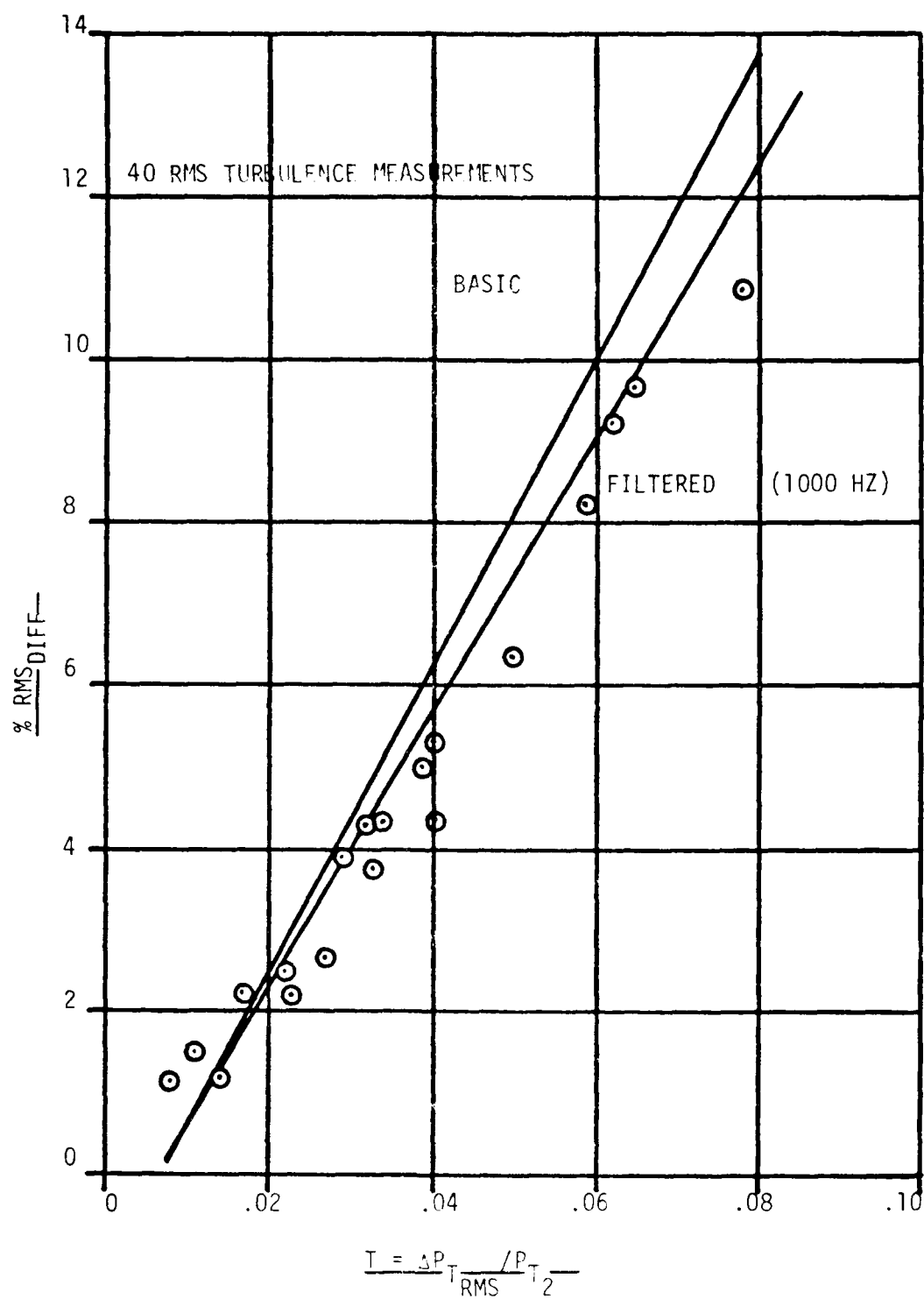


Figure 36 Improved Method (PWA) - Percent RMS Difference

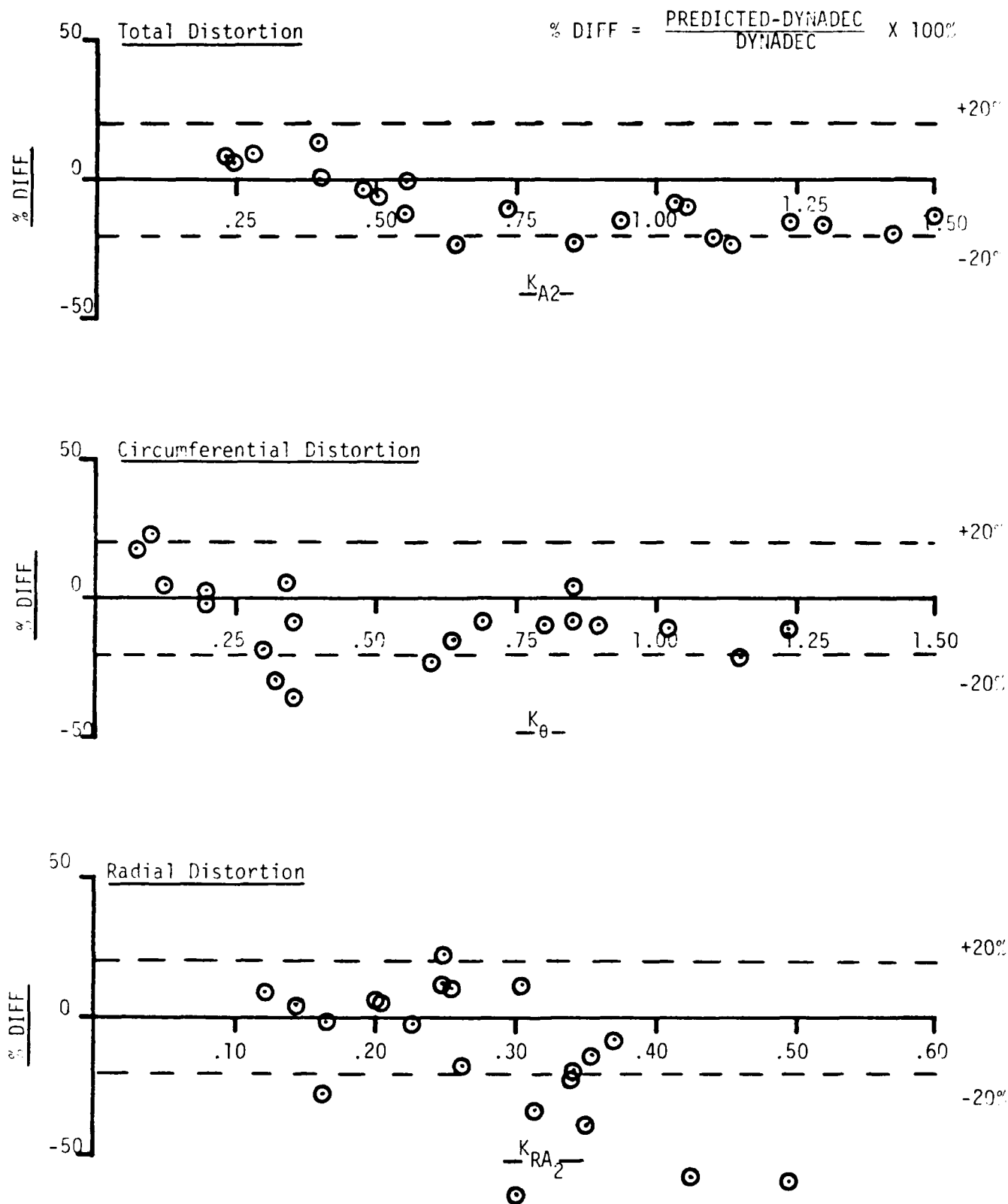


Figure 35 Improved Method (PHA) - Comparison of Predicted to Measured Distortion (Filtered)

Filtering the synthesized pressure reduces the range of the difference between predicted and measured probe recoveries and concentrates more values about the zero difference in recovery.

The results for the prediction model with the PWA distortion parameters are summarized in Figures 35 through 40. The synthesized pressures were filtered at 1000 HZ. Differences between predicted and measured peak distortion levels are shown in Figure 35. The overall trend for the three distortion parameters is similar, although somewhat lower in level, with that obtained with the basic method (Figure 9). The average difference between predicted and measured values of K_{A_2} is -8.9 percent with a standard deviation of 11.4 percent. For K_{θ} , the average difference is -7.3 percent and the standard deviation of 14.5 percent. The average difference and standard deviation between predicted and measured values of K_{RA_2} are -13.5 and 25.7 percent, respectively.

The similarity in the results suggests that the filtering of the synthesized pressures has a much smaller influence on the predicted pressures as compared to results obtained with the GE_1 parameters where the pressures were filtered at 500 HZ. The modest reduction in the percent RMS difference in probe recovery, reflected in the small difference between the two regression lines in Figure 36, would tend to support this observation. However, the regression lines are based on a greater population (several cases were repeated several times) than shown here and the slope of the line for the filtered results is affected by large $\%RMS_{DIFF}$ values for turbulence levels exceeding .06. If that regression line was based solely on those cases having average turbulence levels of less than .06, the slope of the line would be lower and a greater improvement noted.

Evidence of this conclusion can be seen with the substantial improvement to the pressure contour maps and the distribution of the difference in probe pressure recovery presented in Figures 37, 38, and 39. For the low-turbulence case, Figure 37, there is excellent agreement between pressure contours of the predicted and measured distortion maps with thirty-five predicted pressures within .2 percent of their measured values. The $\%RMS_{DIFF}$ is 1.18 which represents a 38 percent improvement over the result obtained with the basic model. The predicted pressure

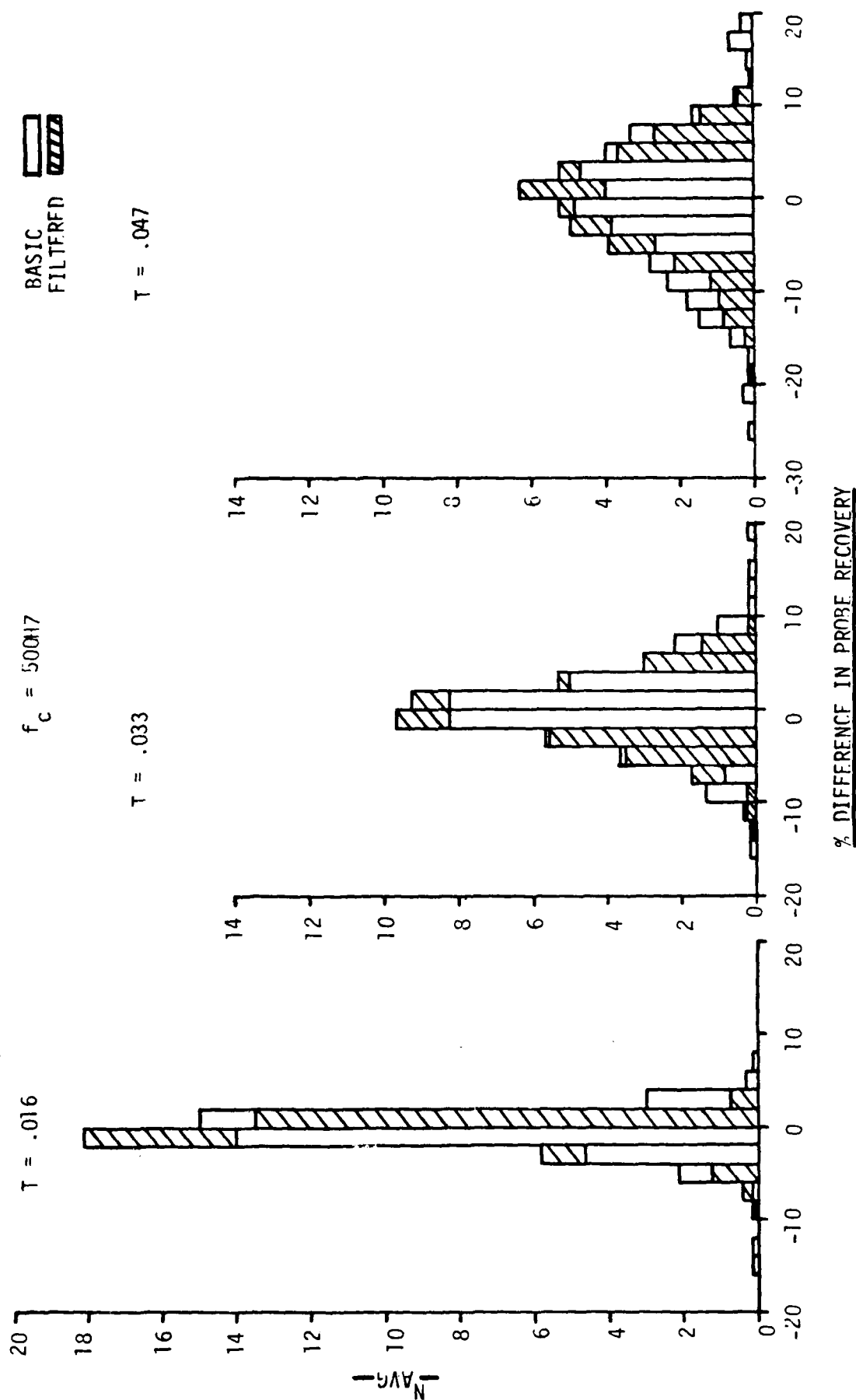


Figure 46 Distribution of Probe Recovery Difference (ΔE_2)

levels show similar results as noted previously, that is, most improvement occurs at low and moderate-turbulence levels. As turbulence increases, the distributions characteristically become flatter and broader, with less than one-third of the predicted pressures being within ± 2 percent of their measured values for the high-turbulence case.

In summary, it has been shown that the filtering of the synthesized pressures provides a significant improvement in the predicted distortion levels and pressure distortion maps. The quality of the predicted pressure distortion maps is a function of the turbulence level and cut-off filter frequency. As the levels of these two parameters increase, the quality of the distortion map decreases. The upper limits for applying the improved model with filtering appears to be approximately .04 for turbulence and a cut-off filter frequency slightly greater than 1000 HZ.

Prediction Model with Filtering and Map Averaging

A map averaging scheme has been included in the model that provides a significant improvement in the accuracy of the pressure distortion map. The predicted distortion map and the level of the distortion parameters are the result of a particular set of random numbers. Another set of random numbers, via a different starting seed value, will generate somewhat different dynamic total pressures and hence, a different distortion map and distortion parameter values. That difference is small for probes with low-turbulence levels, but can be significant for probes located in regions of high-turbulence. All the possible predicted distortion maps are equally valid, and thus each predicted probe pressure is considered to be part of a distribution. The average maximum distortion map, which will be defined as the most probable maximum distortion map, is determined by repeating the solution several times with different sets of random numbers. Individual probe pressures are summed from the individual distortion maps and averaged so that the resulting forty pressures represent the data for the most probable maximum pressure distortion map. For the cases presented, the pressures for six maximum distortion maps were summed and averaged.

The three previous cases with the GE_1 distortion parameters are presented in Figures 47, 48, and 49. Pressure contours for the predicted

map are virtually identical with the measured map for the low-turbulence case, Figure 47. Excellent agreement exists between predicted and measured distortion levels. The $\%RMS_{DIFF}$ is .68, a reduction of 60 percent compared to the results attained with the basic model. Thirty-nine predicted pressures are within ± 2 percent of their measured values. The moderate-turbulence case is presented in Figure 48. Again there is excellent agreement between predicted and measured pressure contour lines. There is correspondingly, excellent agreement between predicted and measured distortion parameter values. Twenty-nine probe pressures agree to within ± 2 percent of their measured values. The percent RMS difference has decreased to 1.87, representing a 44 percent improvement over the basic model. The capabilities of the improved model with the map averaging are further demonstrated with the high-turbulence case presented in Figure 49. The pressure contours of the predicted map show excellent agreement with the measured map with the exception of the pressure recovery contour of .95. Predicted and measured distortion levels exhibit excellent agreement. The number of probes within ± 2 percent of their measured values is twenty-six, a 73 percent improvement over the results with the basic method. The range of the difference decreased 56 percent and the $\%RMS_{DIFF}$ decreased 46 percent compared to the basic model.

Because of the similar substantial agreement between predicted and measured distortion maps for the low-turbulence examples, only moderate- and high-turbulence cases are presented for the PWA and GE_2 distortion parameters. Figure 50 presents the moderate-turbulence case with the PWA distortion parameters. Pressure contours for the predicted and measured maps are almost identical with the only apparent difference at approximately the eleven o'clock position. Predicted distortion levels are in excellent agreement with measured values. The distribution of probe pressure recovery difference shows that twenty-nine probes are within ± 2 percent of their measured values. The range of difference decreased slightly to 11 percent with the percent RMS difference reduced to 2.14, a reduction of 44 percent over the basic model. The high-turbulence case is shown in Figure 51. For this case, there is no improvement in the predicted distortion map compared to what was predicted with filtering. While the range in the probe recovery difference has decreased, the

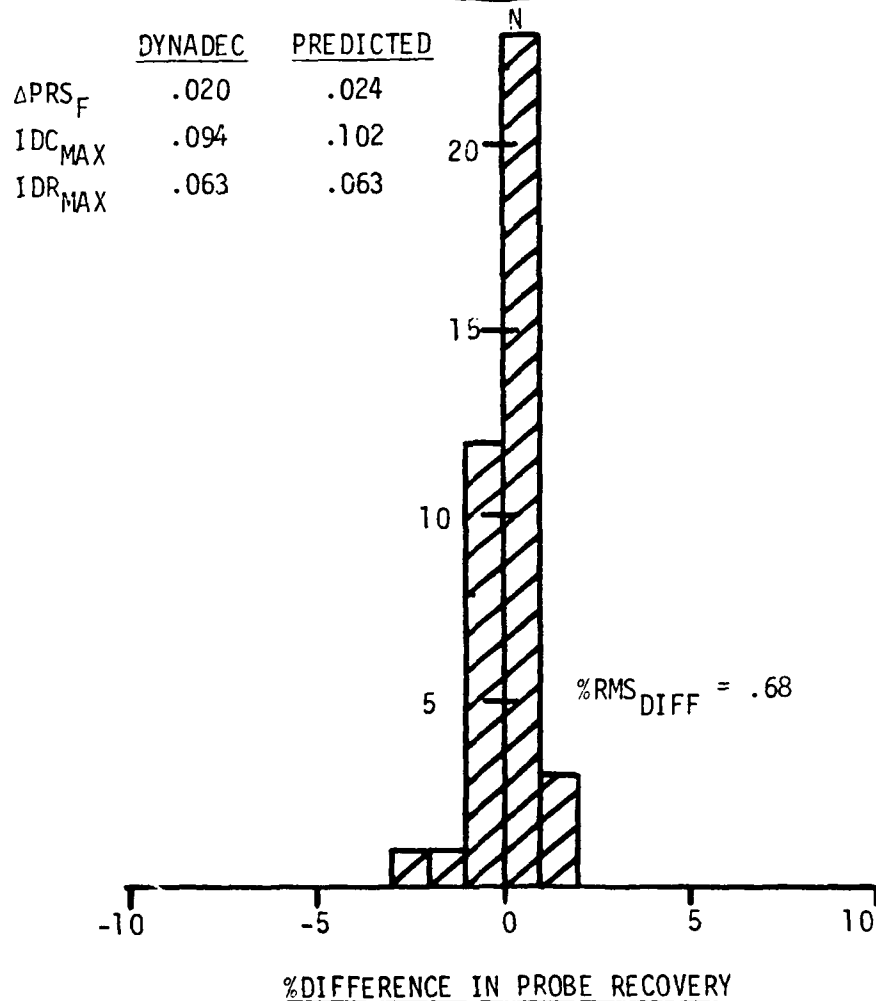
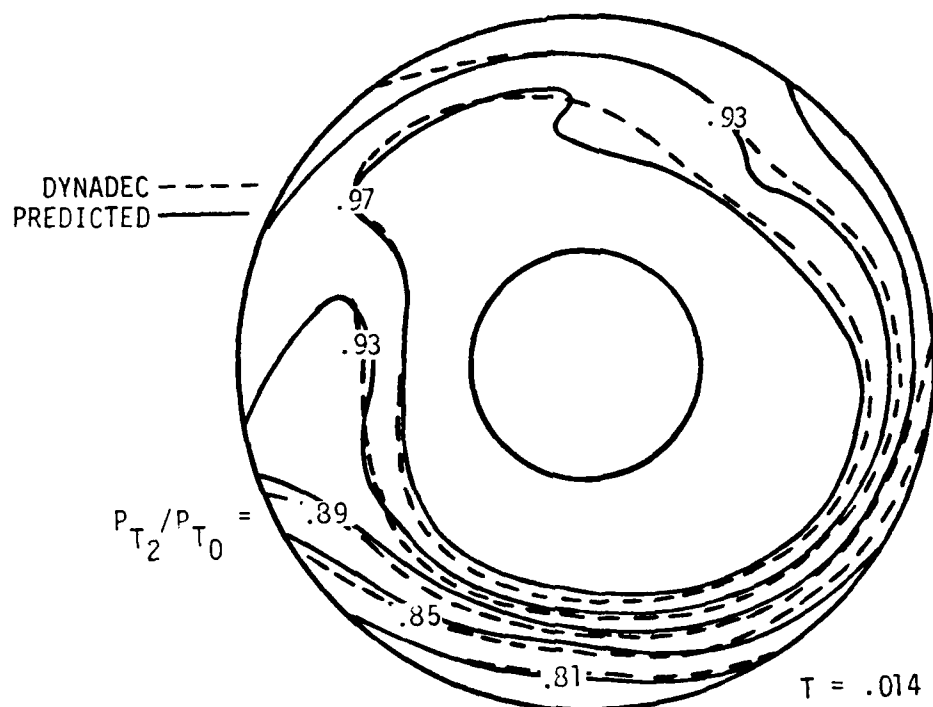
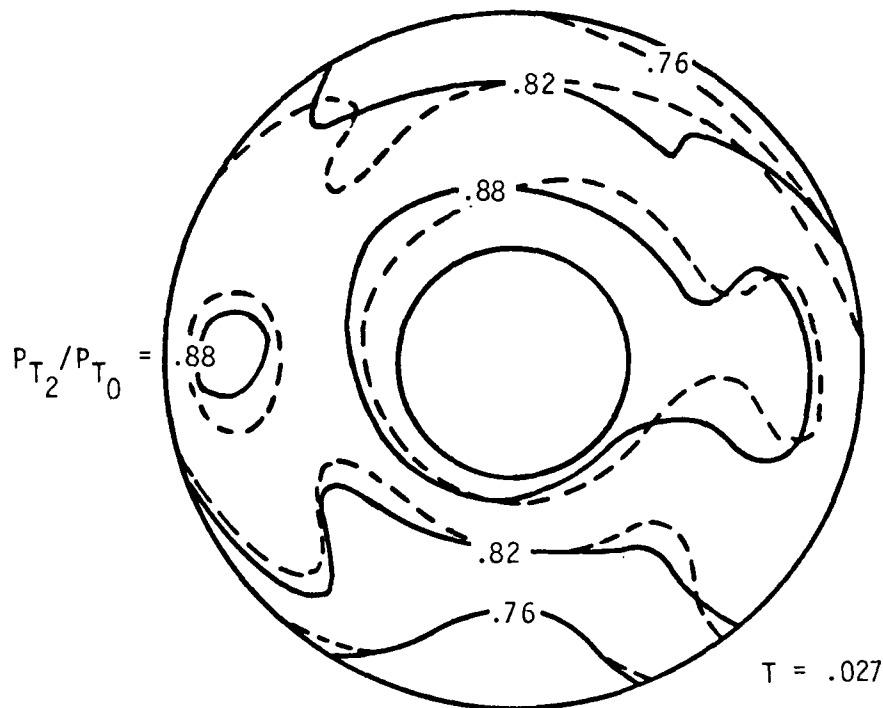


Figure 47 Improved Method (GE_1) - Pressure Contour Map and Histogram, Low Turbulence (Filtered and Map Averaged)

DYNADEC ---
 PREDICTED —



	<u>DYNADEC</u>	<u>PREDICTED</u>
ΔPRS_F	.048	.049
IDC ^{MAX}	.127	.127
IDR ^{MAX}	.033	.030

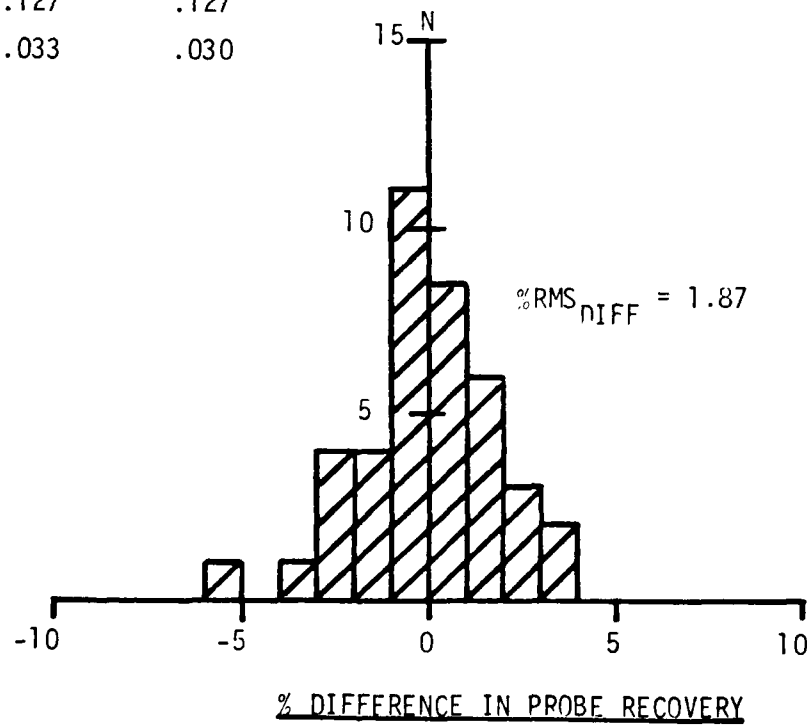


Figure 48 Improved Method (GF_1) - Pressure Contour Map and Histogram, Moderate Turbulence (Filtered and Map Averaged)

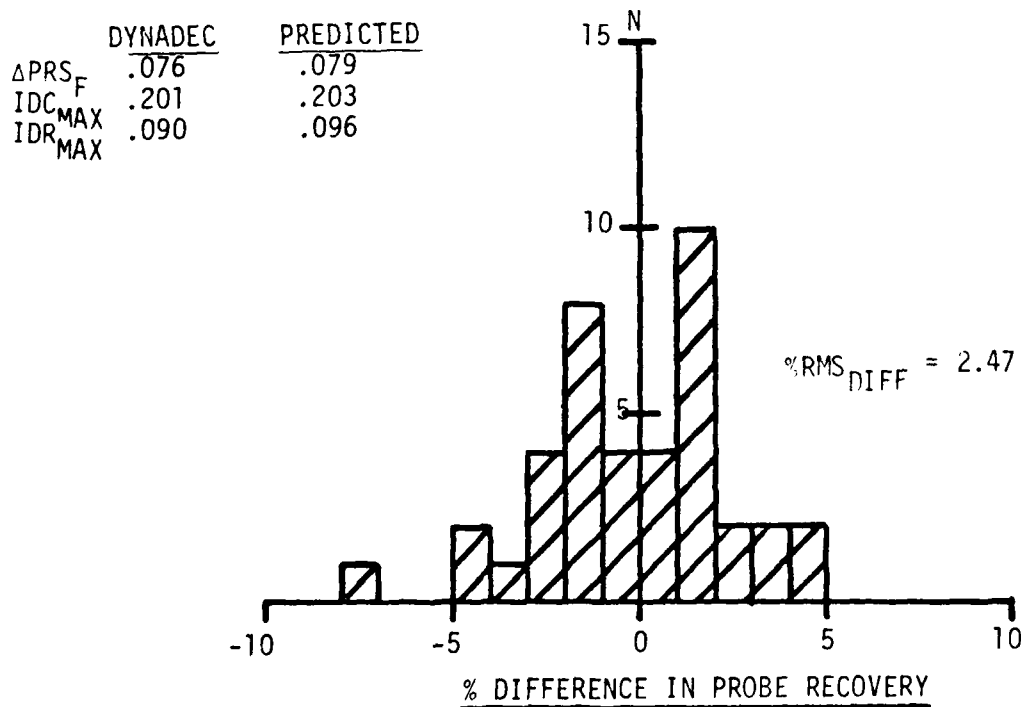
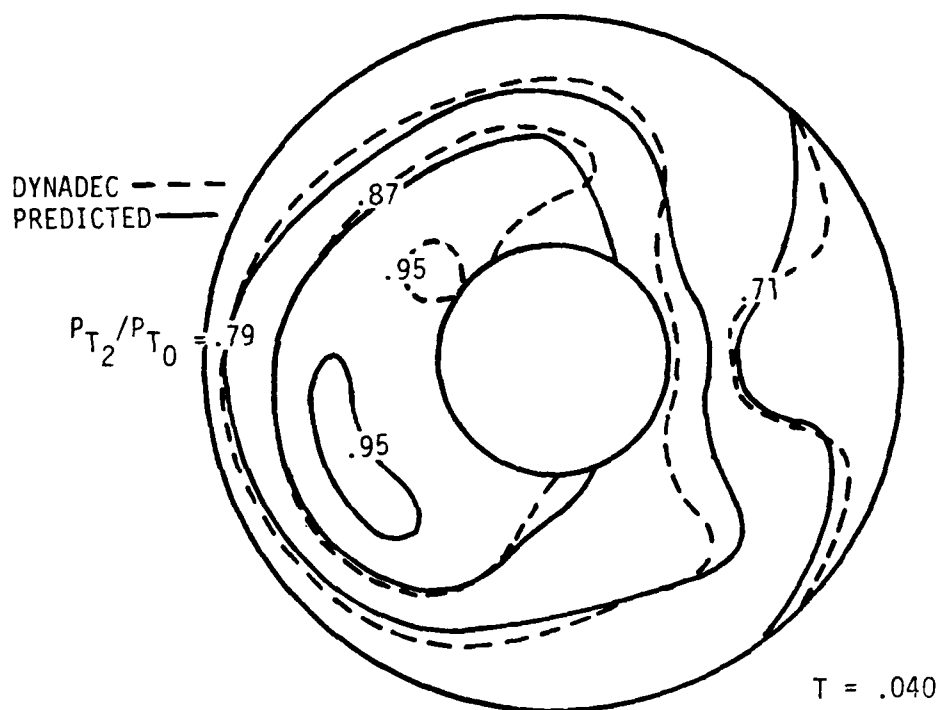


Figure 49 Improved Method (GF_1) - Pressure Contour Map and Histogram, High Turbulence (Filtered and Map Averaged)

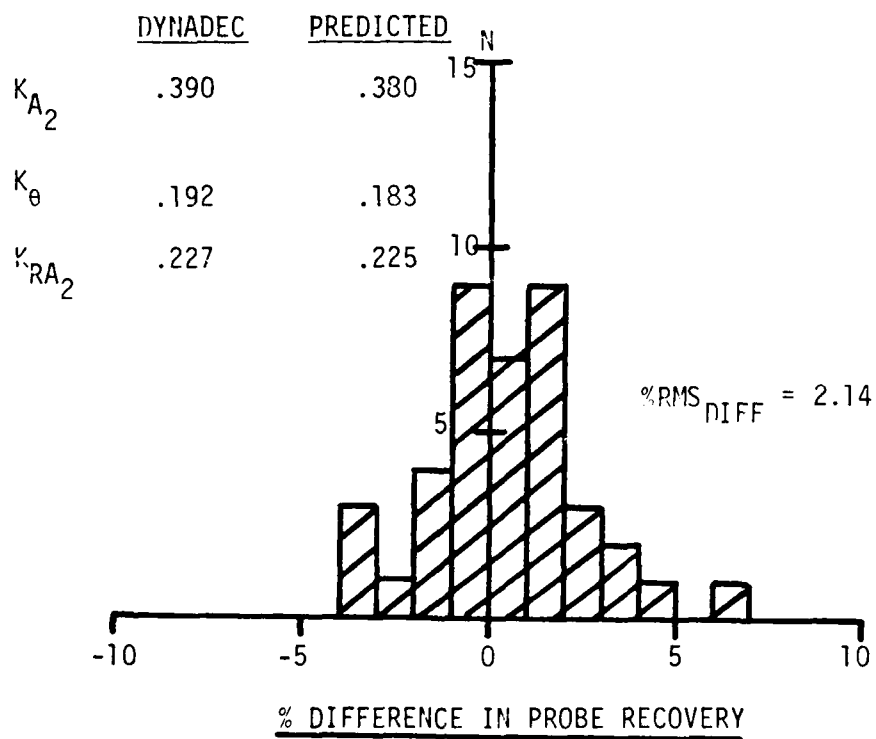
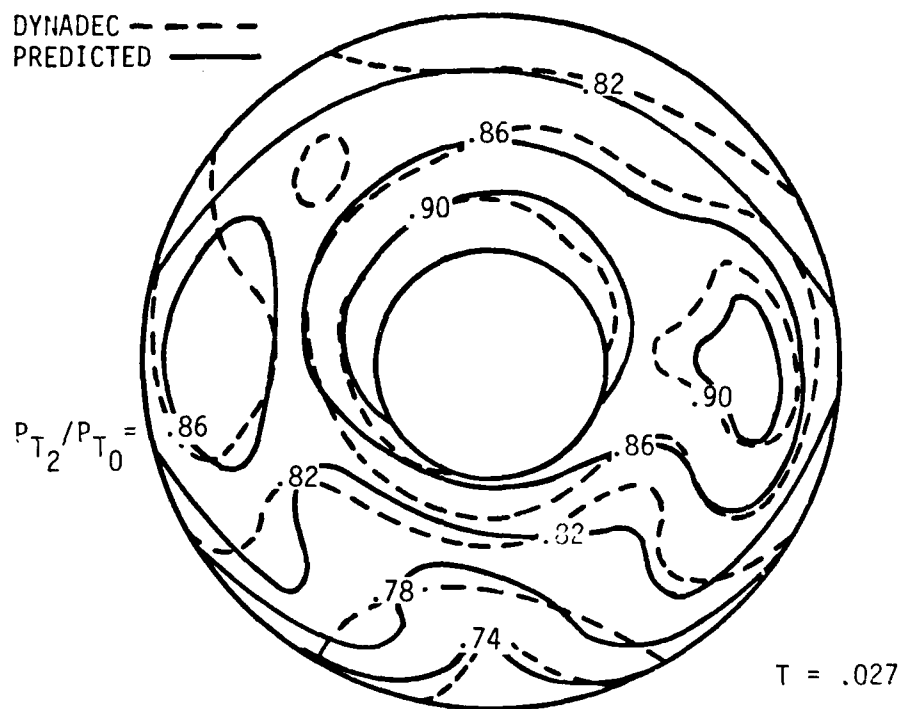
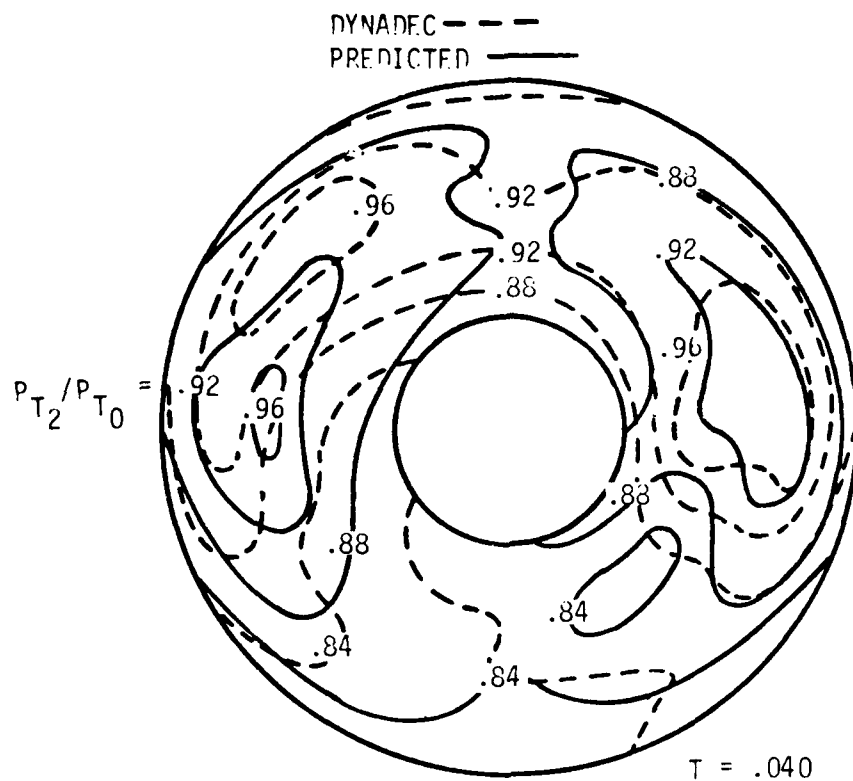


Figure 50 Improved Method (PIA) - Pressure Contour Map and Histogram, Moderate Turbulence (Filtered and Map Averaged)



	<u>DYNADFC</u>	<u>PREDICTED</u>
K_{A2}	.643	.401
K_{θ}	.353	.121
K_{RA2}	.370	.357

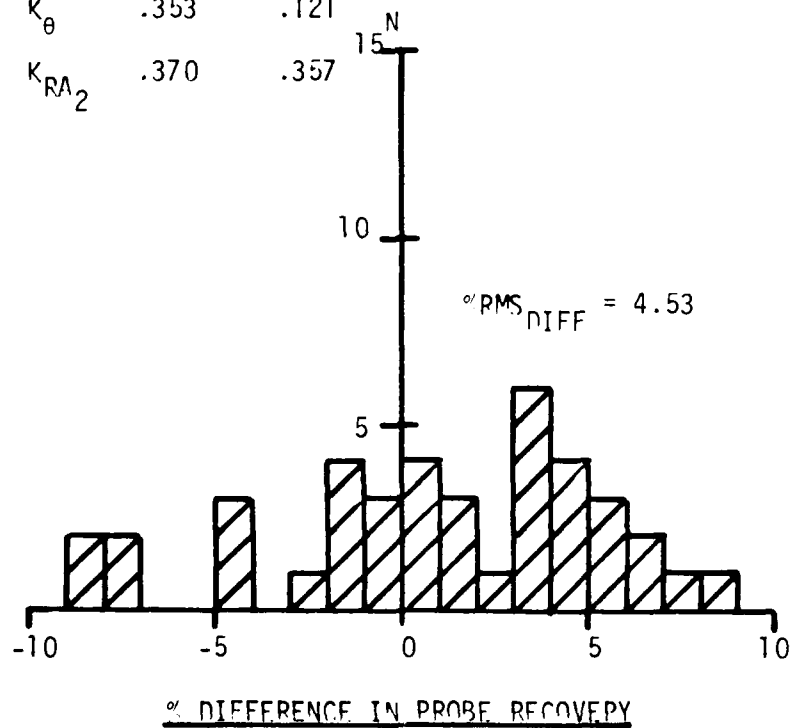
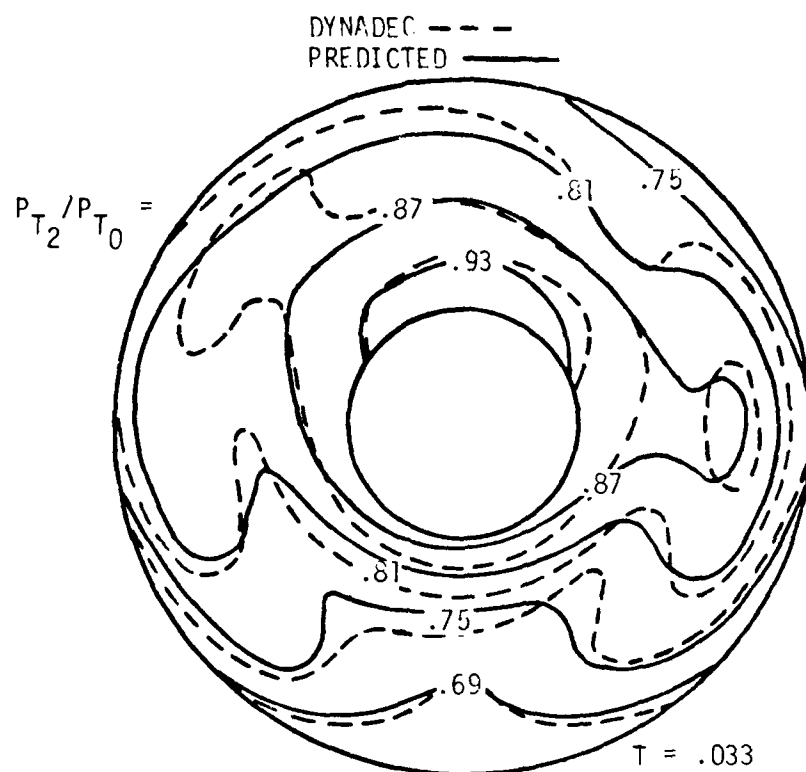


Figure 51 Improved Method (PMA) - Pressure Contour Map and Histogram, High Turbulence (Filtered and Map Averaged)

percent RMS difference increased slightly over the improved model with filtering. This case has a rather complex pattern with two high pressure lobes, and although better results may be achieved with a 180° circumferential distortion pattern, the results again suggest an upper limit of applicability of the improved model with respect to the combination of cut-off filter frequency (1000 HZ) and high-turbulence level (.040). To further define that upper bound, a different case with a turbulence level between the moderate- and high-turbulence level case is presented in Figure 52. Very good agreement exists between predicted and measured contours with the exception in the ten o'clock region of the map. The distortion parameters are in excellent agreement. Twenty-four predicted pressures are within ± 2 percent of their measured values.

The GE_2 moderate-turbulence level case is presented in Figure 53. Very good agreement exists between predicted and measured pressure contours with the exception of contours in the four o'clock region. Excellent agreement exists between predicted and measured levels of total and circumferential distortion. The range of the difference and the percent RMS difference decreased 28 and 40 percent, respectively, over the basic model. The high-turbulence case is shown in Figure 54. Although there is a substantial improvement in the predicted versus measured contours, the distortion parameter levels, the range of difference and percent RMS difference compared to the results obtained with the basic model, there nevertheless are significant differences between the predicted and measured distortion maps. Again, the applicability of the improved model, including map averaging, in this combined region of high-turbulence ($T = .047$) and cut-off frequency is questionable. A lower turbulence level case ($T = .039$) is presented in Figure 55. Better agreement exists between predicted and measured pressure contours, although not as good as that attained for the GE_1 high-turbulence case. Nevertheless, there is excellent agreement between predicted and measured levels of distortion. Eighteen probe pressures are within ± 2 percent of their measured values.

The improvement to the model with filtering and map averaging is summarized in the next six figures using two measures of goodness, the percent RMS difference between predicted and measured probe pressure



	<u>DYNADEC</u>	<u>PREDICTED</u>
K_{A2}	.474	.454
K_{θ}	.339	.337
K_{RA2}	.163	.142

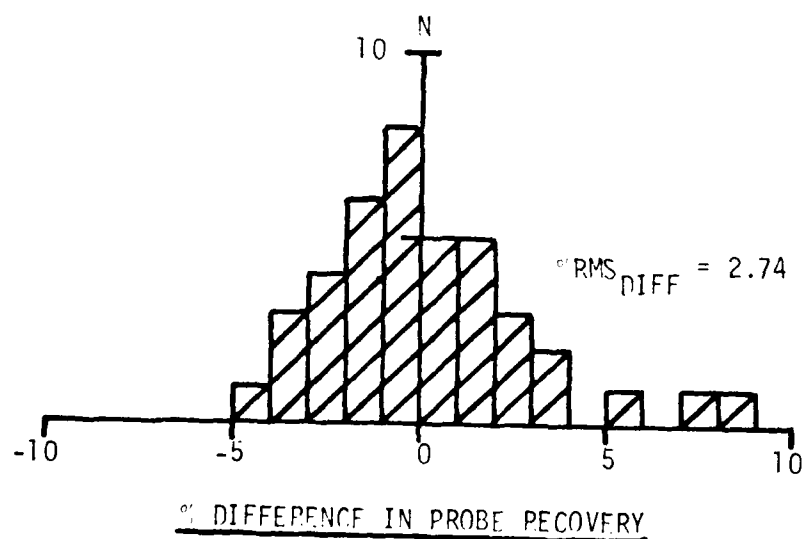


Figure 52 Improved Method (PWA) - Pressure Contour Map and Histogram, Moderate Turbulence (Filtered and Map Averaging)

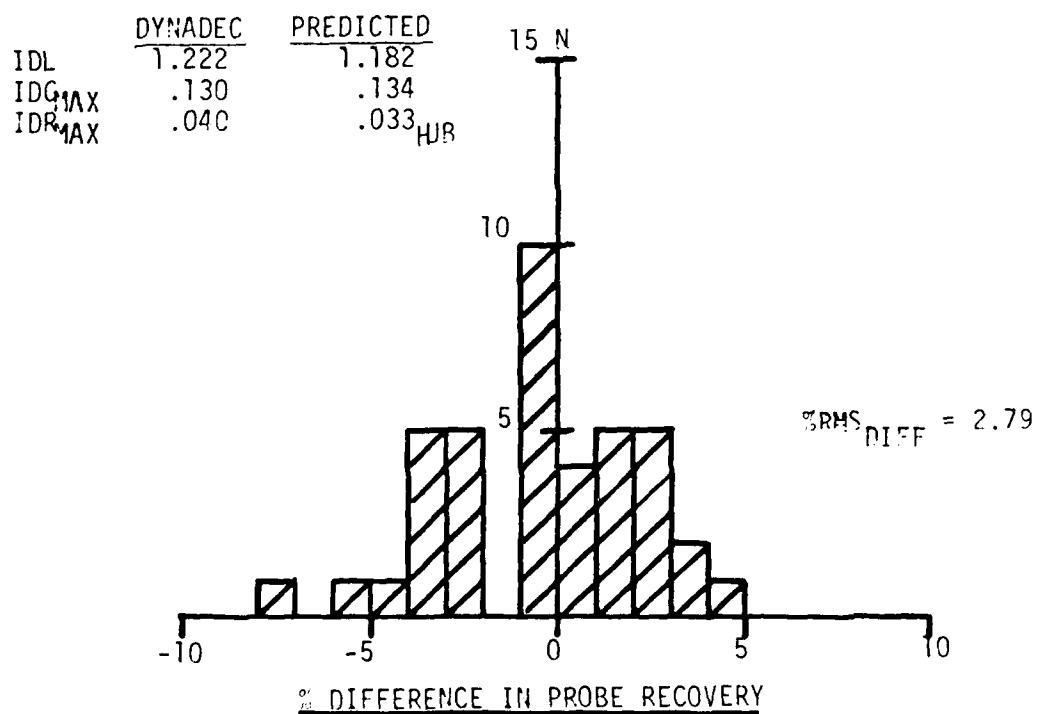
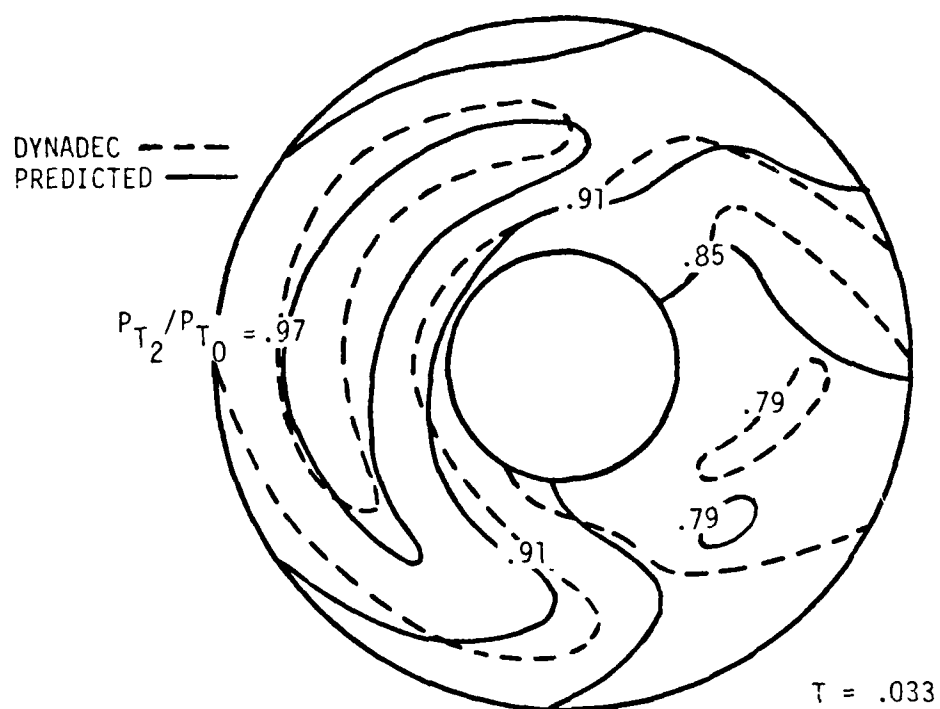


Figure 53 Improved Method (GE₂) - Pressure Contour Map and Histogram, Moderate Turbulence (Filtered and Map Averaged)

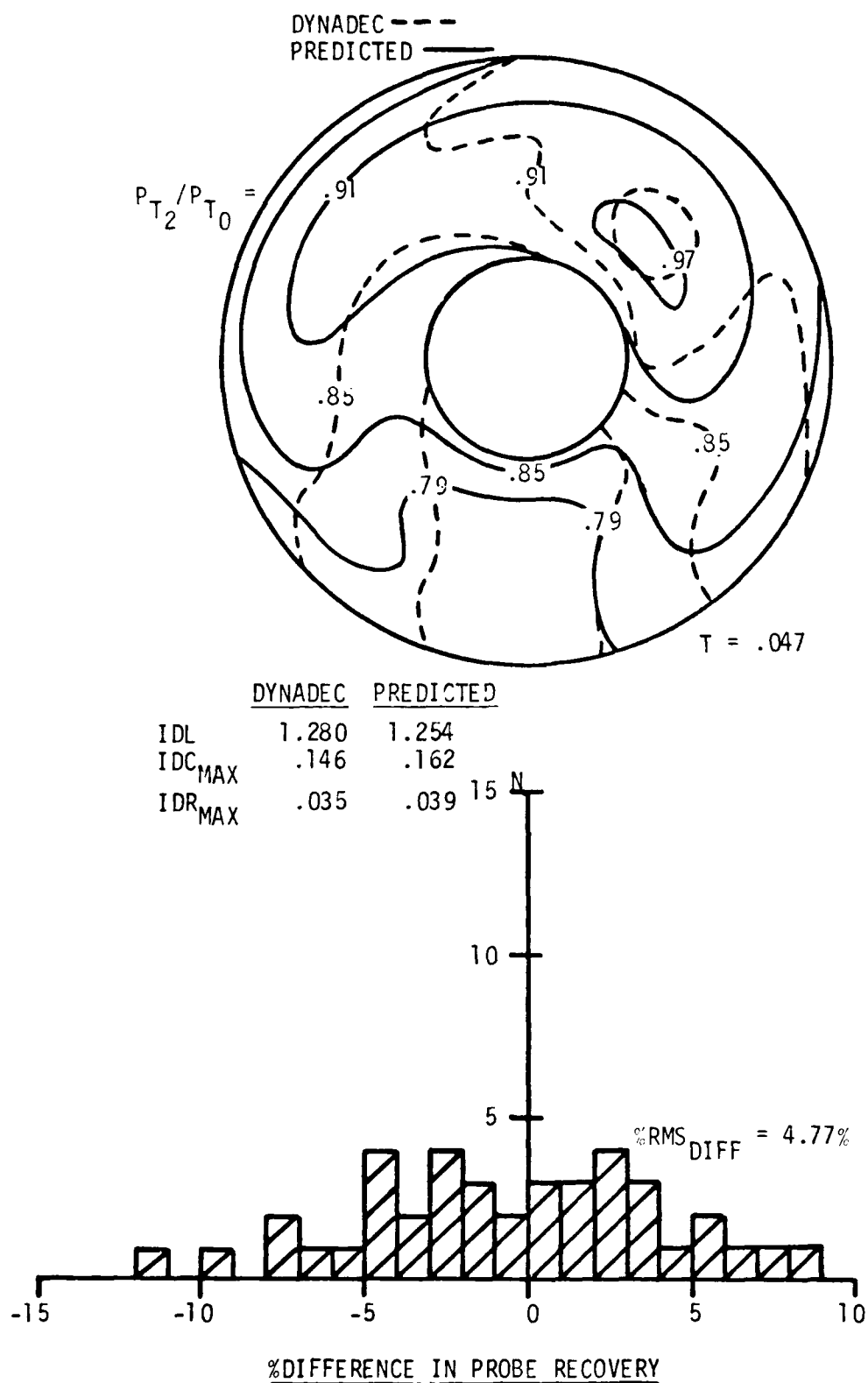


Figure 54 Improved Method (GE_2) - Pressure Contour Map and Histogram, High Turbulence (Filtered and Map Averaged)

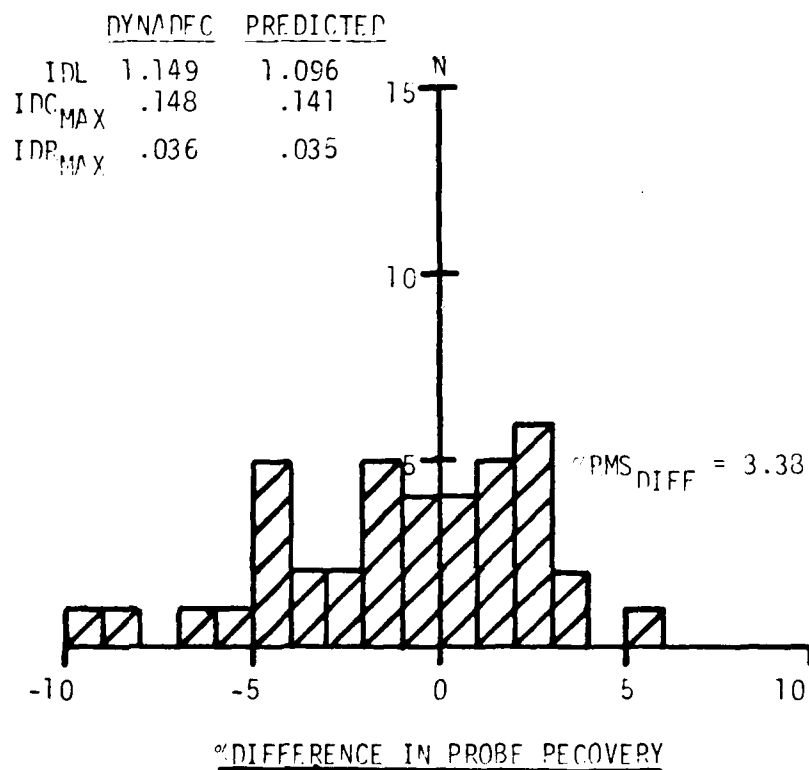
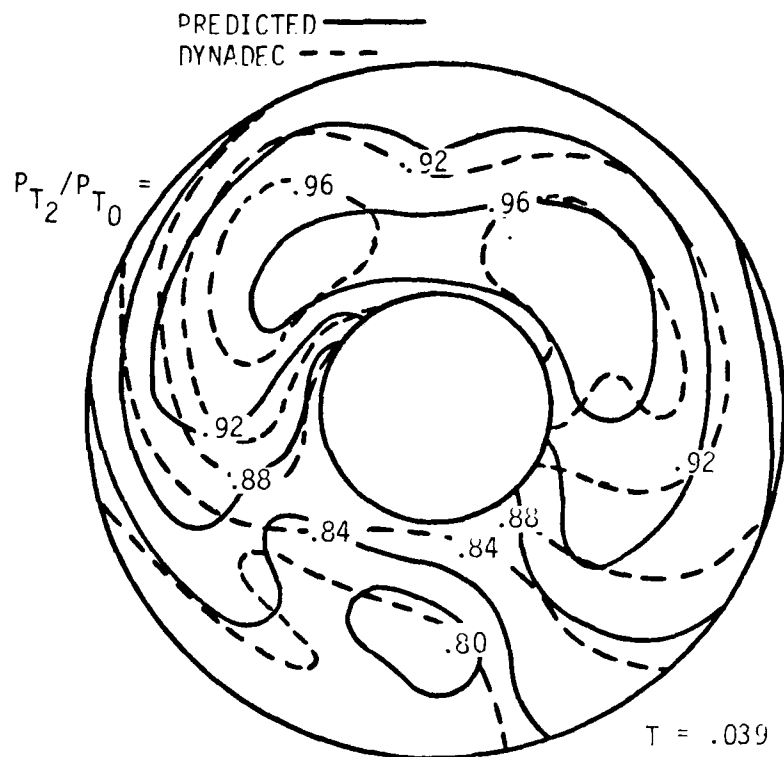


Figure 55 Improved Method (GE_2) - Pressure Contour Map and Histogram, High Turbulence (Filtering and Map Averaged)

recoveries, and the number of probes with predicted values within ± 2 percent of their measured values.

The linear regression lines, Figure 56, illustrate the reduction in the average $\%RMS_{DIFF}$ using filtering and map averaging with the GE_1 distortion parameter methodology. With the exception at low-turbulence levels where there is little difference between the models, the filtering of the random numbers, particularly in combination with map averaging, provides a substantial reduction in the percent RMS difference between predicted and measured pressures. For example, at an average compressor face turbulence level of .04, the average $\%RMS$ difference with map averaging and filtering, is 2.5, a reduction of 56 percent compared to the basic model.

The regression curves in Figure 57 present the other indicator of goodness, the number of synthesized pressures agreeing within ± 2 percent of their measured values using the GE_1 methodology. There is little difference between the basic and improved models for turbulence levels of less than .01 and for levels greater than .06. Maximum benefits with the improved model are in terms of $N(\pm 2\%)$ are in .02 to .04 turbulence range. For a turbulence level of .03, the combined filtering and map averaging offers a substantial improvement in the number of probes predicted to be within ± 2 percent of their measured values. An average of thirty-two pressures are within ± 2 percent of their measured values for the improved model, compared to only eighteen pressures for the basic method.

Figures 58 and 59 present the same summaries with the Pratt & Whitney distortion parameters. The reduction in average $\%RMS_{DIFF}$, Figure 58, is not as dramatic as it was with the GE_1 parameters and is primarily the consequence of filtering the data at a higher cut-off filter frequency. Nevertheless, the filtering and map averaging still provide significant improvements to the pressure contour maps. As was the case with the GE_1 parameters, there is little difference between the basic and improved models at low-turbulence levels. For a turbulence level of .04, the reduction in $\%RMS_{DIFF}$ amounts to 33 percent compared to the basic model.

The effect of the higher cut-off filter frequency is also seen in Figure 59 for the number of predicted pressures within ± 2 percent of

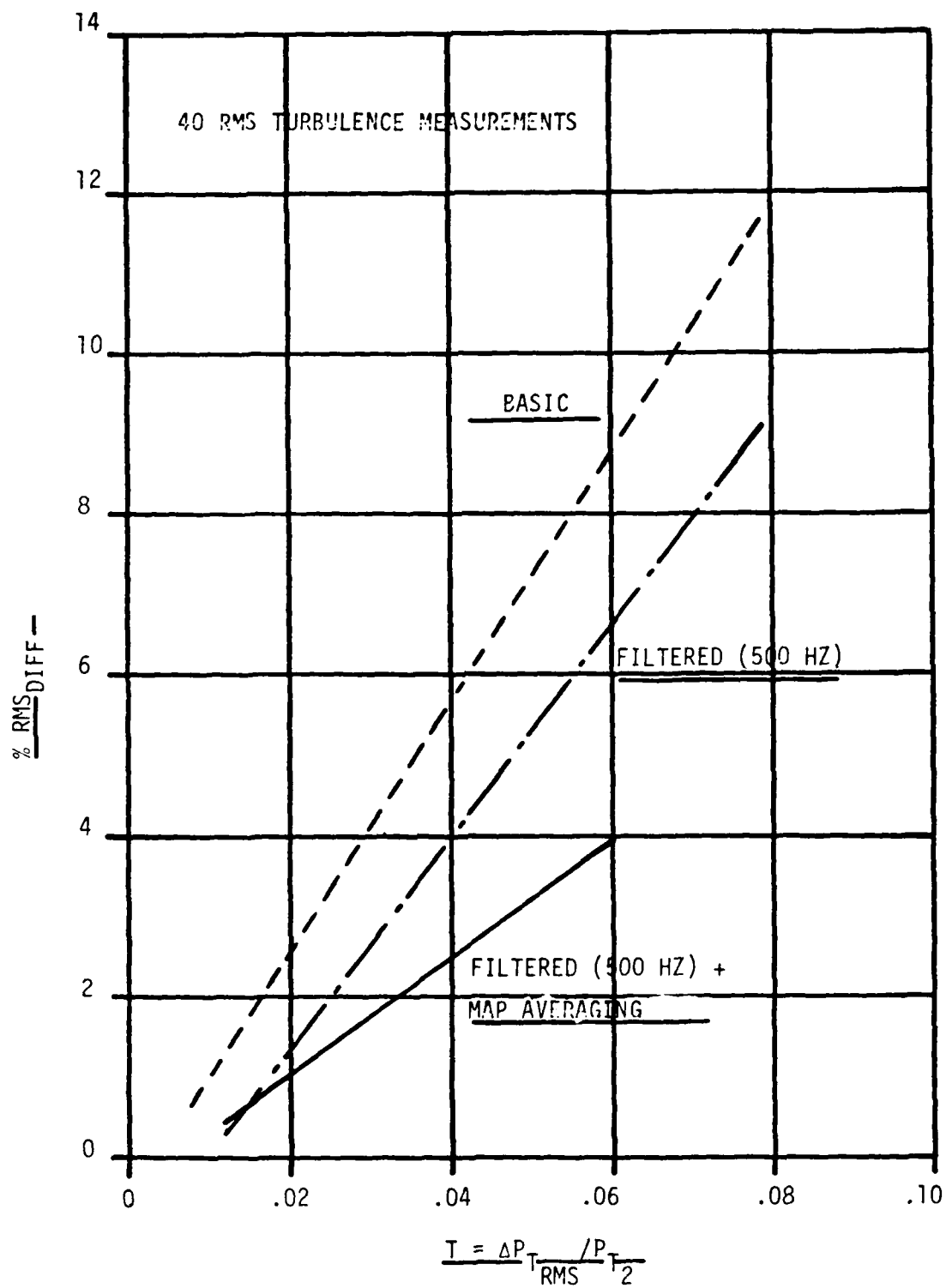


Figure 56 Percent RMS Difference (GE_1)

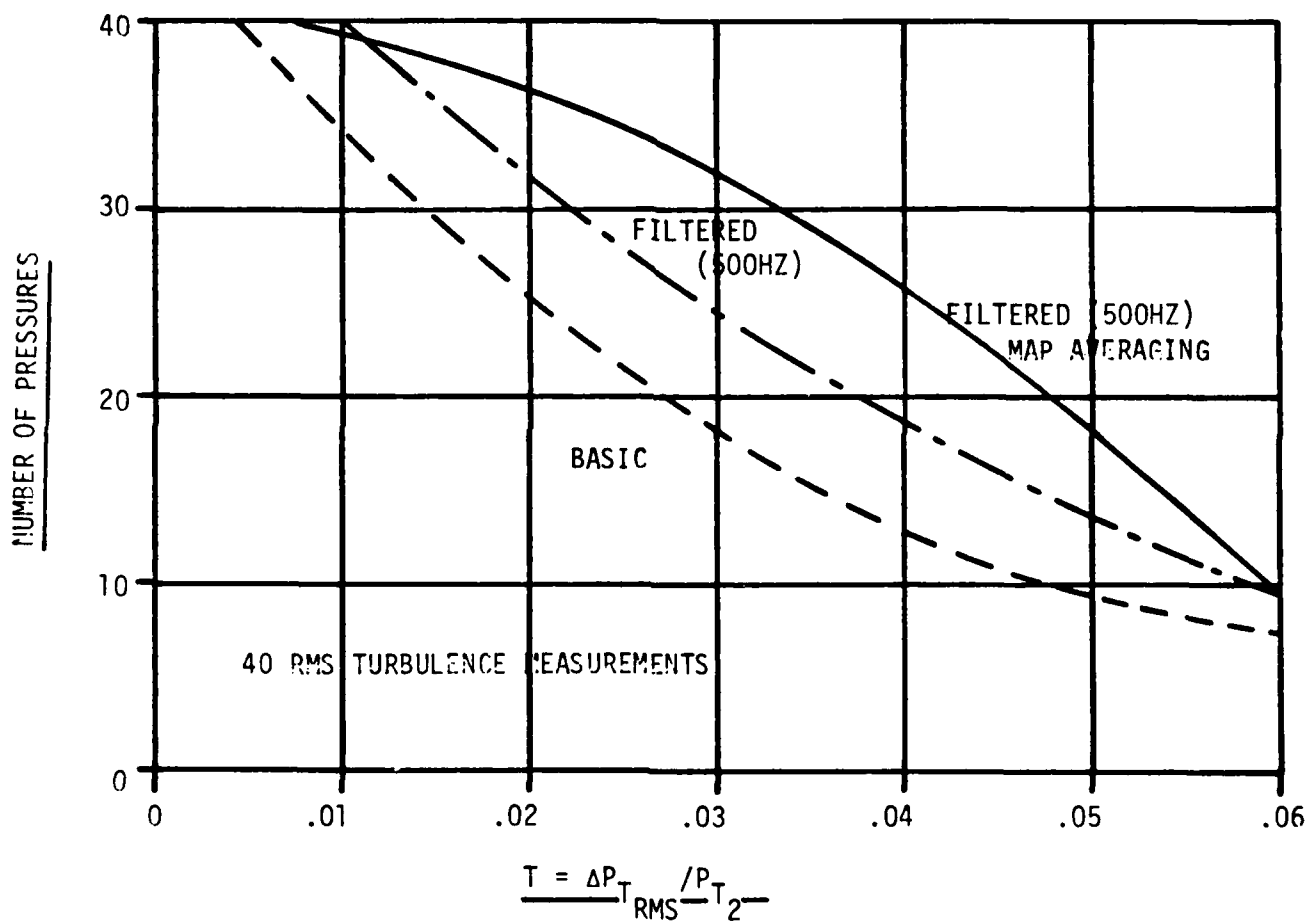


Figure 57 Predicted Pressures within $\pm 2\%$ Measured P_{T1} (GE_1)

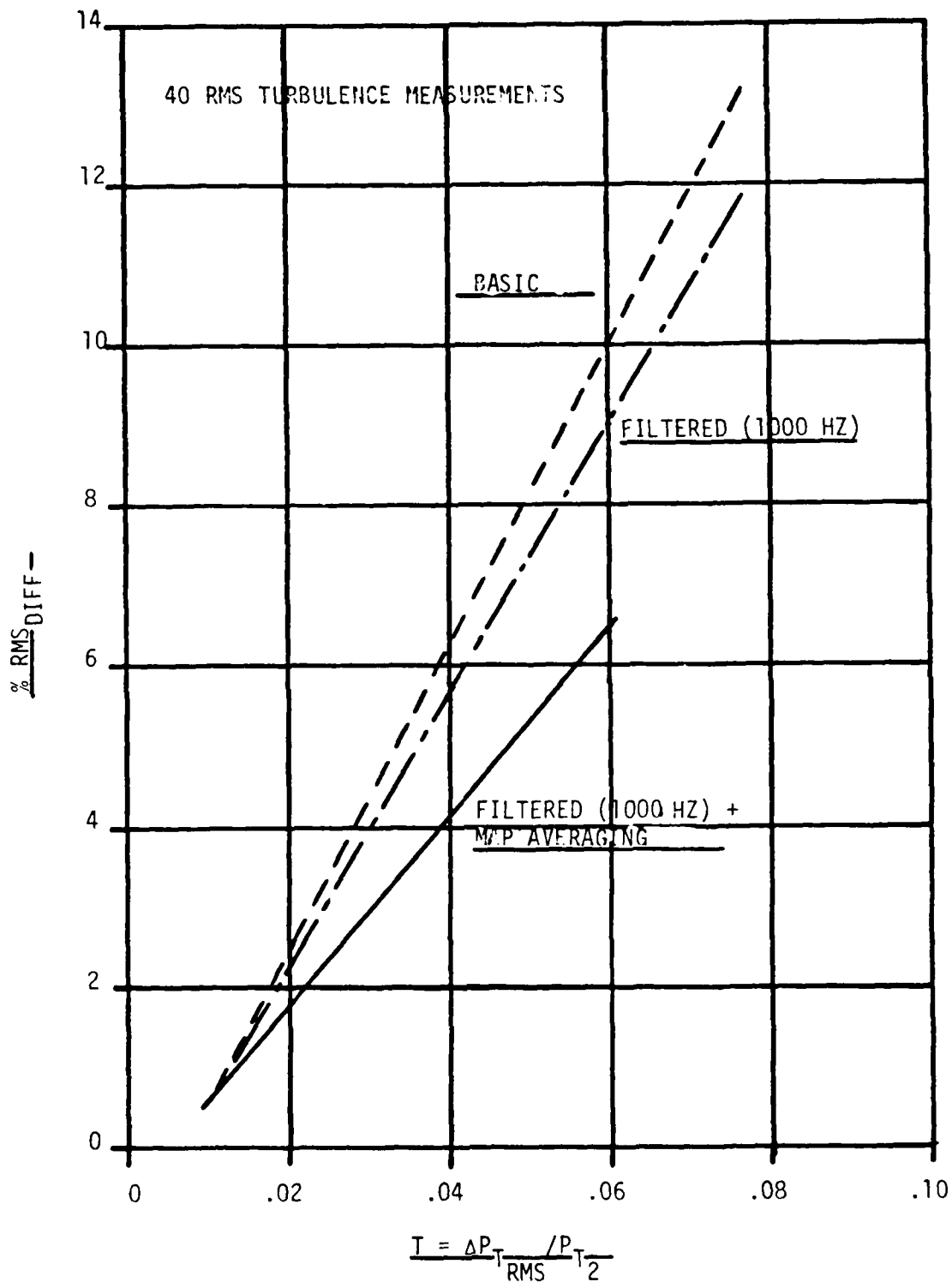


Figure 58 Percent RMS Difference (PIA)

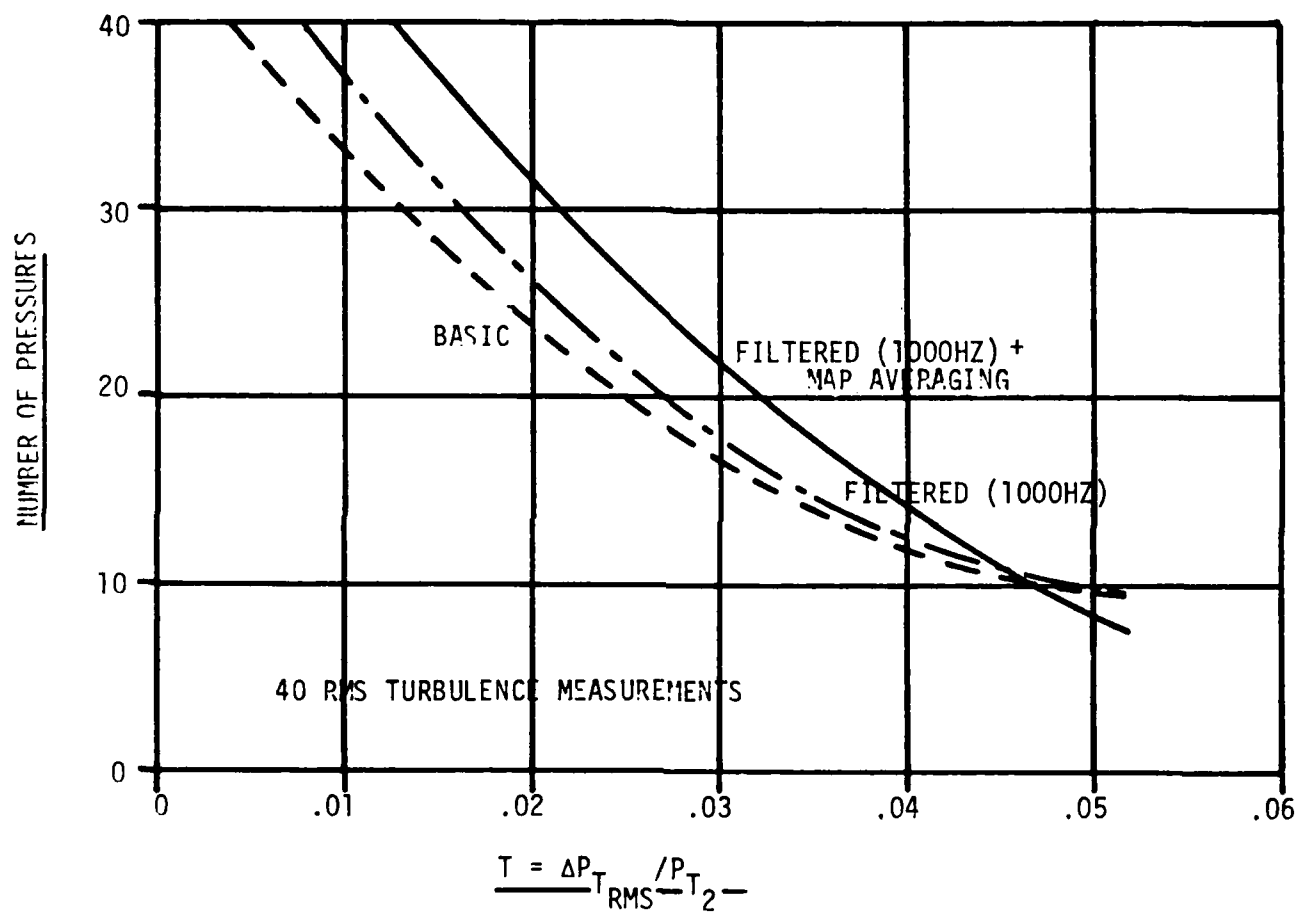


Figure 59 Predicted Pressures within +2% Measured P_{T_i} (PWA)

their measured values. The overall levels of the regression curves with the filtering and map averaging are lower compared to the results in Figure 57. For example, at a turbulence level of .03, an average of twenty-two probes are within ± 2 percent of their measured values. As before, there is little difference between the models at higher turbulence levels ($T > .04$). Substantial benefits can be had with the improved method for turbulence levels as low as .01.

Summaries for the GE_2 distortion parameters are presented in Figures 60 and 61. The average percent RMS difference as a function of turbulence is presented in Figure 60. As was the case with the other two sets of distortion parameters, there is little difference between the basic and improved models for turbulence levels of less than .01. The reduction in the average $\%RMS_{DIFF}$ for the improved model with map averaging, as compared to the basic model results, is not great is that attained with the GE_1 distortion parameters. At a turbulence level of .04, for example, the reduction in $\%RMS_{DIFF}$ amounts to 39 percent as compared to 56 percent with the GE_1 parameters.

The number of predicted pressures agreeing within ± 2 percent of their measured values with the GE_2 parameters is shown in Figure 61. The shapes of the curves are the same as those for the GE_1 parameters, but at a somewhat lower level. At a turbulence level of .03, the average number of predicted pressures within ± 2 percent of their measured values is twenty-four. There is little difference between the models at turbulence levels of less than .01 and for levels exceeding .05.

In summary, it has been shown that substantial improvements can be made to the predicted pressure distortion maps by filtering the synthesized pressure data and by averaging the pressures from several maximum distortion maps. The quality of the distortion map is a function of the turbulence level and cut-off filter frequency defining engine sensitivity. Relative differences between Figures 56, 58, and 60 suggest that depending on the inlet turbulence level, the improved model appears limited to cut-off filter frequencies of less than 1500 HZ.

Prediction Model Using Eight Turbulence Values

The analysis thus far has been based on forty measured turbulence values. Comparisons between predicted and measured pressure contour maps

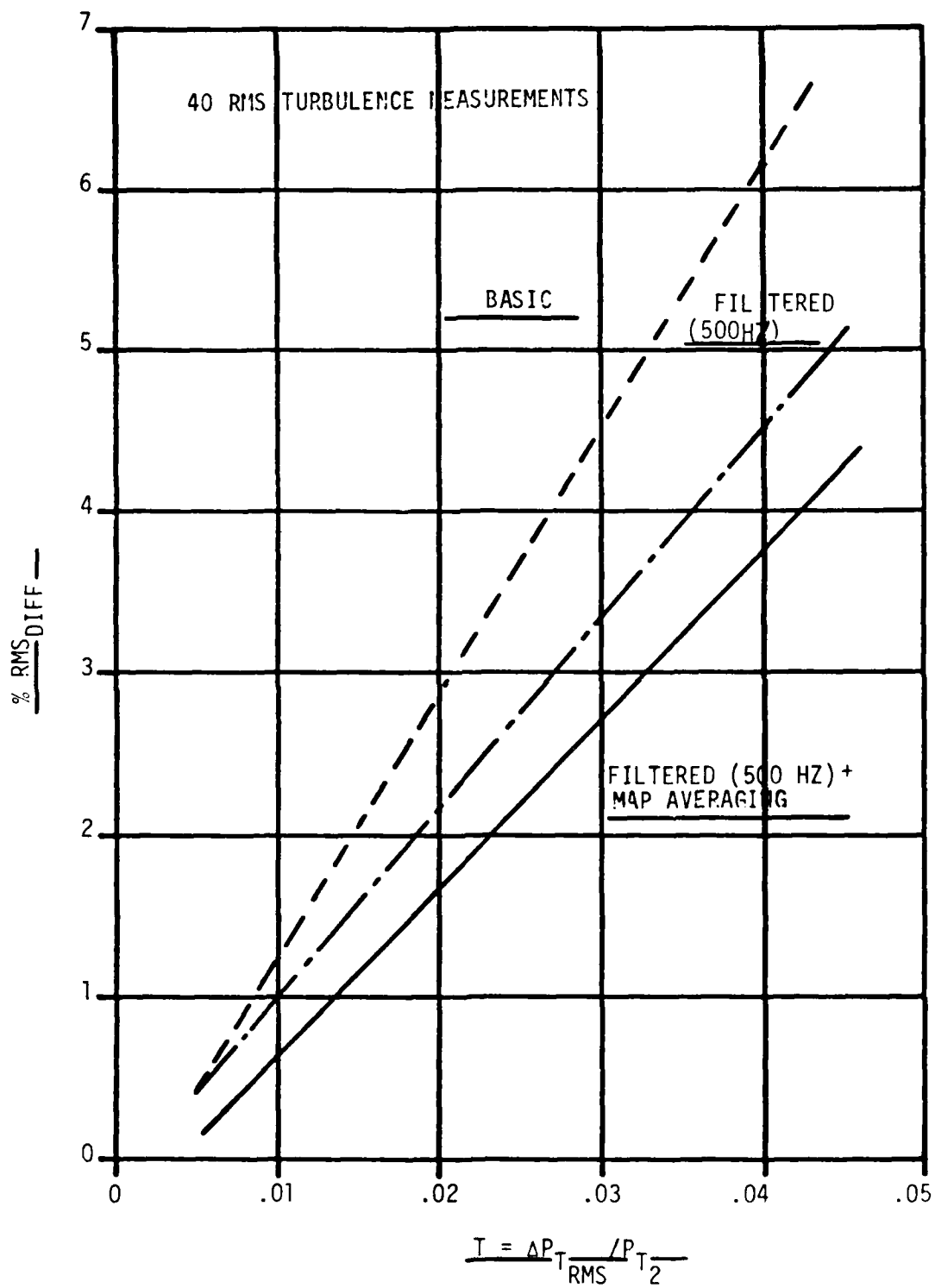


Figure 60 Percent RMS Difference (GE_2)

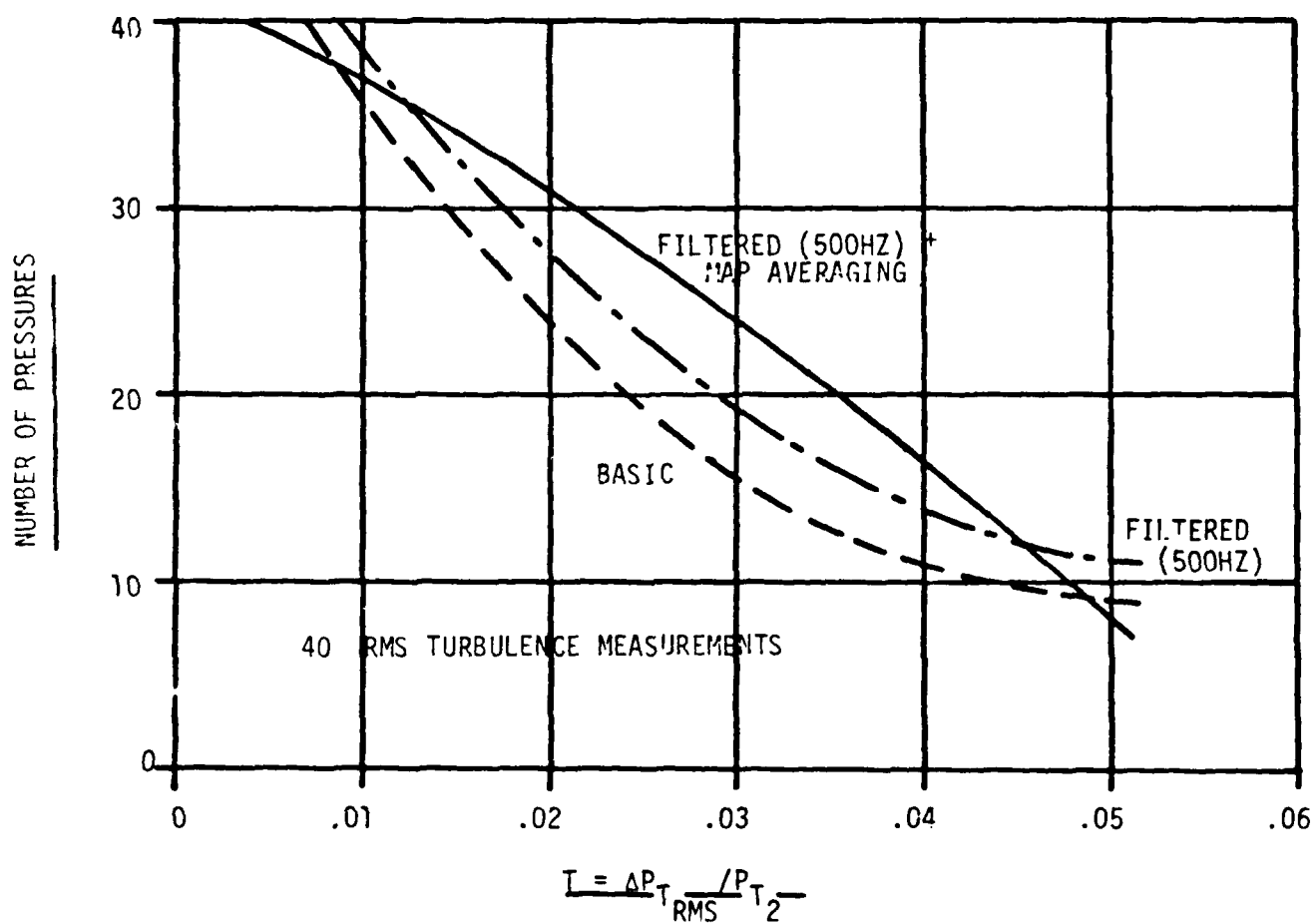


Figure 61 Predicted Pressures within $\pm 2\%$ Measured P_{T_i} (GE_2)

are now presented using eight measured values. The turbulence distribution for each ring is assumed to be the same as that for the third ring of the eight-rake by five-ring array.

Contour maps and histograms based on the GE_1 distortion parameter methodology are presented in the next three figures. The low-turbulence case, previously shown, is presented in Figure 62. Compared to the results based on forty measurements, Figure 47, the range of difference increased from 4 to 8 percent, the number of predicted pressures within ± 2 percent of their measured values decreased from thirty-nine to thirty-five, and the $\%RMS_{DIFF}$ almost doubled to a value of 1.30. Nevertheless, there is excellent agreement between the predicted and measured pressure contours. The moderate-turbulence case is shown in Figure 63. The only difference between the results presented here and those based on forty measurements, Figure 48, is the slightly different distribution in the histogram depicting the difference between predicted and measured probe recoveries. Otherwise, there is excellent agreement between predicted and measured pressure contours and the distortion parameter components, with no change in the range and the number of pressures within ± 2 percent of their measured values. Essentially the same results were obtained for the high-turbulence case, Figure 64. All the indications of goodness; the pressure contours, the distortion levels, and the distribution of the difference in probe recovery show virtually identical results to that based on forty turbulence measurements.

Figure 65 presents for the moderate-turbulence case, the predicted and measured contour maps with the PWA distortion parameter methodology. The agreement between the two maps is considered very good, with some discrepancies in the high recovery contours. The predicted and measured distortion levels are in excellent agreement. In addition, the percent RMS difference between predicted and measured pressure recoveries is identical with the results based on forty measurements. The number of probes agreeing to within ± 2 percent of their measured values decreased to twenty-six, compared to twenty-nine based on forty turbulence measurements.

Finally, the moderate-turbulence case with the GE_2 distortion parameters is shown in Figure 66. Virtually the same results have been attained as that for the distortion map based on forty measurements,

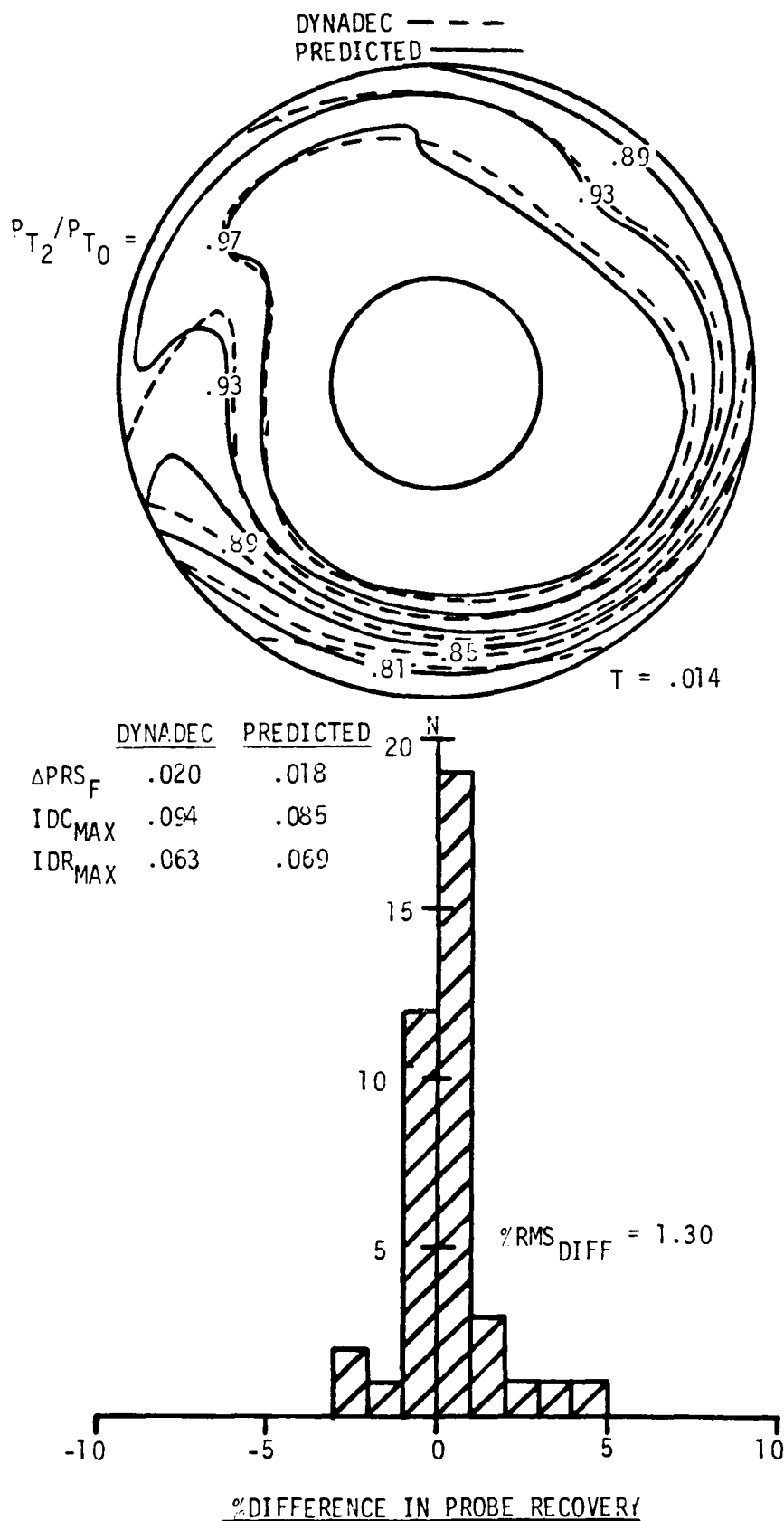
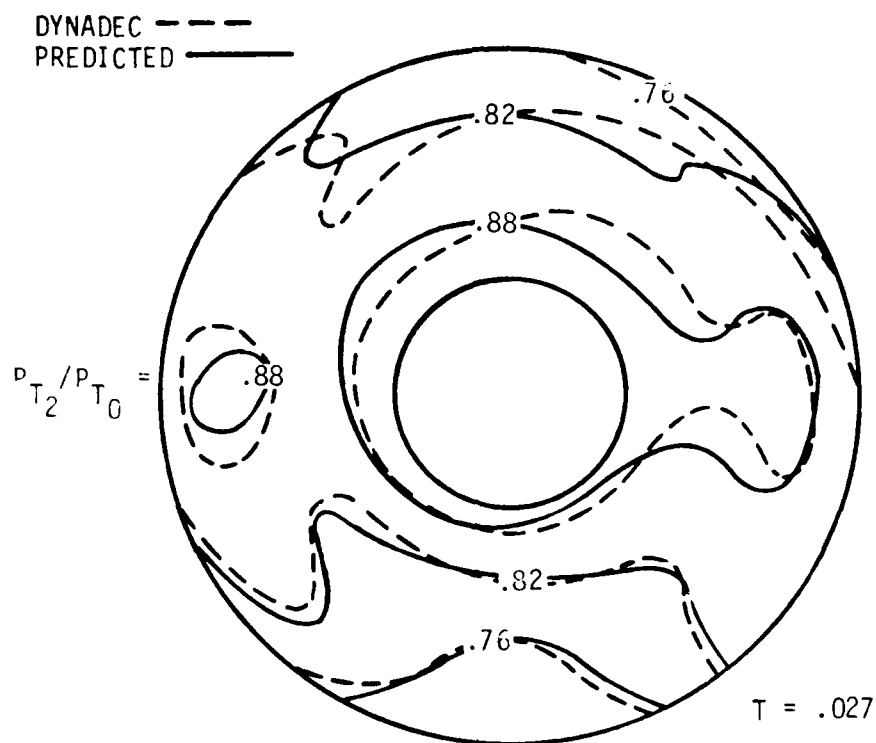


Figure 62 Improved Method (GE_1) - Pressure Contour Map and Histogram - 8 RMS Turbulence Measurements, Low Turbulence



	<u>DYNADEC</u>	<u>PREDICTED</u>
ΔPRS_F	.048	.049
IDC_{MAX}	.127	.126
IDR_{MAX}	.033	.029

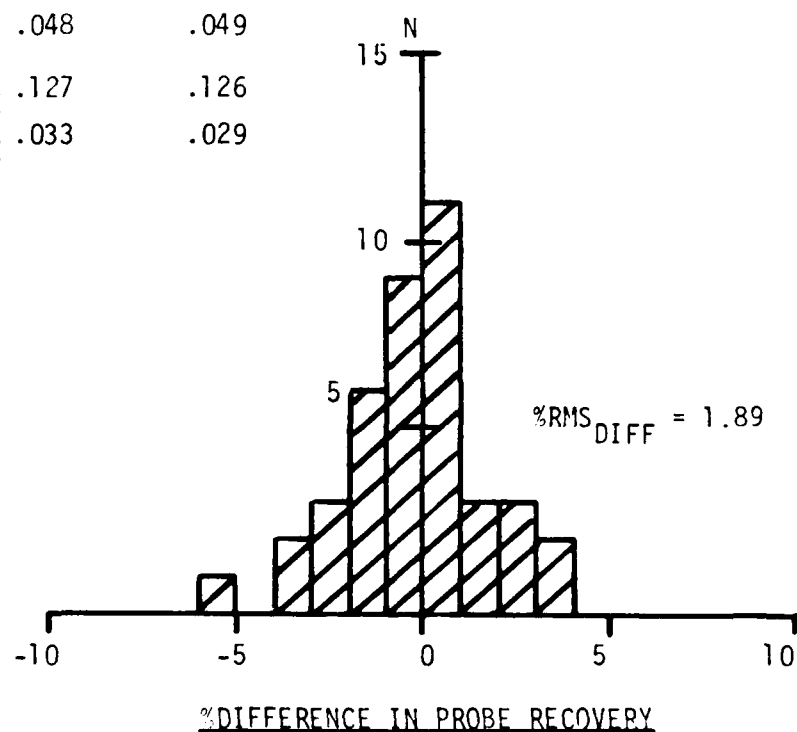
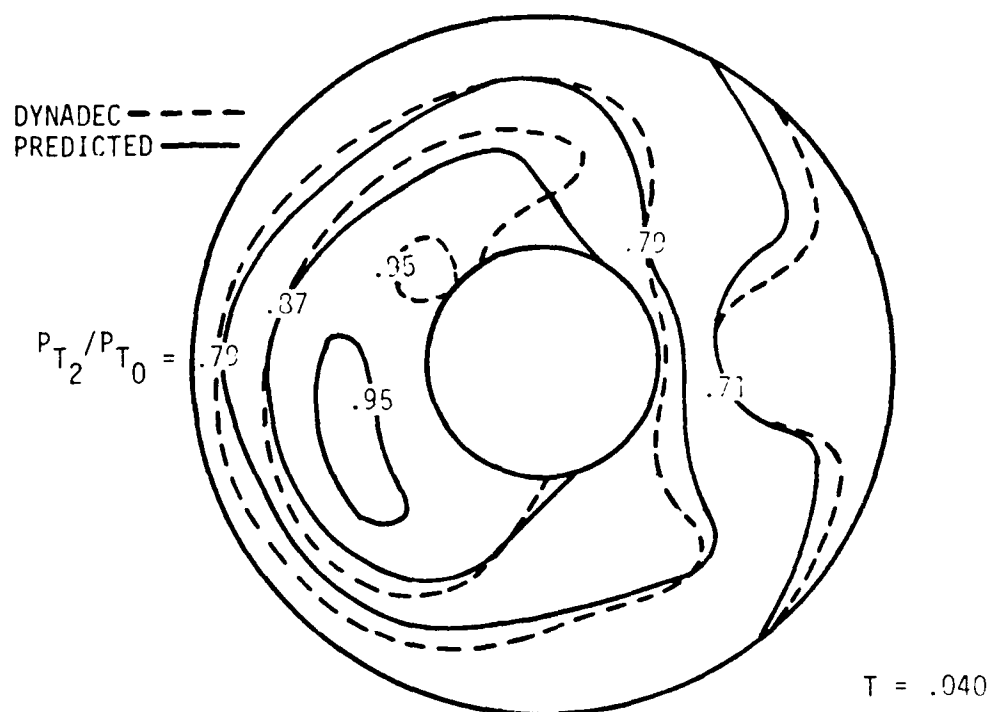


Figure 63 Improved Method (GE_1) - Pressure Contour Map and Histogram - 8 RMS Turbulence Measurements, Moderate Turbulence



	<u>DYNADEC</u>	<u>PREDICTED</u>
ΔPRS_F	.076	.078
IDC _{MAX}	.201	.201
IDR _{MAX}	.090	.099

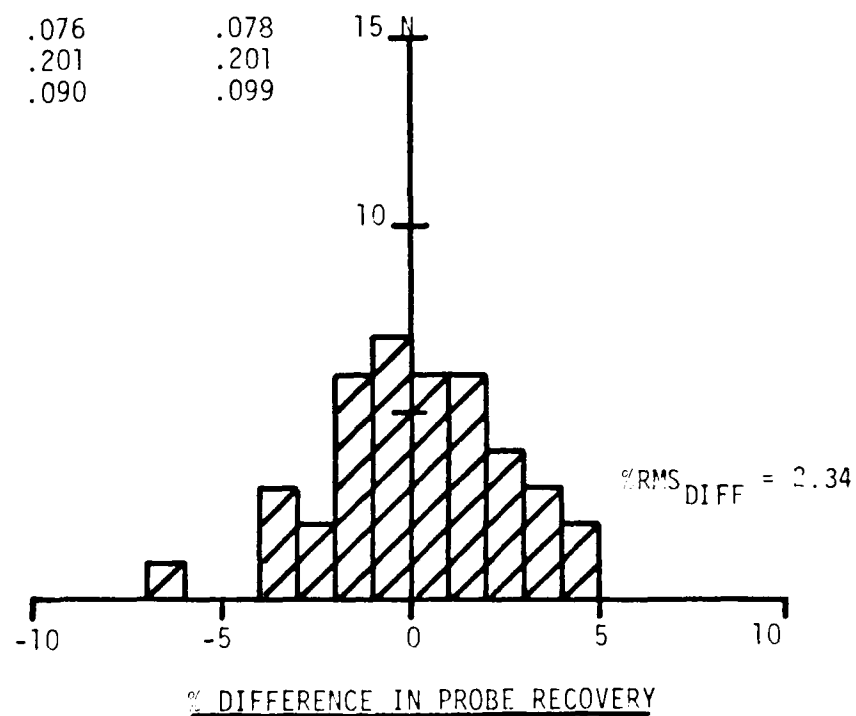
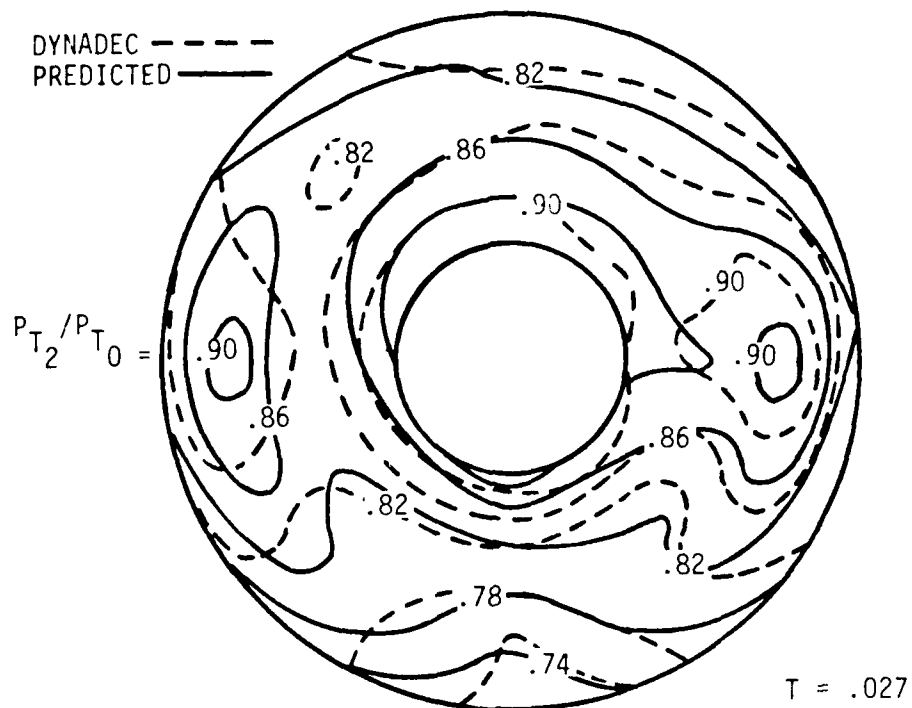


Figure 64 Improved Method (GE_1) - Pressure Contour Map and Histogram - 8 RMS Turbulence Measurements, High Turbulence



	<u>DYNADEC</u>	<u>PREDICTED</u>
K_{A2}	.390	.380
K_e	.192	.183
K_{RA2}	.227	.225

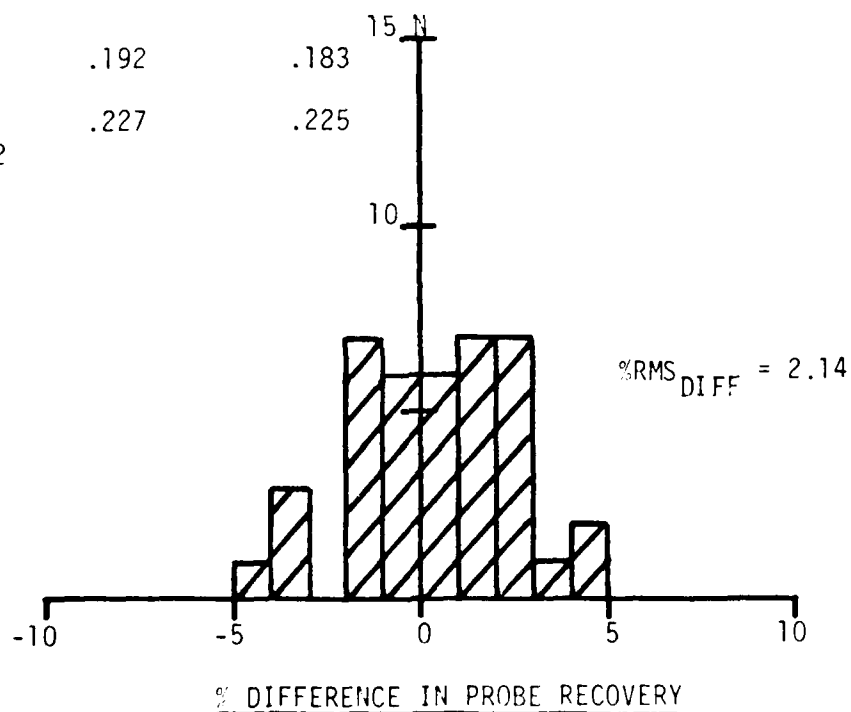
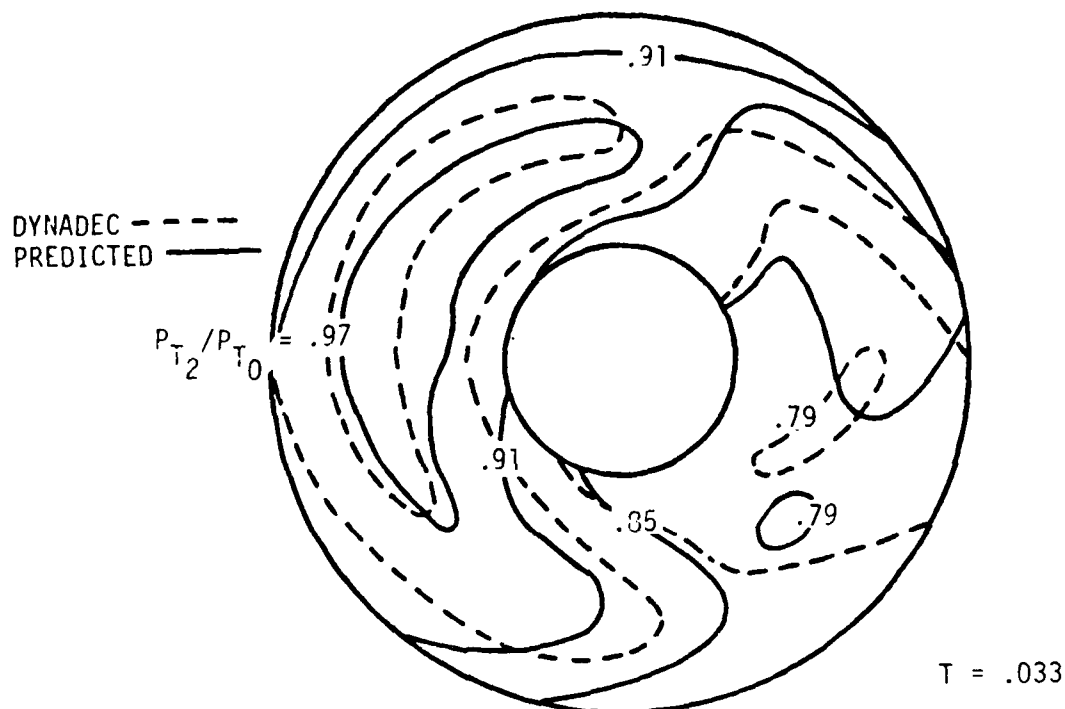


Figure 65 Improved Method (PIA) - Pressure Contour Map and Histogram - 8 RMS Turbulence Measurements, Moderate Turbulence



	<u>DYNADEC</u>	<u>PREDICTED</u>
IDL	1.222	1.143
IDC	.130	.134
IDR ^{MAX}	.040	.025 _{HUB}

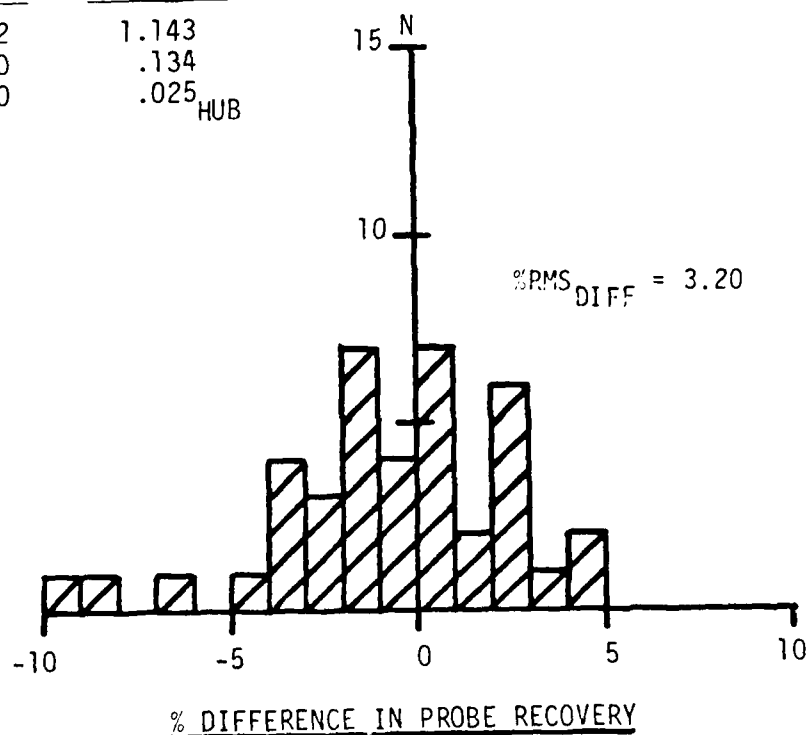


Figure 66 Improved Method (GE_2) - Pressure Contour Map and Histogram - 2.8 RMS Turbulence Measurements, Moderate Turbulence

Figure 53. The percent RMS difference is 3.2, an increase of 15 percent. The range of difference has increased slightly and the number of predicted pressures within ± 2 percent of their measured value remains essentially the same.

Figure 67 presents a comparison of $\%RMS_{DIFF}$ based on eight and forty turbulence measurements for all three sets of engine distortion parameters. With the exception of the small difference at low-turbulence levels with the GE_1 and GE_2 distortion parameters, the effect of using fewer measured turbulence values on the average percent RMS difference between predicted and measured probe recoveries is small. A similar conclusion can be reached upon examining the effect of fewer turbulence measurements on the average number of predicted pressures within ± 2 percent of their measured values shown in Figure 68.

An examination of the magnitude of the terms of the equation defining dynamic total pressure recovery, in particular the fluctuating pressure component term, would suggest that the recovery term and the random number dominate the turbulence value. Consequently, only a reasonable estimate of probe turbulence is required to predict the most probable maximum distortion pressure contour map. Previous investigators have shown that the maximum distortion level can be predicted just as well with fewer turbulence measurements as with forty values. This study has shown that a good estimate of the pressure contour map is possible with fewer turbulence measurements as well.

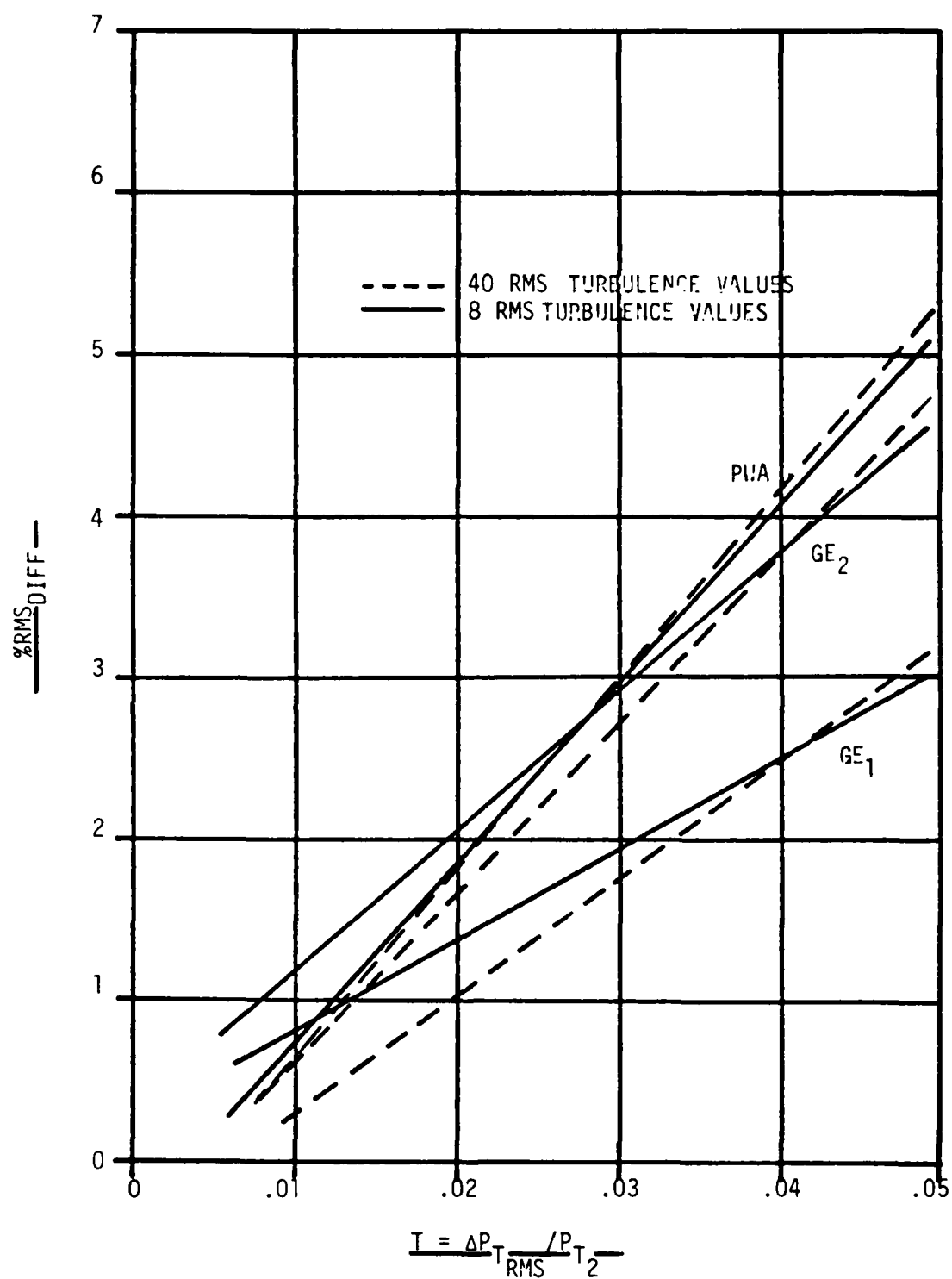


Figure 67 Percent RMS Difference (8 vs 40 RMS Turbulence Values)

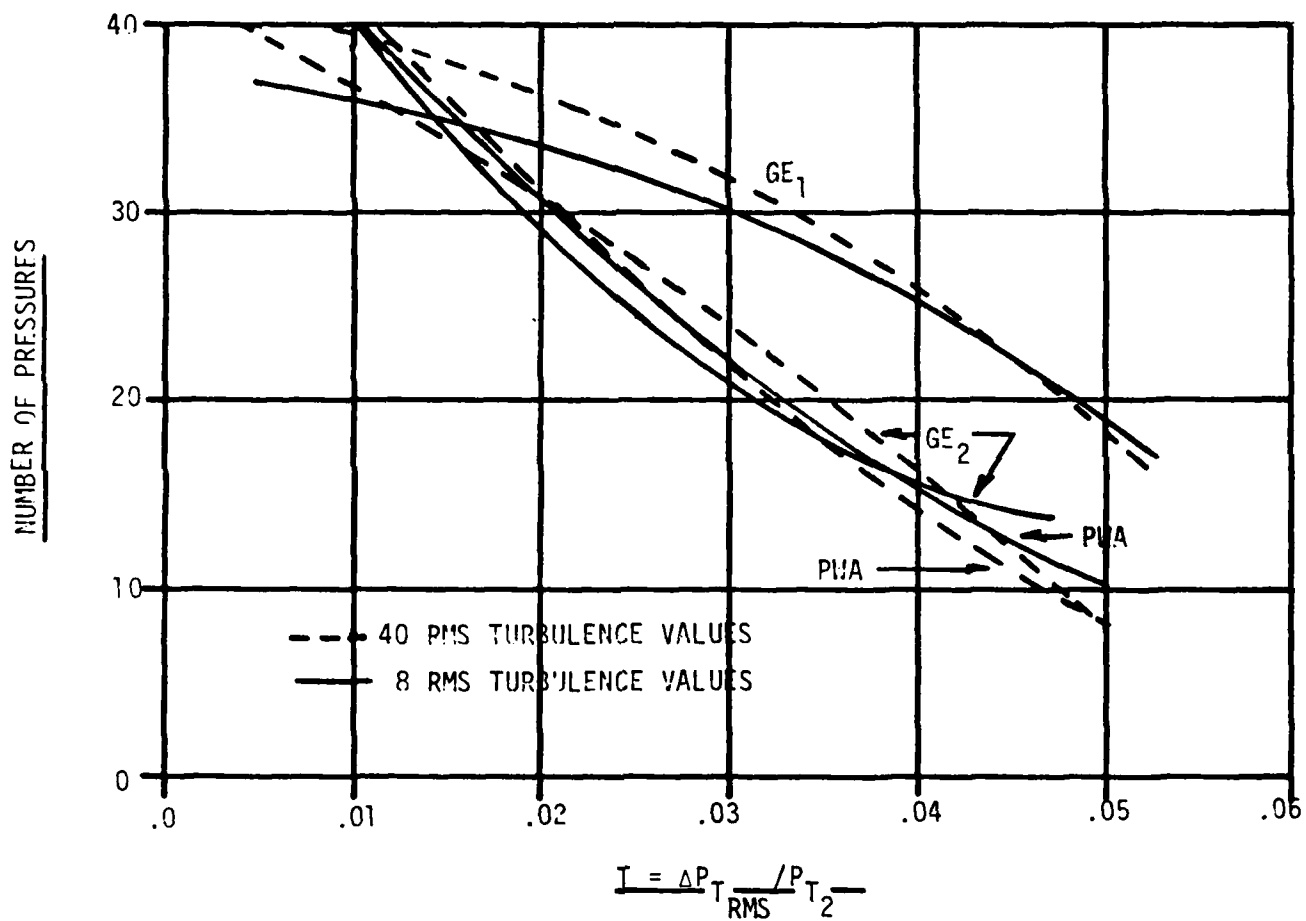


Figure 68 Predicted Pressures within $\pm 2\%$ Measured P_{T_i}

SECTION V

SUMMARY AND CONCLUSIONS

A prediction method that uses the inlet total pressure statistical properties and a random number generator has been developed to predict the most probable maximum distortion and pressure contour map. The model incorporates two digital filters to shape the random number power spectrum to approximate that of inlet pressure data and a map averaging approach that substantially reduces the difference between predicted and measured pressures.

Several measures of goodness have been used to assess the capability of the model. Those factors include: the predicted pressure contour map and distortion level, the distribution of the difference and the standard deviation of the difference between predicted and measured pressures, and the number of pressures agreeing to within ± 2 percent of their measured values.

The improved model with filtering and map averaging offers a substantial improvement over the basic model. Depending on the particular engine distortion parameter methodology and the corresponding cut-off filter frequency defining engine sensitivity, reductions in the percent RMS difference between predicted and measured probe pressures varied from 30 to 60 percent at an average inlet turbulence level of .03. Correspondingly, the number of predicted pressures within ± 2 percent of their measured values increased from 30 to 80 percent compared to the basic model.

The results indicate that the model can be applied to inlet pressure data having average turbulence levels up to .04. The assumption that the pressures have a normal distribution may preclude its application to those situations where there is substantial separation and planar wave phenomena.

The relative benefits of filtering is a function of cut-off filter frequency. As a cut-off filter frequency increases, the standard deviation of the difference between predicted and measured pressures increases and the number of pressures agreeing within ± 2 percent of their measured

values decreases. The application of the method, including map averaging, may be limited to cut-off filter frequencies of less than 1500 HZ.

The improved method has been shown to provide predicted pressure contour maps that are in substantial agreement with measured contour maps based on both forty and eight measured turbulence values.

REFERENCES

1. J. Marcus and D. Sedlock, "An Analog Editing System for Inlet Dynamic Flow Distortion, DYNADEC, Past, Present, and Future," AIAA Paper No.-80-1108, June 1980.
2. R. Borg, "A Synthesis Method for Estimating Maximum Instantaneous Inlet Distortion Based on Measured Inlet Steady State and RMS Pressures," Aerodynamics of Power Plant Installation, AGARD-CP-301, March 1981.
3. D. L. Motycka, "Determination of Maximum Expected Instantaneous Distortion from Inlet Pressure RMS Measurements", AIAA Paper No.-78-970, July 1978.
4. C. H. Stevens, E. D. Spong, and R. C. Oliphant, "Evaluation of a Statistical Method for Determining Peak Inlet Flow Distortion Using F-15 and F-18 Data," AIAA Paper No.-80-1109, June 1980.
5. A. W. Martin, W. D. Beaulieu, and L. C. Kostin, Analysis and Correlation of Inlet Unsteady Flow Data, North American Rockwell Corp., Los Angeles CA, NA-71-1146, 1971.
6. R. W., King, J. A. Schuerman, and R. G. Muller, Analysis of Distortion Data from TF30-P-3 Mixed Compression Inlet Test, NASA Lewis Research Center, NASA CR-2686, June 1976.
7. J. L. Jacocks and K. R. Kneile, Statistical Prediction of Maximum Time-Variant Inlet Distortion Levels, AEDC, Arnold Air Force Station TN, AEDC-TR-74-121, January 1975.
8. H. C. Melick, A. H. Ybarra and D. H. Benze, Estimating Maximum Instantaneous Distortion from Inlet Total Pressure RMS and PSD Measurements, NASA Ames Research Center, NASA TMX-73145, July 1976.
9. H. C. Melick and Ybarra, A. H., "Estimating Maximum Instantaneous Distortion from Inlet Pressure RMS Measurements," AIAA Paper No.-78-970, July 1978.
10. M. E. Sanders, "An Evaluation of Statistical Methods for the Prediction of Maximum Time-Variant Inlet Total Pressure Distortion," AIAA Paper No.-80-1110, June 1980.
11. W. G. Schweikhard, Yen-Sen Chen, K. A. Schweikhard, "Prediction of Dynamic Distortion Using a Minimum of Dynamic Pressure Measurements," AIAA Paper-83-1413, June 1983.
12. J. L. Jacocks, "Statistical Analysis of Distortion Factors," AIAA Paper No.-72-1100, November 1972.

13. J. A. Forner and J. M. Manter, "Prediction of Cruise Missile Inlet Peak Instantaneous Distortion Patterns from Steady State and Turbulence Data Using a Statistical Technique," June 1982.
14. J. S. Bendat and A. G. Piersol, Measurement and Analysis of Random Data, John Wiley & Sons, Inc., New York, 1968.
15. J. Neter and W. Wasserman, Applied Linear Statistical Models, Richard D. Irvin Inc., Homewood IL, 1974.
16. W. G. Gray, Propulsion System Flow Stability Program, TF30 Engine and Compressor Tests and Analysis of Test Data. AF Aero Propulsion Laboratory, WPAFB OH, AFAPL-TR-68-142, December 1968.
17. R. C. Crites and M. V. Heckart, "Application of Random Data Techniques to Aircraft Inlet Diagnostics," AIAA Paper No.-70-597, May 1970.
18. J. Mace and D. Sedlock, "A Perspective on Developing New Inlet Distortion Measurements and Predictive Methods", AIAA Paper No.-81-1589, July 1981.
19. J. O. Hinze, Turbulence, McGraw-Hill Book Co., New York, 1959.
20. Society of Automotive Engineers (SAE), Inlet Total-Pressure-Distortion Considerations for Gas Turbine Engines, AIR 1419, May 1983.
21. B. Gold and C. M. Radar, Digital Processing of Signals, McGraw-Hill Book Co., New York, 1969.